NASA TECHNICAL NOTE

NASA TN D-5007

NASA TN D-5007

HUMAN TRANSFER CHARACTERISTICS IN FLIGHT AND GROUND SIMULATION FOR A ROLL TRACKING TASK

by

Fred D. Newell
Cornell Aeronautical Laboratory, Inc.

and

Harriet J. Smith
Flight Research Center

NATIONAL AERONAUTICS AND SPACE ADMINISTRATION • WASHINGTON, D. C. • FEBRUARY 1969

NASA TN D-5007

HUMAN TRANSFER CHARACTERISTICS IN FLIGHT AND GROUND SIMULATION FOR A ROLL TRACKING TASK

By Fred D. Newell

Cornell Aeronautical Laboratory, Inc.

and

Harriet J. Smith

Flight Research Center
Edwards, Calif.

NATIONAL AERONAUTICS AND SPACE ADMINISTRATION

For sale by the Clearinghouse for Federal Scientific and Technical Information
Springfield, Virginia 22151 – CFSTI price $3.00

CONTENTS

	Page
SUMMARY	1
INTRODUCTION	2
SYMBOLS	3
THE EXPERIMENT	5
$\frac{K}{s}$ and $\frac{K}{s(s - \frac{1}{T})}$ Configurations	6
A-2 and A-2* Configurations	6
Forcing Function	9
Order of Configurations	10
TEST EQUIPMENT	10
T-33 Experiments	10
Ground-Based Simulator—Contact-Analog Display	12
Equipment and Configuration Verification	12
METHODS OF ANALYSIS	13
Cornell Aeronautical Laboratory (CAL)	13
Flight Research Center (FRC)	14
Franklin Institute Laboratories (FIL)	15
DATA PRESENTATION	15
DISCUSSION OF RESULTS	16
Comparison of Analysis Methods	17
Configurations	18
Visual Flight Versus Instrument Flight	24
Difference in K_p	25
The Stationarity Assumption	25
Analysis of Variance	26
CONCLUSIONS	27
APPENDIX - DETAILS OF CAL AND FRC COMPUTER-PROGRAM VERIFICATION TECHNIQUES	29
CAL Spectral Program	29
FRC Spectral Program	30
REFERENCES	31

HUMAN TRANSFER CHARACTERISTICS IN FLIGHT AND GROUND SIMULATION FOR A ROLL TRACKING TASK

By Fred D. Newell
Cornell Aeronautical Laboratory, Inc.

and

Harriet J. Smith
Flight Research Center

SUMMARY

Pilot transfer characteristics for three pilots have been measured in flight and in ground-based simulators for a compensatory roll tracking task with small bank-angle disturbances. The forcing function, in each case, consisted of the sum-of-ten-sine-waves with a bandwidth of 1.5 radians per second. A variable-stability T-33 airplane was used to obtain the flight measurements. Ground-based simulator measurements were obtained with both the T-33 airplane and a general-purpose simulator which used a contact-analog color display. Three different controlled elements were used, two of which were simple single-degree-of-freedom controlled elements that had been studied previously. The third was a multiple-degree-of-freedom element representative of an airplane with good handling qualities and was considered and controlled as a single-degree-of-freedom configuration in roll.

Only the multiple-degree-of-freedom controlled element was flown in actual flight. Two techniques were used to generate the tracking task in the T-33: (1) the forcing function was injected directly into the display, and (2) it was introduced through the aileron control system. In flight the first configuration had to be flown IFR because the motion of the airplane was not necessarily in harmony with the instrument-displayed motion. The second configuration was flown VFR and the motion was in harmony with the visual display. In the contact-analog simulator the display approximated the VFR display of flight but there were no nonvisual motion cues.

The results of the simple controlled-element experiments agreed reasonably well with previous results. For the multiple-degree-of-freedom controlled-element experiment, a noticeable effect of display was found. For this experiment, which was restricted to a small-disturbance bank-angle tracking task with good controlled-element dynamics, nonvisual motion cues appeared to be of less importance than visual cues.

The three pilots who participated in the program exhibited basically similar adaptations to each of the controlled elements, although one pilot consistently used a higher gain in the T-33 ground and flight experiments than did either of the other two.

INTRODUCTION

The combined human—vehicle dynamics are of major interest for determining the suitability of the combined system for the tasks to which the system will be subjected. The dynamics of the vehicle are reasonably susceptible to analysis and are tractable, and a sufficiently complete mathematical description of the human controller is required to permit a proper dynamic analysis of the human—vehicle system.

Pilot transfer characteristics can provide substantial analytic information that does not now exist about the pilot—vehicle system. This information, when combined with pilot evaluation comments, can significantly improve the understanding of the pilot—vehicle system. Initial efforts to study and describe the human controller were made by Tustin (ref. 1) approximately 25 years ago. Since then, the field of study has become primarily concerned with human pilots of aircraft. In the mid 1950's Elkind (ref. 2) extended the knowledge of the field with a study that included the effects of the nature of the input to the system. Shortly thereafter, Hall (ref. 3) examined two-axis airplane-type controlled elements in a ground simulator. The field was then extended to obtaining in-flight measurements as Campbell and Eakin (ref. 4) extracted pilot transfer characteristics from flight data obtained in a variable-stability F-94 airplane. Seckel, Hall, McRuer, and Weir (ref. 5) extracted pilot transfer characteristics from comparative in-flight and ground simulator data obtained in a Navion airplane. Since then, isolated in-flight measurements have been made for specific purposes. Also, theoretical analyses of simple control loops, including the human, have been made by using human transfer characteristics obtained from ground simulator data.

In the interim, McRuer, Graham, Krendel, and Reisener made a study and analysis of ground simulator data in which they showed pilot models that ranged from the very simple to the very sophisticated for the pilot performing a single-degree-of-freedom compensatory task. For this study, which is documented in reference 6, the disturbance input was always the sum of the same 10 sine waves, but the arrangement of the amplitudes of the individual sine waves was varied and thus the effective bandwidth of the summation signal was controllably varied. The effect of the bandwidth of the disturbance signal on the pilot vehicle control loop was studied, as were the effects of the dynamics and gain of several simple controlled elements.

As a continuation of the trend in the development of techniques for obtaining human transfer characteristics, it was felt that an experiment involving the correlation of in-flight as well as ground-based measurements of human transfer characteristics was needed. Such a study would provide information concerning the extrapolation of fixed-base measurements to actual flight consideration.

This report documents the results of a human control-response study which utilized (1) a fixed-base simulator with a contact-analog color display, (2) a variable-stability T-33 airplane as a fixed-base simulator, and (3) a variable-stability T-33 airplane in flight. For all cases examined, the task was compensatory roll tracking with small bank-angle disturbances. The primary objective of this study was the measurement of pilot characteristics in an actual flight environment and the correlation of these data with the results of previous studies that were primarily ground-based simulator investigations. Therefore, this investigation includes ground data obtained with controlled elements that have been studied in the past as well as flight and ground data obtained with an airplane-like controlled element. Additionally, the input used was the same sum-of-ten-sine-waves studied in reference 6. Some of the initial results of this

investigation have been reported in reference 7.

The major part of the work was performed, under contract, by Cornell Aeronautical Laboratory, Inc. (CAL), Buffalo, N. Y., and was sponsored jointly by the NASA Flight Research Center (FRC), Edwards, Calif., and the U. S. Air Force Flight Dynamics Laboratory, Dayton, Ohio. A subcontract was let also to the Franklin Institute Laboratories for Research and Development (FIL), Philadelphia, Pa., to perform certain phases of the analysis.

SYMBOLS

Measurements used in this investigation were generally taken in the U. S. Customary System of Units. Equivalent values are indicated parenthetically in the International System of Units (SI).

F	force, pounds (newtons)
F( ), F*( )	Fourier transform and its complex conjugate, respectively
h	altitude, feet (meters)
i	sum-of-ten-sine-waves input (bank angle)
i′	modified sum-of-ten-sine-waves input (aileron deflection)
$j = \sqrt{-1}$	
K	general gain constant
K_c	controlled-element gain constant
K_p	pilot gain constant
n_y	lateral acceleration
n_z	normal acceleration
r	yaw rate
s	Laplace operator
T	time constant, seconds
T_R	roll-mode time constant, seconds
t	time, seconds
Y_c	controlled-element transfer function, degrees/inch (degrees/centimeter)

Y_p	pilot describing function, inch/degree (centimeter/degree)
α	angle of attack, degrees
β	angle of sideslip, degrees
δ	displacement, inches (centimeters)
δ_a	aileron deflection, degrees
δ'_a	sum of aileron deflection and shaped input, degrees
ϵ	error
ζ	damping ratio
ζ_d	Dutch roll damping ratio
ζ_φ	damping ratio of the second-order term in the transfer-function numerator
θ	pitch angle, degrees
τ	time, seconds
τ_d	time, seconds (see page 16 and fig. 16)
Φ_{ab}	cross-spectral density between data traces "a" and "b"
Φ_{ii}	power-spectral density of sum-of-ten-sine-waves input
φ	display command bank angle, degrees
φ_A	airplane bank angle, degrees
φ_C	display command, degrees
φ_D	displayed bank angle, degrees
φ_{δ_a}	bank angle due to pilot input, degrees
$\left\lvert\frac{\varphi}{\beta}\right\rvert_d$	ratio of bank angle to sideslip angle in Dutch roll mode
ψ	angle of yaw, degrees
ω	frequency, radians/second or cycles per second
ω_d	Dutch roll frequency, radians/second
ω_n	frequency of pilot transfer function, radians/second

ω_φ transfer-function numerator constant

ω_θ short-period longitudinal frequency, radians/second

$\angle$ phase angle

|| absolute value

Subscripts:

as aileron stick

es elevator stick

rp rudder pedal

1,2 refer to different values of t and T

THE EXPERIMENT

Several objectives were relevant to the design of this experiment. They were as follows, essentially in the order of importance:

1. To measure the human pilot's dynamic behavior as a controller in three forms of simulation –

   a. Fixed-base, conventional IFR cockpit display

   b. In-flight variable-stability airplane (same cockpit as in item a (IFR and VFR))

   c. Fixed-base, contact-analog display (VFR)

2. To extend the work of other investigators in human response studies by –

   a. Reexamining the same controlled-element dynamics $\left(\frac{K}{s} \text{ and } \frac{K}{s\left(s - \frac{1}{T}\right)}\right)$

   b. Utilizing several analysis techniques to analyze at least part of the response data

   c. Collecting response data of several pilots in sufficient quantity to suppress the individual pilot variability so that the variability among pilots could be studied

These objectives were incorporated in the design of the experiment. Figure 1 shows the compensatory task studied, and the following table lists the principal configurations (controlled elements) investigated and the number of usable data runs obtained for each pilot for each configuration:

SUMMARY OF CONFIGURATIONS[1]

Pilot	T-33 ground (IFR)				T-33 flight		Contact analog (VFR)		
	$\frac{K}{s}$	$\frac{K}{s(s-\frac{1}{T})}$	A-2	A-2*	A-2 (VFR)	A-2* (IFR)	$\frac{K}{s}$	$\frac{K}{s(s-\frac{1}{T})}$	A-2*
A	10	10	3	10	8	10	4	6	13
B	3	3	10	3	10	3	3	0	10
C	3	3	8	3	10	3	3	0	10

[1]Configurations A-2 and A-2* are defined in the following section.

The original intent was to obtain 10 runs for pilot A in each configuration, 10 runs for each pilot in configuration A-2, and 3 runs in each remaining configuration for pilots B and C. However, because time and money were limited, not all these runs could be made. Also, some of the runs that were obtained were not usable.

$\frac{K}{s}$ and $\frac{K}{s(s-\frac{1}{T})}$ Configurations

For the $\frac{K}{s}$ controlled element, the value of K in terms of roll rate per aileron stick deflection is 50 degrees/second per inch (20 degrees/second per centimeter). The aileron stick spring rate is 2.5 pounds/inch (4.4 newtons/centimeter) for the T-33 airplane and 3.0 pounds/inch (5.3 newtons/centimeter) for the contact-analog simulator.

For the $\frac{K}{s(s-\frac{1}{T})}$ controlled element, the value of K in terms of aileron stick deflection is 120 degrees/second^2 per inch (48 degrees/second^2 per centimeter), and the value of T is 1 second. The aileron stick spring rates were the same as for $\frac{K}{s}$.

No longitudinal control task was mechanized for either the $\frac{K}{s}$ or the $\frac{K}{s(s-\frac{1}{T})}$ controlled elements. The pilot's control task consisted of the use of the ailerons to minimize bank-angle excursions from zero. No rudder was required with either of these simple, single-degree-of-freedom controlled elements.

A-2 and A-2* Configurations

The A-2 and the A-2* configurations for the T-33 ground-based simulations were full six-degree-of-freedom mechanizations of the airplane equations of motion. These equations, of course, operate implicitly in actual flight. The two configurations were the same except for the manner in which the forcing function was introduced into the system.

For the contact-analog experiments, only one configuration, referred to as the "A-2* contact analog," was considered. Only the lateral-directional equations of motion were mechanized on the analog computer.

For the A-2 and the A-2* configurations, the aileron stick spring rate was 2.5 pounds/inch (4.4 newtons/centimeter) for the T-33 airplane and 3.0 pounds/inch (5.3 newtons/centimeter) for the contact analog. The lateral-directional characteristics, shown in the following table, were the same for both configurations:

A-2 AND A-2* LATERAL-DIRECTIONAL CHARACTERISTICS

	T-33 ground	T-33 flight	Contact analog
Y_c	$\frac{\varphi}{\delta_{as}} \approx \frac{K_c}{s(s + \frac{1}{T})}$	$\frac{\varphi}{\delta_{as}} \approx \frac{K_c}{s(s + \frac{1}{T})}$	$\frac{\varphi}{\delta_{as}} \approx \frac{K_c}{s(s + \frac{1}{T})}$
K_c, $\frac{deg/sec^2}{in.}$ $\left(\frac{deg/sec^2}{cm}\right)$	60 (24)	45 (18)	55 (22)
T_R, sec	0.35	0.35	0.39
$\left\|\frac{\varphi}{\beta}\right\|_d$	0.6	0.6*	0.6
ω_d, rad/sec	2.28	2.30	2.30
ζ_d	0.11	0.09	0.10

*Phase angle improper (φ lagged β rather than led it).

The aileron characteristics were such that aileron motion caused only a very small sideslip disturbance and, consequently, the pilots did not use the rudder. Although the bank-angle-per-aileron-stick-deflection transfer function was of the form

$$\frac{\varphi}{\delta_{as}} = \frac{K\left(s^2 + 2\zeta_\varphi \omega_\varphi s + \omega_\varphi{}^2\right)}{s(s + \frac{1}{T_R})\left(s^2 + 2\zeta_d \omega_d + \omega_d{}^2\right)}$$

the numerator approximately canceled the Dutch roll quadratic term in the denominator of the transfer function. Thus the transfer function for the two configurations was reduced to a second-order function in which the first-order roll modes were explicit.

The differences between K_c and $\left|\frac{\varphi}{\beta}\right|_d$ as shown in the table for T-33 ground and flight were unintentional. However, the roll mode was so easy to fly that the only difference to be expected in the results is a different pilot gain K_p. Credence for this assumption is gained from consideration of figures 35 and 36 in reference 6, in which the variability caused by changes in gain is no different from typical run-to-run variations. Thus, the assumption that pilots compensate rather completely for changes in controlled-element gain for the same controlled element is considered valid. The pilots did not mention any noticeable difference in K_c between ground and flight. Only one pilot suspected the change in sign of $\left|\frac{\varphi}{\beta}\right|_d$. The pilot, however, could not be certain of his observation, which was made as the airplane responded to a calibration

rudder input. The difference in $\left|\frac{\varphi}{\beta}\right|_d$ is probably of little consequence in this experiment because the pilot's use of ailerons excited very little sideslip. The maximum excursion of β noted on several runs was ±0.3°. The side acceleration generated was neglected by the pilots.

The longitudinal characteristics for the T-33 simulations were the same for both configurations and were the same for flight as for ground-based simulation. These characteristics were as follows:

A-2 AND A-2* LONGITUDINAL CHARACTERISTICS

T-33 ground and flight	Contact analog
ω_θ = 2.94 radians/second ζ = 0.54	No longitudinal degrees of freedom

The tracking task for the A-2 and the A-2* configurations, both in flight and in each of the fixed-base simulators, was a compensatory bank-angle task. Very little longitudinal control was necessary in the T-33 to maintain an altitude of 23,000 feet (6900 meters) and an indicated airspeed of 250 knots (128.6 meters/second). No purposeful perturbation of the pitch attitude was introduced in the experiment, and the pilots did not find the longitudinal subtask in the T-33 to be disturbing. All flights were made in smooth air.

As stated before, the controlled element was the same for configurations A-2 and A-2*. The only difference between the two configurations was the manner in which the forcing function was introduced. For the A-2* configuration, the forcing function was injected at the display (attitude indicator for the T-33 experiments), as indicated in figure 2, whereas for the A-2 configuration the forcing function actually disturbed the aircraft. The forcing functions were required to correspond for the two configurations. This was accomplished by preshaping the input to the ailerons by the inverse of the bank-angle-per-aileron-deflection transfer function so that the resulting disturbance in the bank angle has the desired spectral density. The block diagram for the A-2 configuration is shown in figure 3. The forcing function i, which is made up of 10 sinusoids, is referred to as the sum-of-ten-sine-waves input, and the forcing function i' is termed the modified sum-of-ten-sine-waves input. These inputs gave maximum displayed bank angles of ±8°.

As far as the pilot was concerned, the A-2 and A-2* configurations were the same on the T-33 ground-based simulator and both were flown by reference to the instruments. However, in actual flight, the experiments were completely different. For the A-2 configuration in which the airplane was disturbed by the forcing function, the task was to maintain wings level; thus, the actual airplane bank angle and the error were the same (see fig. 3) and the motion of the airplane was in harmony with the visual cues. The A-2 configuration could be flown by reference to either the instruments or the outside world. For this experiment, however, the airplane was flown only by reference to the outside world (VFR). For the A-2* configuration in which the forcing function was applied directly to the display (attitude indicator), the pilots' task was to maintain zero error on the attitude indicator. Therefore, this configuration could be flown IFR only.

Because the angle (error) displayed on the attitude indicator included the disturbance, whereas the actual airplane bank angle was a result of the pilot's inputs only, the airplane motion was not in harmony with the displayed bank angle.

The pilot was aided in flight with the A-2 configuration by four grease-pencil lines on the windscreen which helped to define small roll angular displacements and rates from steady wings-level flight. The placement of these lines is shown in figure 4(a).

For the simulation involving the contact analog, the forcing-function input was the unmodified sum-of-ten-sine-waves interjected in the same manner as in the A-2* configuration on the T-33 (fig. 2); therefore, this case is referred to as A-2*. However, because the visual display was a simulation of the outside world, the experiments were actually more like the A-2 flight experiments without the motion cues. It should also be noted that the contact analog had no reference lines similar to the lines on the T-33 windscreen.

Forcing Function

Three forcing-function signals were used in the experiment. There were several generalities by which these signals were the same or produced the same results, and there were some specific differences.

Each forcing function had a Gaussian-like amplitude distribution and was generated by summing 10 sine waves in a digital computer. Although these signals appeared to the pilots to be random, they were actually periodic. The lower six sinusoid frequencies of the signals had a relative amplitude of unity, and the remaining four frequencies had a relative amplitude of one-tenth. This sum-of-ten-sine-waves forcing function was chosen in order to correlate the results with those of reference 6. For use with the analog system in the fixed-base simulators and the T-33 in flight, the signals were converted to analog signals in a digital-to-analog converter. The summation of the 10-sine-wave signals was in accordance with the method shown in figure 20 of reference 6 and defined a bandwidth of 1.5 radians/second. The frequency content of the forcing functions is summarized in the following table:

FREQUENCY CONTENT OF FORCING FUNCTIONS

Contact analog (FRC)		T-33 ground and flight (CAL)	
radians/sec	cycles/sec	radians/sec	cycles/sec
0.157	0.025	0.157	0.025
.262	.042	.262	.042
.419	.066	.393	.062
.576	.092	.603	.096
.942	.148	.969	.154
1.518	.242	1.492	.238
2.618	.417	2.539	.404
3.979	.633	4.032	.642
7.592	1.208	7.566	1.201
13.980	2.224	13.797	2.193

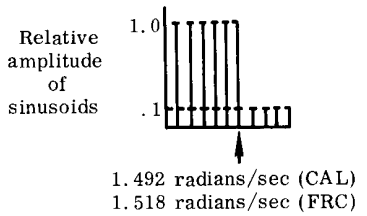

For the T-33, the forcing functions were recorded on FM tape as analog signals. As mentioned previously, there was the sum-of-ten-sine-waves signal i and the modified sum-of-ten-sine-waves signal i′. The signal i′ was produced in the same manner as i with the additional procedure of shaping i through a filter with the characteristics of the inverse of the bank-angle-per-aileron transfer function. The starting point of the forcing-function tape for each run was not controlled in any way in the T-33 tests.

For the FRC contact analog, the forcing function was stored in an on-line digital computer, converted to an analog signal, and fed directly to the simulator during each run. The forcing function was started at the same point for each run.

A specific difference between the signals is noted in the frequency content shown in the preceding table. The forcing functions used in the CAL measurements had the same frequency content as those used in the study of reference 6. These forcing functions had periods of 4 minutes. Because of storage-capacity limitations due to on-line functions of the digital computer used for the FRC measurements, only 2 minutes of data could be stored. Therefore, the frequencies were adjusted so that the forcing function was made periodic, with a period of 2 minutes. Each run for each configuration at both FRC and CAL was of 4 minutes duration, and there is no evidence that the pilots learned either the 2-minute-period or the 4-minute-period forcing functions, other than obviously becoming aware of the approximate size of the expected disturbances.

Order of Configurations

No attempt was made to randomize the order in which the pilots flew the several configurations either on the ground or in the air. The lack of randomness was dictated by the short time available with the participating pilots.

Although the pilots were given time to practice with each configuration before data runs were made, in general, little practice was required. The principal exception was the $\frac{K}{s(s - \frac{1}{T})}$ configuration, which was divergent and required the pilot's complete attention. The little practicing that was done implies that the data presented herein are representative of normal piloting effort rather than maximum performance after considerable practice.

TEST EQUIPMENT

T-33 Experiments

The equipment used in the T-33 experiments included a variable-stability T-33 airplane, three TR-10 analog computers and one TR-20 analog computer, and an FM record/reproduce magnetic-tape unit.

The variable-stability T-33 is a standard U. S. Air Force T-33 that has been modified and is operated by Cornell Aeronautical Laboratory for handling-qualities studies under contract to the USAF Flight Dynamics Laboratory. Variable-stability

characteristics are achieved by modulating, through gain changers, the electrical signals from angle-of-attack and angle-of-sideslip probes and from angular position, rate, and acceleration sensors and by summing the signals in appropriate combinations to drive the elevator, rudder, and ailerons of the airplane. Response characteristics of the airplane can be varied according to the combinations and magnitudes of the signals that are summed. The system is described in detail in reference 8.

When the airplane is used as a ground-based simulator, one of two techniques can be employed. One technique is to program the equations of the desired airplane on an associated analog computer and bypass the variable-stability equipment. This technique was used for the $\frac{K}{s}$ and $\frac{K}{s(s - \frac{1}{T})}$ configurations. The other method is to program the normal T-33 equations of motion on the analog and to use the variable-stability equipment to obtain the desired simulation. This technique was used for the ground-based simulation of the A-2 and A-2* configurations because it allowed more accurate matching between ground-based simulation and in-flight simulation. The variable-stability-system characteristics were then automatically included in both simulations.

The instrument displays used in the T-33 are shown in figure 4(a) for the in-flight simulator and in figure 4(b) for the ground-based simulator. Placement of the instruments was identical for flight and ground tests, but some of the physical instruments were in different units so that each instrument would be compatible with the instrumentation system in use. The instruments that were active for the ground-based simulation were: the normal acceleration n_z; airspeed; altitude h; angle of attack α; rate of climb $\frac{R}{C}$; the Lear all-attitude indicator with bank angle φ, sideslip angle β, pitch angle θ, and yaw rate r; the compass card of the ADF radio magnetic indicator; and the percent rpm indicator. For the in-flight IFR simulation, all the instruments on the panel were operable, but the pilot concentrated on using the same instruments that were used in the ground-based simulation.

The analog computers used in the ground simulation were transistorized computers. The servo interface equipment between the analog computers and the servo instruments in the airplane was produced at Cornell Aeronautical Laboratory and had been used on several previous programs. Previously, pilots had complained about a "stickiness" or "jittery" response of the attitude display in bank angle, which was subsequently traced to a high-frequency oscillation. For this program, rate feedback was added to the interface transmitter servos to eliminate the "jitter" effect. A frequency response of the bank-angle servo loop, except for the bank-angle indicator, is shown in figure 5. The bandwidth (3.5 cps) of the bank-angle-display servo loop is considerably wider than the defined bandwidth (0.238 cps) of the forcing function, although the servo does tend to attenuate slightly the two highest frequencies of the forcing function. The response characteristics of the bank-angle indicator are shown in figure 6. The phase lags of the display system probably affected the $\frac{K}{s(s - \frac{1}{T})}$ configuration most. All three pilots felt that the bank-angle presentation in the T-33 ground-based simulator was normal.

The elevator and rudder control static characteristics of the T-33 are shown in figure 7. The aileron stick characteristics are the same for all configurations and are

shown in figures 8 and 9. Although the elevator-stick and rudder-pedal feel systems were operative, the elevator and rudder deflections were not mechanized for the $\frac{K}{s}$ and $\frac{K}{s(s - \frac{1}{T})}$ configurations. Figure 8 shows that the aileron stick had a hysteresis loop between stick force and stick position. The hysteresis was noticeable to all three pilots but was not considered to be objectionable. Because the stick position was used to drive the aileron, there is no direct effect of the hysteresis loop in the data. There is, however, an implicit effect, since the hysteresis may affect the pilot.

Ground-Based Simulator—Contact-Analog Display

The equipment used at FRC for the ground-based simulator experiments included an analog computer, a color contact-analog display, a digital computer, an FM tape record/reproduce unit, and a cockpit. For simplicity these experiments will be referred to as "contact analog" experiments. The cockpit and contact-analog display are illustrated in figure 10. The display was positioned approximately 24 to 30 inches (60 to 75 centimeters) ahead of the pilot, subtending a total angle at the eye of approximately 28° to 30° and thus allowing considerable peripheral vision.

An attempt was made to duplicate the aileron control-stick characteristics of the T-33. The stick gearing was essentially the same as that in the T-33 although the forces were slightly higher (3 pounds (13.3 newtons) for 1 inch (2.5 centimeters) and 8 pounds (35.6 newtons) for 3 inches (7.5 centimeters)). Lateral stick forces were produced by compression springs attached to the control stick. There was approximately 0.7 pound (3.1 newtons) of coulomb friction in the aileron stick and a force deadband of ±0.1 inch (0.25 centimeter).

The forcing-function input was stored in the digital computer and put through a digital-to-analog converter to the analog computer. The controlled-element response was computed on the analog computer and summed with the forcing-function input, forming the error. The error in bank angle was sent to the contact-analog color display. The controller deflection, displayed error, and controlled-element response were sent to the digital computer through analog-to-digital converters and with the forcing-function input were recorded on tape using a digital format. FM tape recordings were made simultaneously.

Equipment and Configuration Verification

The individual configurations were verified by analysis of transient responses to control impulse and step inputs and spectral analysis of the tracking records. The transfer functions obtained from the spectral analysis are shown in figures 11 to 13. Because the computed transfer functions varied very little from run to run, only one run is plotted for each case. A transfer function computed from the recorded data for the A-2 configuration used on the T-33 is not shown, since the total input $(\delta_a + i')$ to Y_c was not recorded because of insufficient channels in the tape recorder. However, the A-2 configuration transfer function is necessarily the same as that shown for the A-2* configuration, since precisely the same analog-computer settings and T-33

variable-stability-system gains were used for the two configurations. It is seen from the transfer functions for the A-2* configuration (page 7) that the Dutch roll mode is absent.

The A-2 configuration was established during a previous program, which is described in reference 9. This reference also contains the longitudinal and lateral-directional equations of motion that were programed on the analog computer for the T-33 ground-based simulation portion of this program. For the contact-analog program, the longitudinal equations were omitted.

METHODS OF ANALYSIS

Cornell Aeronautical Laboratory (CAL)

Spectral method. – The data recorded on FM tape were the forcing function i or i′, the true aileron stick displacement δ_{as}, the airplane bank angle φ_A, and the bank-angle error displayed on the attitude indicator ϵ. The taped data were digitized in an analog-to-digital converter to fixed-point digital data. These data were then analyzed by digital computers for the pilot random-input describing function Y_p, and controlled-element transfer function Y_c, and the open-loop random-input describing function Y_pY_c. The power-spectral-density ratios presented in reference 10 were used in the analysis; namely, $Y_p = \frac{\Phi_{i\delta_{as}}}{\Phi_{i\epsilon}}$, $Y_pY_c = \frac{\Phi_{i\varphi_A}}{\Phi_{i\epsilon}}$, and $Y_c = \frac{\Phi_{i\varphi_A}}{\Phi_{i\delta_{as}}}$. The symbol Φ_{ab} represents the cross-spectral density between data trace "a" and data trace "b". Details of the computer-program verification are discussed in the appendix.

Deterministic theory. – One run was also analyzed by using the deterministic theory presented in reference 11 for obtaining the time-varying characteristics of a time-varying system. This technique adjusts the gain of a set of characterizing filters according to the criterion of minimizing the integral square error between the pilot's output and the output of the model for the same input. The available choice of gains is constrained to account for the fundamental uncertainty which always accompanies time-varying identification processes. This constraint, for instance, makes it impossible for the deterministic technique to force a fit of the pilot's output with a single-pole filter and rapidly varying gain. The time interval over which the filter gains are computed can be chosen for any interval greater than approximately 5 seconds. In the limit, the time interval can be so long that the technique determines a set of constant coefficients. This limit form of the analysis can be expressed in a standard Bode diagram form.

Variance analysis. – An analysis of variance was performed on the amplitude data for Y_p and Y_pY_c for the T-33 ground simulator runs. The analysis was based on the first three runs by each pilot. This approach was used to make whatever effect of learning there might have been as consistent as possible among the three pilots and to perform an analysis that did not bias the results toward pilot A, who usually performed more runs per configuration than either of the other pilots. The analysis was designed to determine the significance of the exhibited differences in Y_p and Y_pY_c due to the

configurations and the pilots and the interaction between the pilots and the configurations. Thus, the model for the analysis was

$$Y_{ijk} = m + c_i + P_j + e_{ijk}$$

where

Y = pilot describing function or open-loop describing function

m = mean value of describing function

c = effect of configuration on the describing function

P = effect of the pilot on the describing function

e = error term

Subscripts:

i = configuration index (1, $\frac{K}{s}$; 2, $\frac{K}{s(s - \frac{1}{T})}$; 3, A-2; 4, A-2*)

j = pilot index (1, A; 2, B; 3, C)

k = run number

The analysis was performed at four frequencies, 0.0625 cps, 0.237 cps, 0.4042 cps, and 1.204 cps for the $|Y_p|$ data and at 0.0625 cps, 0.237 cps, 0.4042 cps, and 0.642 cps for the $|Y_pY_c|$ data, to determine if significant differences varied with frequency.

For the variance analysis of the Y_pY_c data, the values of Y_pY_c for the A-2 configuration were generated by multiplying the Y_p determined for the A-2 configuration with the Y_c determined from the A-2* configuration. This is an accepted procedure because the only difference between the two configurations is the point of injection of the forcing function.

Flight Research Center (FRC)

The Flight Research Center used a spectral method of analysis; however, the technique used to obtain the spectral densities made use of the following expression (see ref. 12):

$$\Phi_{xy} = \frac{F^*(x)F(y)}{2T}$$

where F( ) and F*( ) represent the Fourier transform and its complex conjugate, respectively. The equations for the pilot describing function, airplane transfer function, and open-loop describing function then become

$$Y_p = \frac{F^*(i)F(\delta_{as})}{F^*(i)F(\epsilon)}$$

$$Y_c = \frac{F^*(i)F(\varphi_A)}{F^*(i)F(\delta_{as})}$$

and

$$Y_pY_c = \frac{F^*(i)F(\varphi_A)}{F^*(i)F(\epsilon)}$$

Because the forcing-function input consisted of sine waves, no smoothing was considered necessary. Therefore, the preceding expressions were simplified as follows:

$$Y_p = \frac{F(\delta_{as})}{F(\epsilon)}$$

$$Y_c = \frac{F(\varphi_A)}{F(\delta_{as})}$$

and

$$Y_pY_c = \frac{F(\varphi_A)}{F(\epsilon)}$$

In addition to analyzing the contact-analog runs by this technique, nine runs obtained on the T-33 were analyzed. Further details of the use and application of the FRC spectral technique in this program are presented in the appendix.

Franklin Institute Laboratories (FIL)

Eight of the T-33 runs that were analyzed by both CAL and FRC spectral techniques were also analyzed on the analog spectral analyzer at the Franklin Institute Laboratories for Research and Development. This analyzer, described in reference 6, used tuned oscillators and operated directly with the recorded FM analog signal. The analyses of all eight runs were performed after the oscillators were adjusted for one of the runs.

DATA PRESENTATION

The primary form of presentation of the data is the Bode diagram. Figures 11 to 13 show Bode diagrams for the controlled elements $\frac{K}{s}$, $\frac{K}{s(s - \frac{1}{T})}$, and A-2*,

respectively, as determined from both the T-33 and contact-analog experiments. The asymptotes shown in the figures are those that are theoretically expected.

Figures 14(a) to 14(h) are Bode diagrams on which the CAL, FRC, and FIL spectral analyses of eight T-33 runs are plotted. These plots compare the results of the different analysis techniques as applied to the same original data.

Figures 15 and 16 present the results of the application of the deterministic theory to T-33 flight run 106 for configuration A-2 and pilot A. Figure 15 compares the constant-coefficient case of the deterministic theory with CAL and FRC spectral analyses of the same data. Figure 16 shows the time-varying case of the deterministic theory analysis. In figure 16(a) the presentation of the response of the pilot model to a step input has two time axes, t and τ. The time axis t represents the time throughout the run at which the pilot model is sampled with a step input. The time axis τ is the axis for plotting the time history of the output of the pilot model at time t in response to a step input at $\tau = 0$. If the pilot model varies from time t_1 to t_2, the variation will be depicted by different step-response time histories at these two times. Because the model characterizes the pilot, changes in the model reflect changes in the pilot. The time base used in the truncation function of the time-varying analysis of this run is 20 seconds, and the total data analyzed are the last 100 seconds of the run. The first portion of the run is used to determine the initial values of the filter variables of the analysis method.

Presented in figure 16(b) are the input signal to the pilot, the pilot's output, the output of the model for the same input, and the error trace, which is the time history of the difference between the pilot's output and the output of the model.

Figures 17 to 19 present Bode diagrams of the pilot transfer characteristics and the open-loop characteristics obtained by CAL and FRC. The spectral method of CAL was used in the analysis of the T-33 data shown in these figures, and the spectral method of FRC was used in the analysis of all contact-analog data. In these figures, the data symbol at any frequency for any pilot represents the average of the pilot's data at that frequency. The pilot's data points, except for figure 18, are separated at each frequency for clarity, and the specific frequency is noted by a tick mark on the frequency scale. The vertical lines at each data point represent plus and minus the standard deviation (based on N-1) applicable to that point.

In figure 18, the magnitude data for the pilot-transfer characteristic of IFR flight and visual, heads-up flight obtained in the T-33 and visual, heads-up ground simulation obtained with the contact analog are compared.

DISCUSSION OF RESULTS

Perhaps the most fundamental concern of this program was the demonstration that reliable pilot describing-function data could be obtained in flight. Toward this purpose, it was important to measure the variability exhibited from run to run with the same pilot. It is noted, from the values of standard deviation shown in the figures, that the data are consistent throughout most of the frequency range. At the lowest and highest frequencies there was often insufficient power to accurately measure the pilot

describing function for the easily flown configuration. The consistency of the inflight data is compatible with the consistency of the ground-based simulator data. Thus, comparisons of the flight and ground data can be made directly. Furthermore, it is a matter of interest to compare the data for the simple controlled elements $\left(\frac{K}{s}\right.$ and $\left.\frac{K}{s(s-\frac{1}{T})}\right)$ with data previously obtained with those controlled elements in the study of reference 6. The present data and the referenced data are of comparable consistency and are directly compared. To indicate the comparisons with the referenced data, faired representations of those data are presented. These are merely "eyeball" fairings and do not constitute polynomial fits to the reference 6 data. They are presented only as a convenient reference to previous experimental data. Because all the data for the present experiment were obtained with a forcing function of bandwidth 1.5 radian/sec, the comparisons are restricted to the data of reference 6 that were obtained for the same forcing function. It should be noted that the equipment used in the experiments reported in reference 6 differed from that used in the present experiment (see page 10). The equipment used in the experiments discussed in reference 6 consisted of a chair, an arm rest, a minimum inertia and minimum damping 4-inch (10-centimeter) moment-arm stick that was spring restrained, and an oscilloscope. The stick presumably had no hysteresis, and the presentation on the scope was a dot that moved back and forth horizontally, according to the error signal. The pilot's task was to minimize the error.

Prior to the experiment, it was hoped that turbulence would not present an insurmountable distortion of the flight data. During the program, the pilots reported very little turbulence, and usually none. The consistency of the flight data, as compared with the ground data, gives credence to the claim that turbulence did not affect the flight data.

Comparison of Analysis Methods

Figure 14 presents the results of using the three (CAL, FRC, and FIL) different spectral-analysis techniques for several selected T-33 runs. The agreement is acceptable for most cases and, therefore, any significant differences between the contact-analog data and the T-33 data can be expected to result from differences in simulation rather than in analysis technique.

Figure 15 compares results from a constant-coefficient case of the deterministic theory with the standard cross-spectral-density-ratio analysis of CAL and the Fourier transform spectral analysis of FRC for a flight run (configuration A-2). The spectral analyses agree in magnitude and phase, and the magnitude ratios compare favorably with the constant-coefficient analysis. However, the phase angles at the lower frequencies for the constant-coefficient analysis do not compare well with either of the spectral analyses. Part of the difference between the methods is attributed to the shorter run length analyzed by the constant-coefficient technique. Because of limited computer storage capacity, only 3 minutes of the data could be analyzed by the constant-coefficient analysis, whereas 4 minutes of data were analyzed by the spectral-density analysis of Cornell and the Fourier transform spectral method of FRC. Further study of this particular comparison is needed.

$Y_c = \frac{K}{s}$. – The data for the $Y_c = \frac{K}{s}$ configuration, in terms of amplitude ratio and phase angle, are presented in figures 17(a) and 17(b) and 19(a) and 19(b) for Y_p and Y_pY_c, respectively. For the T-33 data the three pilots showed similar characteristics in both the Y_p and Y_pY_c data and had a characteristic that is "second-order-like" with a relatively low damping ratio "resonant" peak at approximately 1.2 cps. The pilots' phase-angle diagram in figures 17(a) and 17(b) is similar to that of a second-order system, although at the higher frequencies the phase-angle change of the pilot is too rapid for a second-order system which has a moderate damping ratio, and it passes through -180°.

For the contact-analog data of figure 17(b), the amplitude ratio of Y_p is more constant throughout the frequency range than are the T-33 data, so that below 0.7 cps it is greater than the T-33 amplitude ratio and in the region of 0.7 cps the two amplitude ratios are equal. The contact-analog data do not show the "resonant" peak, and, except at the highest frequency, the phase angle matches the phase angle determined in the T-33 airplane. The contact-analog Y_pY_c data of figure 19(b) accurately reflect the Y_p data and have a general slope of -20 dB per decade.

The data presented in figure 17(a) are compared with Y_p data deduced from figure 41(a) or figure 48 of reference 6, and the data shown in figure 19(a) are compared with the data of figure 48 of the reference. The Y_p data deduced from the reference are shown in figure 17(a). The $|Y_p|$ data from the reference are constant throughout the frequency range, and the "resonance" in the data from the present experiment does not occur. The Y_p phase-angle characteristic deduced from the reference agrees well with the results of the present experiment. Only above 1.0 cps do the characteristics differ appreciably, in that the phase angle determined in both the contact-analog and the T-33 experiments changes more rapidly than does the phase angle of the referenced data at the higher frequencies.

The open-loop Y_pY_c data are shown in figures 19(a) and 19(b) for the T-33 and contact analog, respectively, and the data from reference 6 are included in figure 19(a). The similarity of the sets of data is good. The "resonance" of the pilot at approximately 1.2 cps evident in the T-33 data is absent in the contact-analog data and the referenced data. The gain crossover frequency (the frequency at which the gain is 1) of the T-33 data is 0.4 cps, as contrasted to 0.6 cps for the contact-analog data and 0.72 cps for the referenced data. The phase-angle characteristics are comparable up to 1 cps and then differ, in that the phase angle for the present experiment changes more rapidly than that of the referenced experiment.

The T-33 ground data presented in figures 17(a) and 19(a) show that the pilots were operating as higher-order systems than was shown in either the contact-analog data or the reference 6 data. This is noted in the nonconstant slopes of the amplitude data and the faster phase-angle change at the high frequencies, with the suggestion that the roots that represent the pilot are closely spaced. It is also noted that in the mid-frequency range of the T-33 data pilot A uses a slightly higher gain than used by either pilot B or

pilot C. In the contact-analog data pilots A and B generally used a higher gain than pilot C. However, the three pilots have essentially the same gain for both experiments near 0.7 cps.

A possible cause of the resonance displayed by the pilots in the T-33 data may be the implicit effect of the aileron stick feel system. The feel-system dynamics were shown in figure 9. For this figure, an attempt was made to remove the effects of the hysteresis loop from the data. The figure shows two peaks, at 1.75 cps and at 3 cps. An association between the feel-system dynamics and the "resonance" displayed by the pilots can be made because the damping ratio and the undamped natural frequency implied by the lower frequency peak in figure 9 are reasonably close to those obtained for the second-order pole of a polynomial fit to some of the Y_p data. This polynomial fit is discussed later. However, because of the "parallel" nature of the feel system and the unknown pilot reaction to the system, an explicit demonstration of the effects of the feel system cannot be obtained.

$Y_c = \frac{K}{s(s - \frac{1}{T})}$, $T = 1.$ – The amplitude and phase data for the $Y_c = \frac{K}{s(s - \frac{1}{T})}$ configuration are presented in figures 17(c) and 17(d) and 19(c) and 19(d) for Y_p and Y_pY_c, respectively.

For the T-33 data in figures 17(c) and 19(c), the three pilots show the same characteristics, within an experimental accuracy of 10 percent to 15 percent, except for the amplitude-ratio data in figure 19(c) at the highest frequency. The amplitude ratio of figure 17(c) for each of the pilots has a slope of approximately 20 dB per decade but with the same tendency toward a low damped "resonance" at 1.2 cps as noted in the discussion of the $\frac{K}{s}$ data for the T-33.

In the contact-analog data for pilot A in figure 17(d), the amplitude ratio of Y_p is comparable to that obtained in the T-33 above a frequency of 0.16 cps, but it has a slope that is nearer 20 dB per decade. The phase-angle data of figure 17(d) are equivalent to the T-33 phase-angle data except at the two highest frequencies where the contact-analog data show less lag. The Y_pY_c data of figure 19(d) reflect the Y_p data accurately and have a slope of -20 dB per decade. As would be expected from the Y_p data, the contact-analog phase data for the Y_pY_c match those for the T-33 data except at the two highest frequencies where they show less lag than shown by the T-33 data.

The Y_p data deduced from figure 44 of reference 6 are shown in figure 17(c) for comparison. The amplitude ratio from the reference 6 data has a general slope of 20 dB per decade. In general, the phase angle obtained in the present experiment indicates a greater phase-angle lead than is evident from the referenced data from the low frequencies up to a frequency of 0.7 cps where the phase-angle diagrams match. Above this frequency, the phase-angle lag of the present data increases more rapidly than that of the referenced data.

For the comparison of the open-loop Y_pY_c data, the data of figure 19(c) are compared with those of figure 51 of reference 6. From figure 51, straight-line fits to the amplitude data for values of $\frac{1}{T}$ of 1 and 1.5 in the controlled element $Y_c = \frac{K}{s(s - \frac{1}{T})}$ are taken and are shown in figure 19(c). The phase-angle curve in figure 19(c) represents the phase angle for both values of $\frac{1}{T}$ from the reference data. It is noted that the amplitude data from the present T-33 experiment are more like those for the $\frac{1}{T} = 1.5$ case of the reference data, but that the "resonant" peak shown by the pilots in the present T-33 data reduces the Y_pY_c gain margin of the present data from what it is for either case of the reference data. As a matter of interest, it is noticed from figure 51 of reference 6, which shows data for values of $\frac{1}{T}$ of 0, 0.5, 1.0, and 1.5, that for $\frac{1}{T} = 0$ the slope of the Y_pY_c amplitude ratio is -20 dB per decade and that as $\frac{1}{T}$ increases this slope decreases. As $\frac{1}{T}$ increases, the controlled element $Y_c = \frac{K}{s(s - \frac{1}{T})}$ becomes more difficult to control. An intuitive suggestion is that the more difficult a system is to control the more inclined a pilot may be to operate in a manner that is described by amplitude-ratio slopes that are not integer multiples of 20 dB per decade. This characteristic suggests that the pilot has an increasing tendency to operate as a higher-order system which has closely spaced poles and zeros.

The gain crossover frequencies of the present and the referenced data are approximately the same, and the phase-angle diagrams are similar. For the T-33 data the crossover frequency is 0.44 cps, for the contact-analog data it is 0.47 cps, and for the referenced data it is 0.55 cps. The phase-angle data, in contrast to the referenced data, for both the T-33 and the contact analog in the mid-frequency range show somewhat less lag, but in the region of crossover all three phase-angle diagrams are the same as shown in figures 19(c) and 19(d). For the higher frequencies the phase-angle lag for the T-33 data increases more rapidly than that for either the contact-analog data or the referenced data. Each of the experiments indicates the tendency for low-frequency phase-angle droop.

Y_c = A-2, A-2* ground. – The A-2 and A-2* ground experiments should be identical, and the fact that for the T-33 experiments the input signal was injected into the system loop in different ways is immaterial. The Y_p data are shown in figures 17(e) and 17(f) for the T-33 data and in figure 17(g) for the contact-analog data. The Y_pY_c data for the A-2* ground case are shown in figures 19(e) and 19(f) for the T-33 and contact analog, respectively. The manner in which the data were recorded in the T-33 precluded direct computation of either Y_c or Y_pY_c for the A-2 ground case; however, Y_c was obtained and checked periodically from transient responses and was identical for the A-2 and A-2* ground cases. Therefore, because the Y_p data of figures 17(e) and 17(f) are comparable, the Y_pY_c data of figure 19(e) are representative of the A-2 ground case as well as the A-2* ground case from which they were obtained. The three figures for the T-33 data are internally consistent and do not strongly indicate the

pilots' tendencies for a "resonance" near 1 cps. In general, pilot A used a higher gain at each frequency than used by either of the other pilots.

For the contact-analog data of figure 17(g) the amplitude ratio for Y_p is, except at 0.6 cps, generally greater than that for the T-33 data. Pilot A used a generally higher gain than pilot B and pilot C in the T-33, but for the contact analog pilot A is similar to pilot B. The Y_p phase diagram for the contact-analog data is identical to the phase angle obtained in the T-33 up to a frequency of 0.6 cps, and then at the two highest frequencies the contact-analog data show noticeably less lag than do the T-33 data. Each of the experiments shows a slight tendency for low-frequency phase-angle droop.

From the T-33 Y_pY_c amplitude data of figure 19(e) the most striking characteristic is the tendency of each pilot to obtain a crossover frequency that is lower than any chosen for the $\frac{K}{s}$ or $\frac{K}{s(s - \frac{1}{T})}$ configuration. Also, each pilot is individualistic in the choice of crossover frequency. For the T-33 A-2* ground data, the gain crossover frequencies are 0.3 cps for pilot A, 0.105 cps for pilot C, and 0.07 cps for pilot B.

The contact-analog Y_pY_c amplitude-ratio data in figure 19(f) are more consistent among the three pilots than are the T-33 data, generally greater than the T-33 amplitude ratio, and have a slope that more nearly approaches -20 dB per decade. The crossover frequencies for all three pilots for the contact analog are between 0.45 cps and 0.50 cps.

The contact-analog Y_pY_c phase data are the same as the T-33 phase-angle data through a frequency of 0.6 cps; however, at the highest frequencies, the T-33 data show considerably more lag than the contact-analog data.

Although there are no previous data to compare with the data of this study, similar configurations are often approximated by $\frac{K}{s}$. Therefore, the Y_pY_c data of reference 6 for $Y_c = \frac{K}{s}$ are shown in figure 19(e), for both amplitude and phase angle. For this comparison the crossover frequencies are considerably different, although the phase-angle characteristics are similar. Hence, the gain and phase-angle margins for the present data are considerably larger than they are for the $\frac{K}{s}$ data of reference 6. This same situation is indicated, although not as strongly, by comparing the $\frac{K}{s}$ data of figures 19(a) and 19(b) with the data of figure 19(e).

The Y_pY_c phase data of figures 19(e) and 19(f) do not show any strong tendency for a low-frequency phase-angle droop.

Y_c = A-2, A-2* flight. – The A-2 and A-2* flight experiments are different in that A-2 flight was flown by visual reference to the natural horizon and the forcing function was contained in the motion of the airplane, whereas A-2* flight was flown by reference to the roll-attitude instrument and the forcing function was not contained in the motion of the airplane. The forcing function, although injected into the system loop in

different ways, was visually the same bank-angle forcing function in both the A-2 and A-2* configurations.

The Y_p data are shown in figures 17(h) and 17(i) for the A-2 flight and A-2* flight cases, respectively, and the Y_pY_c data are shown only for the A-2* flight case in figure 19(g). Because the recorded data for the A-2 flight case did not permit direct computation of Y_c or Y_pY_c, Y_c was calibrated from transient response records and found to be the same as Y_c for the A-2* flight case. From both transient-response measures of Y_c for the A-2 flight and A-2* flight cases and from spectral measures of Y_c for the A-2* flight case, it was determined that, dynamically, the value of Y_c for the A-2 flight and ground and A-2* flight case was the same but the gain of Y_c was different between flight and ground. This difference in gain is noted in the table of constants on page 7.

A comparison of the Y_p data of figures 17(h) and 17(i) indicates different pilot adaptations to the two configurations. However, before the differences are discussed, it should be recalled that the motion cues of the airplane for the A-2* flight case are not necessarily in harmony with the motion that is displayed to the pilot on the roll-attitude indicator, whereas all cues are in harmony for the A-2 flight case. The resulting differences may be small and negligible or they may have an effect, but this experiment does not provide the information that is necessary to make a conclusive determination. In figures 17(h) and 17(i) the amplitude ratio for the heads-up A-2 flight case shows a somewhat flatter response than the amplitude ratio for the instrument A-2* flight case, and there is a tendency for a low-frequency phase-angle droop in the A-2 heads-up flight data that is not indicated in the A-2* instrument flight data. Also, the phase-angle lag above 0.4 cps increases less rapidly for the A-2 heads-up flight data than it does for the A-2* instrument flight data. It is interesting to note in the comparisons of the Y_p data from the T-33 experiments that the A-2 ground, A-2* ground, and A-2* flight amplitude and phase-angle diagrams are comparable for the Y_p data of figures 17(e), 17(f), and 17(i). Although pilots A and B show a tendency to use a somewhat higher gain for A-2* flight at frequencies below 0.3 cps than they use for either A-2 ground or A-2* ground, pilot behavior in flight is similar to pilot behavior in a ground simulator for this task.

A further comparison of the amplitude-ratio data of Y_p for the A-2 (ground and flight) cases is made in figures 18(a) to 18(c). It will be recalled that the gain K_c of the controlled element for these cases was different between ground and flight. In figure 18 the amplitude ratios of Y_p for the flight data have been adjusted to account for the difference in K_c by multiplying the flight data by the ratio of K_c flight to K_c ground. As suggested earlier, credence for this correction is gained from figures 35 and 36 of reference 6. The most evident implication of figure 18 is the significantly larger amplitude ratio chosen by all three pilots for the heads-up A-2 flight case and the contact analog as compared with A-2 ground and A-2* flight or ground for frequencies below 0.6 cps. It appears from the data presented in these figures that fixed-base visual simulation is a better approximation to visual flight than either IFR inflight

simulation or IFR ground-based simulation. This is most evident for pilots B and C; however, the difference between flight and ground VFR shown here for pilot A was not evident in a similar previous experiment (ref. 7). From the data of this experiment, an exact comparison of inflight IFR with inflight heads-up flight cannot be made because the A-2 configuration, which is the only configuration that could be flown both IFR and VFR, was flown only heads-up in flight.

The flatter amplitude-response curve for Y_p for the A-2 flight case and the contact analog is evident in figure 18. The pilot transfer characteristics obtained from both the A-2 flight and contact-analog data can be described by the general polynomial

$$\frac{e^{-\tau_d s} K\left(s + \frac{1}{T_1}\right)}{\left(s + \frac{1}{T_2}\right)\left(s^2 + 2\zeta\,\omega_n s + \omega_n{}^2\right)}$$

The most interesting outcome of this approximation is the necessity to include the second-order pole not contained in the expression for Y_p in reference 6. An example of the fit that can be obtained is shown in figure 20 in relation to Y_p obtained for pilot A. It is noted in figure 20(a) for the contact-analog data that the polynomial can be made to closely match the experimental results in both phase angle and amplitude. For the flight data (fig. 20(b)) the amplitude fit is also excellent; however, a complicated expression for τ_d is required to match the phase-angle data as well. A list of the constants obtained for the preceding polynomial is shown in table I for the A-2 configuration of the T-33 and the A-2* configuration for the contact analog.

TABLE I

CONSTANTS IN THE FUNCTION $Y_p = \dfrac{e^{-\tau_d s} K\left(s + \frac{1}{T_1}\right)}{\left(s + \frac{1}{T_2}\right)\left(s^2 + 2\zeta\,\omega_n s + \omega_n{}^2\right)}$

[Configurations A-2 and A-2*]

Pilot	Simulator	τ_d	K	T_1	T_2	ω_n	ζ
A	T-33 flight	0	23.63	2.295	0.834	9.1	0.45
A	Contact analog	0.175	16.68	1.053	.500	8.9	.45
B	Contact analog	.190	42.19	1.000	.333	12.5	.40
C	Contact analog	.260	3.38	.8333	0	7.5	.75

As an outcome of the amplitude fit, it is recognized that the noninteger slope tendency for the A-2 and A-2* data is a result of the proximity of the poles and zeros required to fit the data.

The Y_pY_c data of figure 19(g) are consistent with the Y_p data of figure 17(i) and the known Y_c. The crossover frequency for pilots A and B for the A-2* flight case is

approximately 0.3 cps, and for pilot C it is approximately 0.1 cps. The phase-angle diagram is consistent for all three pilots. Because of the repeatability of Y_c as measured from in-flight transient-response records, the difference that would be expected between Y_pY_c for the A-2 heads-up flight case would be a reflection of the generally higher gain used by the pilots for the A-2 flight configuration than for the A-2* flight configuration. This in turn would be reflected in higher crossover frequencies for each pilot, that is, a crossover frequency of approximately 0.6 cps for pilots A and B and approximately 0.33 cps for pilot C. The phase-angle diagram for Y_pY_c of the A-2 heads-up flight case would be expected to reflect the low-frequency phase-angle droop and slower increase of high-frequency phase-angle lag that is shown in the Y_c phase-angle data in figure 17(h). The $\frac{K}{s}$ data from reference 6 are shown again for comparison.

Visual Flight Versus Instrument Flight

The data of this experiment do not permit a direct comparison of instrument flight with strictly heads-up visual flight to provide definitive, conclusive results. For the A-2* instrument flight case, the motion of the airplane is entirely a result of the control inputs made by the pilot and does not reflect the forcing function, which is displayed only on the roll-attitude indicator. However, for the A-2 heads-up flight case, the motion of the airplane is a result of both the forcing function and the control motions made by the pilot. The contact analog had only visual cues. Thus, the nonvisual cue field is different among the experiments and the sources of visual information differ in both form and dynamic characteristics. As a result, there are too many variables to permit a conclusive discussion.

In an attempt to obtain a factually based and reasonable, though necessarily hypothetical, explanation of the data, a review of some of the literature (refs. 13 to 16) that pertains to visual and motion cues was made. This review suggested that visual sensing can be of finer resolution than vestibular or tactile sensing and that it can operate for small motion perception without phase-angle lag or time delays up to a frequency of 0.4 cps and with small phase-angle lag but not great loss of information up to a frequency of 1.6 cps. It is expected that a subject's use of visual and nonvisual motion cues can be affected by the resolution of the visual information that is presented to him, the magnitude and frequency content of both the visual and nonvisual motion, and perhaps by the rates of change of acceleration that occur in the forcing function.

The input for the present experiment was for small bank angles and relatively small roll accelerations. It is expected, then, that the visual input played a major role in the ability of the pilot to perform the compensatory tracking task. It is also estimated from the geometry of the roll-attitude indicator and the geometry of the natural outside-world presentation with the addition of the horizontal lines on the windscreen that the pilot had at least twice the static visual resolution of information from the natural outside world as he had from the attitude indicator. Also, as discussed by Jones in reference 15, all of the large-amplitude portion of the forcing function is within the frequency range which, for the small amplitude used, is within the visual capability with zero phase lag. It therefore seems natural that the pilot will use the higher-resolution, zero-phase-lag visual information of the heads-up visual cases to increase his gain and thereby reduce the closed-loop phase-angle lag at least over a frequency range up

to 0.4 cps to 0.6 cps. This suggestion is considered to be the reason for the increased amplitude ratio for visual flight over IFR either ground or flight that is shown in figures 18(a) to 18(c) for frequencies up to at least 0.6 cps.

The difference in phase angle in Y_p for the A-2 flight and A-2* flight cases at and above 0.6 cps may indicate that for the visual flight case the pilot is able to reduce his transport time delay. This reduction may be attributed to lead from vestibular-sensed motion inputs, because the effectiveness of the eye diminishes as frequency increases and because for constant-amplitude motion the associated acceleration increases with frequency. However, the lead may still come from the visual system because the eye is still a good sensor over the frequency range of the forcing function used in this experiment. It appears from a comparison of phase-angle data among the T-33 experiments and the contact-analog experiment that the type of visual presentation does affect the pilot's phase angle at higher frequencies. However, more work in this area is needed before the suggestions made can be completely accepted as the explanation of the data.

Difference in K_p

From a study of all the T-33 $|Y_p|$ and $|Y_pY_c|$ data, it is noted that pilot A generally used a higher gain than the other pilots used. It is suggested that this tendency of pilot A is the major contribution to the significant difference among the pilots that occurs in the results of the analysis of variance as shown in table II. However, the data of all three pilots tend to coalesce and be most similar in or slightly above the frequency region of unity gain crossover for Y_pY_c. This is perhaps the most important characteristic displayed in the variance shown in table II, wherein the pilots are not significantly different in the region of 0.64 cps. However, there is a tendency for the pilots to be different at 0.4 cps, which can still be within the crossover region.

From the contact-analog data the tendency for pilot A to use larger gain than the other pilots used is not evident. However, except for the divergent $\frac{K}{s(s - \frac{1}{T})}$ configuration, the pilots all tended to use a larger gain in the contact analog than in the T-33 IFR configurations, either ground or flight, especially for frequencies below 0.65 cps.

The Stationarity Assumption

The time-varying data presented in figure 16 indicate that pilot A, for the one run analyzed, is rather consistent. It may therefore be concluded that there is little nonstationarity exhibited in the range of periods from 10 seconds to 90 seconds. This conclusion is based on a consideration of all the step responses except the first, which appears to be anomalous. The first step response may be traced to either anomalous behavior of the pilot or to improper initialization of the model. The limited scope of this investigation precluded detailed investigation of this peculiarity. The pilot model for this analysis was composed of seven poles and six zeros. The poles ranged from 0.25 radian/second to 16 radians/second.

Because the digital data available for analysis by the time-varying technique were limited to a maximum of eight data points per second, a pole of high enough frequency to define the pilots' reaction times could not legitimately be included in the model. This limitation is probably the reason that a definite pilot reaction time is not displayed in the step responses of figure 16.

The normalized integral square error (NISE) figure of merit of 18.39 expresses the fact that the output of the model, for the same input as the pilot had, accounts for 81.61 percent of the variance of the pilot's output. A comparison of the "model output" and the pilot's "stick output" which are included in figure 16 indicates that the wave forms of the two outputs are very similar. A point-by-point comparison of the two outputs is included in the figure as the "error (stick minus model)" trace, which is the arithmetic difference between the two output traces. The "error display" trace is the input to the pilot and to the model.

Analysis of Variance

The results of the analysis of variance performed on the T-33 ground simulator data are shown in table II.

TABLE II
ANALYSIS-OF-VARIANCE RESULTS FOR
T-33 GROUND-BASED MEASUREMENTS

		Frequency, cps				
		0.0625	0.237	0.404	0.642	1.20
Configurations	$\lvert Y_p \rvert$	(a)	(a)	(a)	---	(a)
	$\lvert Y_p Y_c \rvert$	(a)	(a)	(a)	(a)	---
Pilots	$\lvert Y_p \rvert$	(b)	(a)	(a)	---	(a)
	$\lvert Y_p Y_c \rvert$	(c)	(a)	(a)	(c)	---
Interaction	$\lvert Y_p \rvert$	(c)	(a)	(a)	---	(b)
	$\lvert Y_p Y_c \rvert$	(c)	(b)	(b)	(b)	---

(a) Significant at a level very much smaller than 1-percent level
(b) Significant at the 1-percent level
(c) Not significant
---No test made

As expected, a significant difference due to configuration was found. Although there were no significant differences among the pilots at a frequency of 0.64 cps, there were differences at the other frequencies. It is believed that these differences resulted primarily from the consistent differences in the gain used by pilot A in the T-33 tests, as compared with pilots B and C. Further, the nonsignificant difference among the pilots at 0.64 cps is another indication of the often-stated characteristic that pilots tend to behave alike in the region of crossover.

In summary, it can be stated that the similarity exhibited among the pilots in their adaptation to each controlled element strengthens the potential of correlating measured transfer characteristics of the pilot with his verbal assessments and rating of handling qualities. Caution is recommended in interpreting this conclusion because meaningful, mission-oriented tasks usually involve multivariable, multicontrol roles for the pilot, whereas this experiment concentrated on a single variable, single control task. Appreciable research effort must be expended in both theoretical and experimental areas of the multivariable, multicontrol problem to extend the techniques of this program to the broad area of handling-qualities research.

CONCLUSIONS

Pilot transfer characteristics for three pilots were measured in flight and in ground-based simulators. The flight measurements were obtained with a T-33 variable-stability airplane. Ground measurements were obtained with the T-33 and a general-purpose simulator which used a contact-analog color display. Three different computation techniques were used to obtain the pilot transfer characteristics. Except for one unstable configuration, the controlled-element dynamics were easy to fly. In addition, the task was compensatory tracking in roll for which the bank-angle disturbances were small and only aileron control was used to maintain zero bank angle. Within these limitations the following general conclusions can be made:

1. The pilot transfer characteristics indicated that pilot behavior in flight was similar to pilot behavior in a ground simulator for this task. For the multiple-degree-of-freedom configuration, the fixed-base ground visual data were a better approximation to inflight visual data for all three pilots than either IFR ground data or IFR flight data. This result was especially evident for two of the pilots and indicated that, for the task investigated, more reliable results can be obtained in ground-based simulators if the visual display provided is compatible with the flight situation being simulated. There was a significant tendency for the pilots to use a higher gain for the visual ground and flight cases than for either ground or flight IFR. For the higher frequency range of the data, the adaptations the pilots made appeared to be somewhat individualistic.

2. Limited examination of the data indicated that for the "good" airplane controlled element, the pilot exhibited relatively constant dynamic behavior over at least 100 seconds of a 4-minute tracking run. Therefore, the stationarity assumption of the data-analysis technique appeared to be substantiated.

3. Often, at the lowest and the highest frequencies of the forcing-function input, there appeared to be insufficient power to accurately measure the pilot transfer characteristic for the easily flown controlled elements. At the other frequencies of the forcing function, consistently satisfactory data were extracted.

4. Variations of pilot describing function with different controlled elements were obtained that compared favorably with similar variations in controlled element found in other experiments by other investigators.

5. The flight data showed a consistency that was compatible with the ground-based simulator data. The variance of the extracted transfer characteristics was approximately unchanged between T-33 ground and flight runs.

6. The results from the different computation techniques used were in excellent agreement; therefore, the results obtained should not be affected by the computation techniques involved.

7. Each of the three pilots exhibited basically similar adaptations to each of the controlled elements in the T-33 and the contact-analog simulator. Detailed differences were exhibited in the amplitude-ratio adaptation, particularly that shown by one of the pilots who used a consistently higher amplitude ratio than the other two pilots in the T-33 airplane.

8. The similarity exhibited among the pilots in their adaptation to each controlled element strengthens the potential of correlating measured transfer characteristics of the pilot with his verbal assessments and rating of handling qualities. Caution is recommended in interpreting this conclusion because meaningful, mission-oriented tasks usually involve multivariable, multicontrol roles for the pilot. Appreciable research effort must be expended in both the theoretical and experimental areas of the multivariable, multicontrol problem in order to extend the techniques of this program to the broad area of handling-qualities research.

Flight Research Center,
National Aeronautics and Space Administration,
Edwards, Calif., July 5, 1968,
125-19-06-06-24.

APPENDIX

DETAILS OF CAL AND FRC COMPUTER-PROGRAM VERIFICATION TECHNIQUES

CAL Spectral Program

Because the digital program for computing spectral densities had been developed for continuous-spectrum random signals, whereas the forcing function was actually a discrete sum-of-ten-sine-waves, there was some question of the accuracy of the spectral-density computations. The accuracy of the computations was investigated empirically in several ways. One way was to implement two known linear transfer functions in the forward loop of a unity feedback closed loop on an analog computer. The transfer functions used were $(1 + \frac{1}{s})$ and $\frac{K}{s}$. Sinusoidal frequency responses were obtained to verify each transfer function, and then closed-loop data were taken on FM tape for both the sum-of-ten-sine-waves input and a random input to the closed loop. By using the spectral-density technique, the closed-loop data were analyzed and compared with the transfer function $(1 + \frac{1}{s})$. For the sum-of-ten-sine-waves data, the results were excellent except at the two lowest frequencies of the input where the error signal power was extremely small. The results for the random input data were not as good as for the sinusoidal input data until considerably higher frequencies were reached. This effect is attributed to the spectral window of the computation process not being narrow enough to adequately resolve the power of the closely packed frequencies of the low-frequency end of the random input. A comparison of the results of the two sets of data indicated that the results for the sum-of-ten-sine-waves were reliable only at the discrete frequencies of input, whereas the random input results were equally as reliable for a specific frequency as they were for any frequency near the specific frequency. This difference in the results was not surprising because the computation procedure chooses, from each data trace, only those frequencies that are coherent with the input. Therefore, for the sum-of-ten-sine-waves input, results will be obtained only at the frequencies of the individual sine waves of the input. For the random input, meaningful results will be obtained at all frequencies at which the input power is sufficiently larger than that of the pilot's remnant.

Several playback and recording operations were involved in the production of the digital tape. As a result, the effective frequencies of the input signal varied slightly from run to run. The variations were on the order of 0.005 cps at the lower frequencies and sometimes as much as 0.2 cps at the highest frequency, enough to affect the results of the data analysis. Therefore, for each data run, the spectral content of the forcing function was obtained by determining Φ_{ii}. Then the required spectral-density ratios were computed at the effective frequencies of the input (i.e., frequencies where Φ_{ii} peaks) as determined from Φ_{ii}. It was possible to program the digital computer to compute Φ_{ii} for each run, search the record for the effective frequencies, and compute the desired ratios of cross-spectral densities only at these frequencies. To maintain a check on this system, a complete printout of all the spectral and cross-spectral density computations was obtained. The printouts were used to determine if a wild-appearing point in the computed ratios of cross-spectral densities was valid.

Some wild points did occur, always at the two lowest frequencies of the input and the highest frequency of the input. It was always found that the power in one of the cross-spectral densities of the pertinent ratio of spectral densities was so low that the computation of the spectral density was subject to error, probably due primarily to digital noise. Such points were deleted from the data.

A rigid internal check on the digital scale factors that resulted from the analog-to-digital conversion of the data on the FM tapes was maintained by having an accurate 1-volt step on the FM tapes at the beginning of each recorded run.

FRC Spectral Program

In the FRC computational technique, use is made of the known frequencies of the forcing function. However, because of the variation of frequencies in the recorded T-33 data, a scale shift of the known frequencies of the forcing function was required to obtain the effective frequencies of the data. To determine this scale factor, Φ_{ii} was computed for the higher frequency range, and the frequencies determined from this function were compared with the known frequencies of the forcing function. An average, constant scale factor was thus determined for each T-33 run. The run lengths were changed accordingly so that complete periods were analyzed. The tape recordings from the contact-analog runs did not require searching for the precise input frequencies because the digital tapes were recorded on line. Therefore, no tape-playback operations that could alter the frequencies were involved.

For the $\frac{K}{s}$ and $\frac{K}{s(s - \frac{1}{T})}$ configurations on the contact analog, the wrong signal for φ_A was inadvertently recorded during the contact-analog runs. To compute Y_c and $Y_p Y_c$ for these cases, φ_A was obtained by subtracting the error signal from the forcing-function signal in the digital program. This technique was also applied to some of the known A-2* cases to determine what, if any, differences occurred as a result of this computational procedure. There was little difference in the computed and measured φ_A; however, there was a significant difference in Y_c at the highest frequency. The gain of Y_c was consistently higher and the phase lag consistently lower than expected at this frequency. Many arithmetic operations are involved in computing Y_c and, apparently, small errors were additive.

REFERENCES

1. Tustin, A.: The Nature of the Operator's Response in Manual Control, and Its Implications for Controller Design. J. Inst. Elec. Engrs., vol. 94, Part IIA, no. 2, 1947, pp. 190-202.

2. Elkind, Jerome I.: Characteristics of Simple Manual Control Systems. Tech. Rep. No. 111, Mass. Inst. Technol., Lincoln Lab., April 6, 1956.

3. Hall, Ian A. M.: Effects of Controlled Element on the Human Pilot. Tech. Rep. 57-509 (ASTIA No. AD 130979), Wright Air Dev. Center, U.S. Air Force, Aug. 1958.

4. Eakin, G. J.; and Campbell, G. F.: Human Operator Transfer Function Investigation. Rep. No. TE-665-F-5, Cornell Aero. Lab., Inc., Oct. 1, 1957. (Available from ASTIA as AD 278 190.)

5. Seckel, Edward; Hall, Ian A. M.; McRuer, Duane T.; and Weir, David H.: Human Pilot Dynamic Response in Flight and Simulator. Tech. Rep. 57-520 (ASTIA No. AD 130988), Wright Air Dev. Center, U.S. Air Force, Aug. 1958.

6. McRuer, Duane; Graham, Dunstan; Krendel, Ezra; and Reisener, William, Jr.: Human Pilot Dynamics in Compensatory Systems. Theory, Models, and Experiments With Controlled Element and Forcing Function Variations. Tech. Rep. AFFDL-TR-65-15, Air Force Flight Dynamics Lab., Wright-Patterson Air Force Base, July 1965.

7. Smith, Harriet J.: Human Describing Functions Measured in Flight and on Simulators. Second Annual NASA - University Conference on Manual Control, NASA SP-128, 1966, pp. 279-290.

8. Key, David L.: A Functional Description and Working Data for the Variable-Stability System T-33 Airplane. Rep. No. TC-1921-F-2, Cornell Aero. Lab., Inc., Oct. 1965.

9. Meeker, J. I.: Evaluation of Lateral-Directional Handling Qualities of Piloted Re-entry Vehicles Utilizing Fixed-Base and In-Flight Evaluations. Cornell Aero. Lab., Inc. (NASA CR-778), 1967.

10. McRuer, Duane T.; and Krendel, Ezra S.: Dynamic Response of Human Operators. Tech. Rep. 56-524 (ASTIA No. AD-110693), Wright Air Dev. Center, U.S. Air Force, Oct. 1957.

11. Wierwille, Walter W.; and Gagne, Gilbert A.: A Theory for the Optimal Deterministic Characterization of the Time-Varying Dynamics of the Human Operator. Cornell Aero. Lab., Inc. (NASA CR-170), 1965.

12. Taylor, Lawrence W., Jr.: A Comparison of Human Response Modeling in the Time and Frequency Domains. Third Annual NASA - University Conference on Manual Control, NASA SP-144, 1967, pp. 137-153.

13. Meiry, Jacob L.: The Vestibular System and Human Dynamic Space Orientation. Mass. Inst. Technol. (NASA CR-628), 1966.

14. Webb, Paul, ed.: Bioastronautics Data Book. NASA SP-3006, 1964.

15. Jones, G. Melvill; and Drazin, D. H.: Oscillatory Motion in Flight. FRPC 1168, Flying Personnel Research Committee, Inst. of Aviation Medicine, RAF, Air Ministry, July 1961.

16. Derevyanks, Ye. A.; and Myl'nikov, V. G.: Biological Effects of Gravitational Acceleration. Voprosy Psikhologii (Questions of Psychology), vol. X, no. 3, May-June 1964 (Moscow), pp. 131-139. (Trans. available from OTS, U.S. Dept. Com. as JPRS 25,929.)

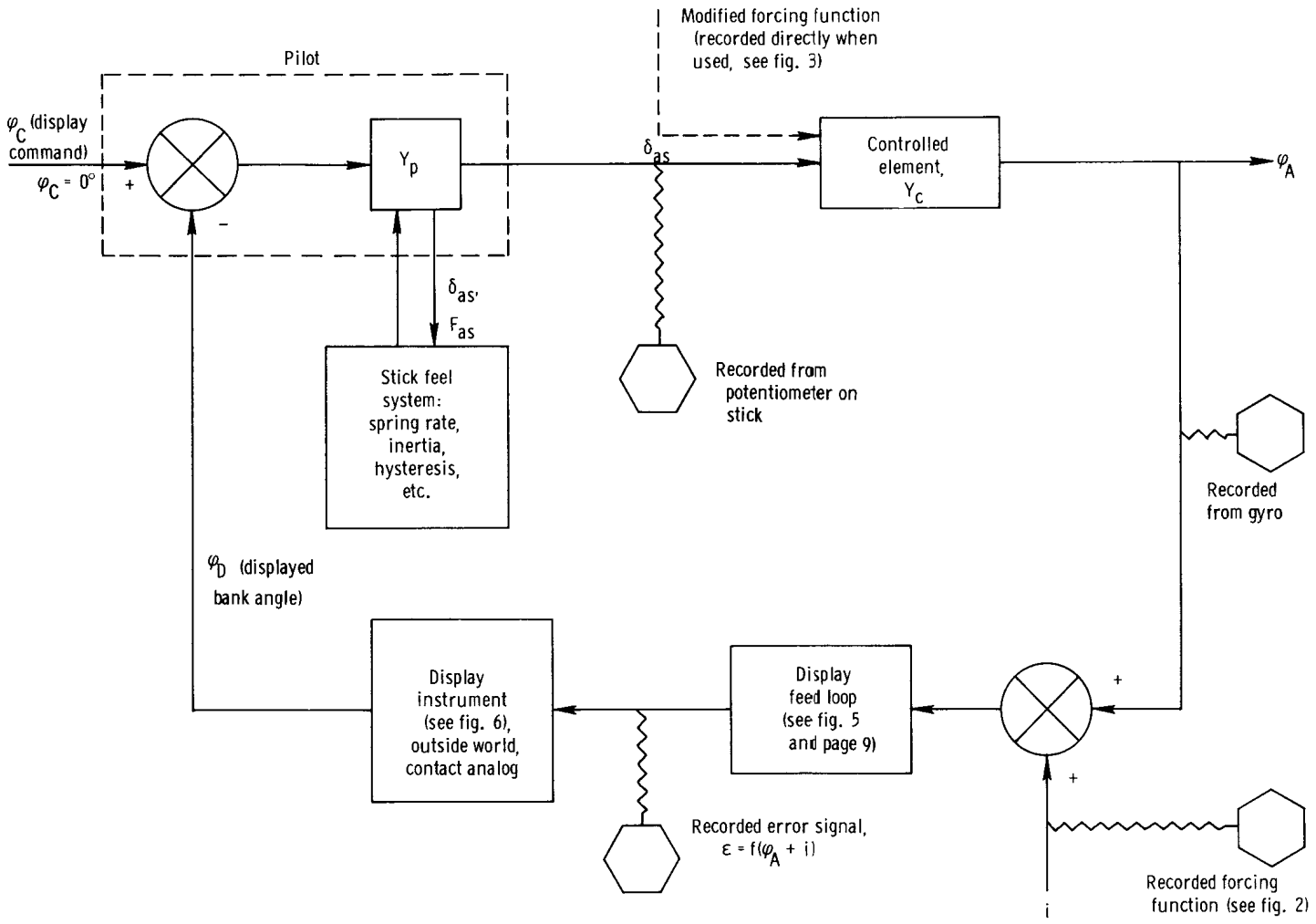

Figure 1. – General block diagram of the experiment.

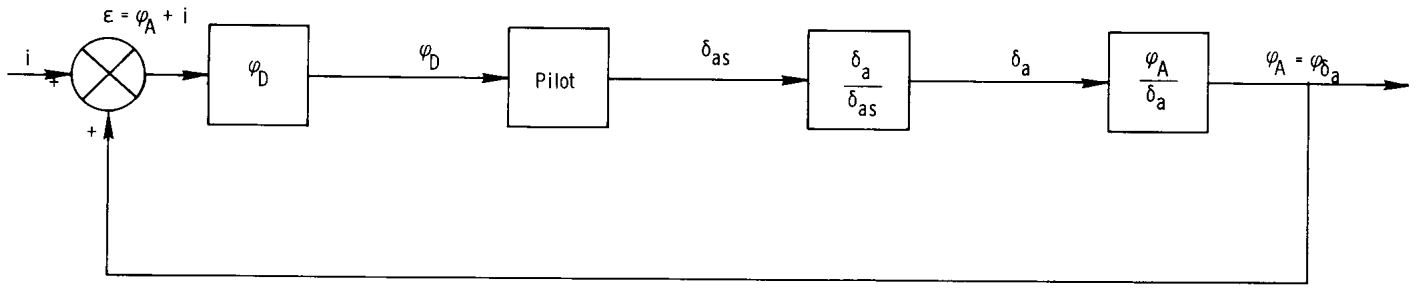

Figure 2. – Block diagram of compensatory tracking task with unshaped input i (for configuration A-2*, $\frac{K}{s}$, and $\frac{K}{s(s - \frac{1}{T})}$).

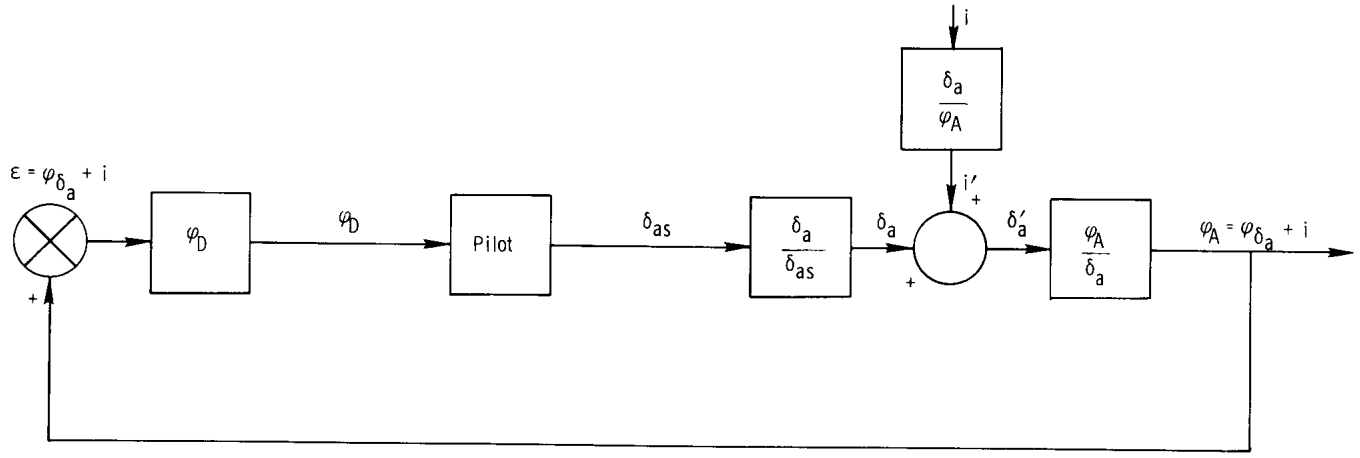

Figure 3. – Block diagram of compensatory tracking task with shaped input i′ (for configuration A-2).

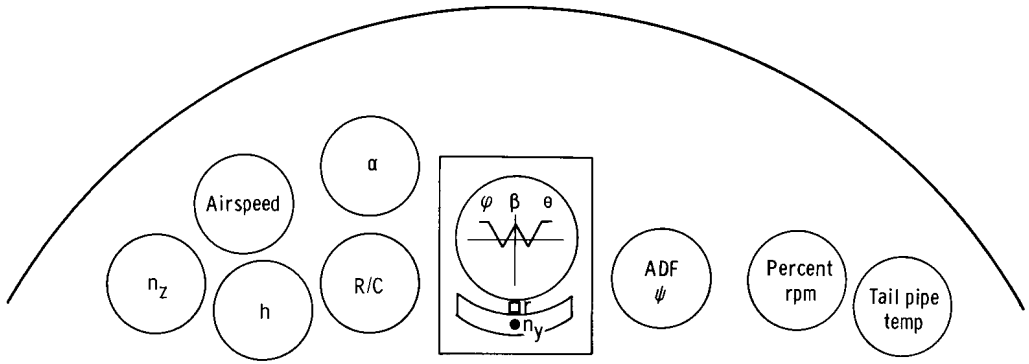

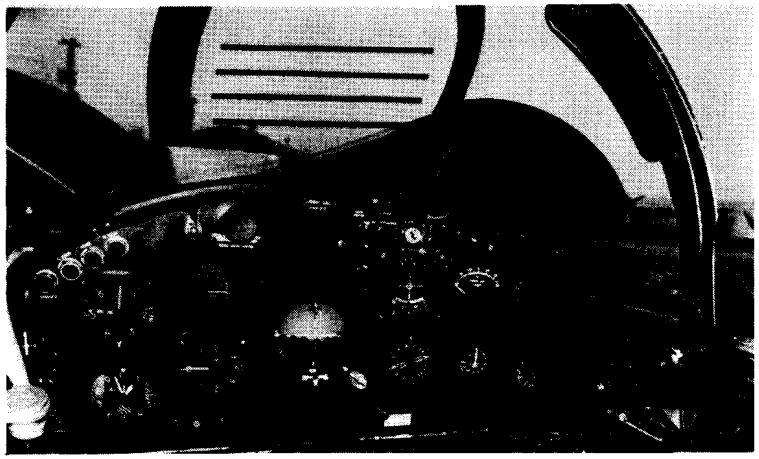

(a) In-flight simulator.

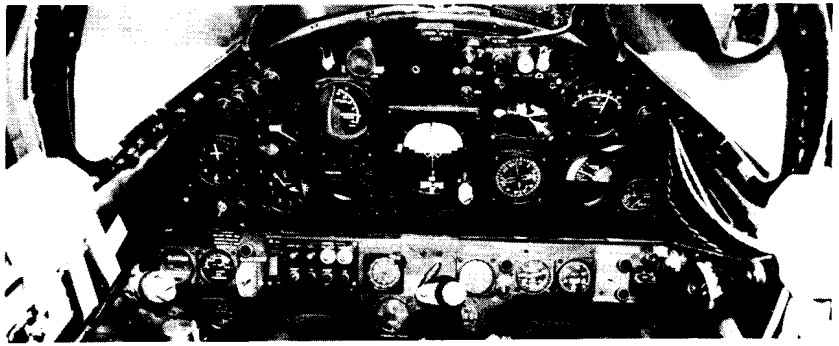

(b) Ground-based simulator.

Figure 4. – T-33 instrument displays.

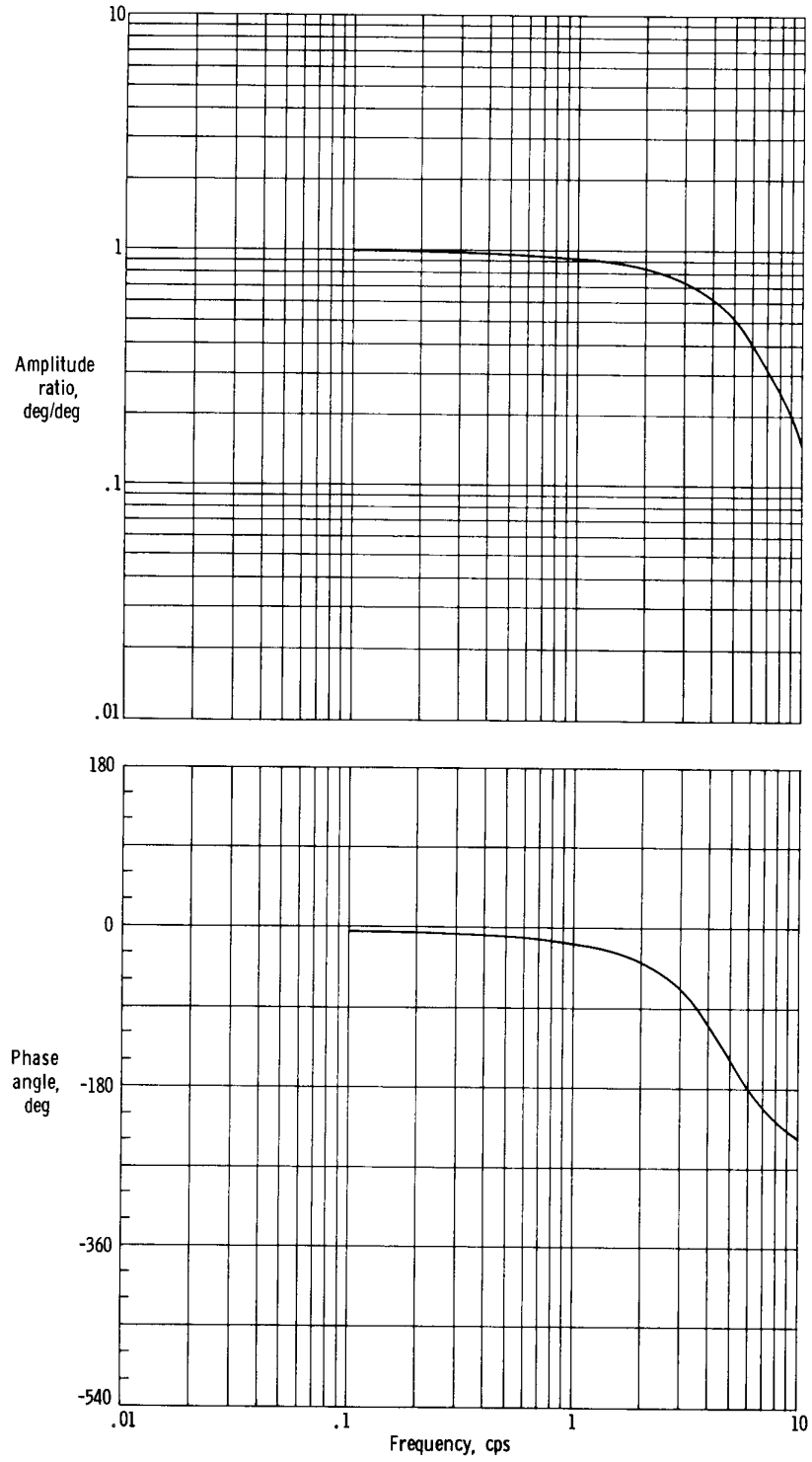

Figure 5. – Frequency response of bank-angle servo in computer interface equipment (T-33).

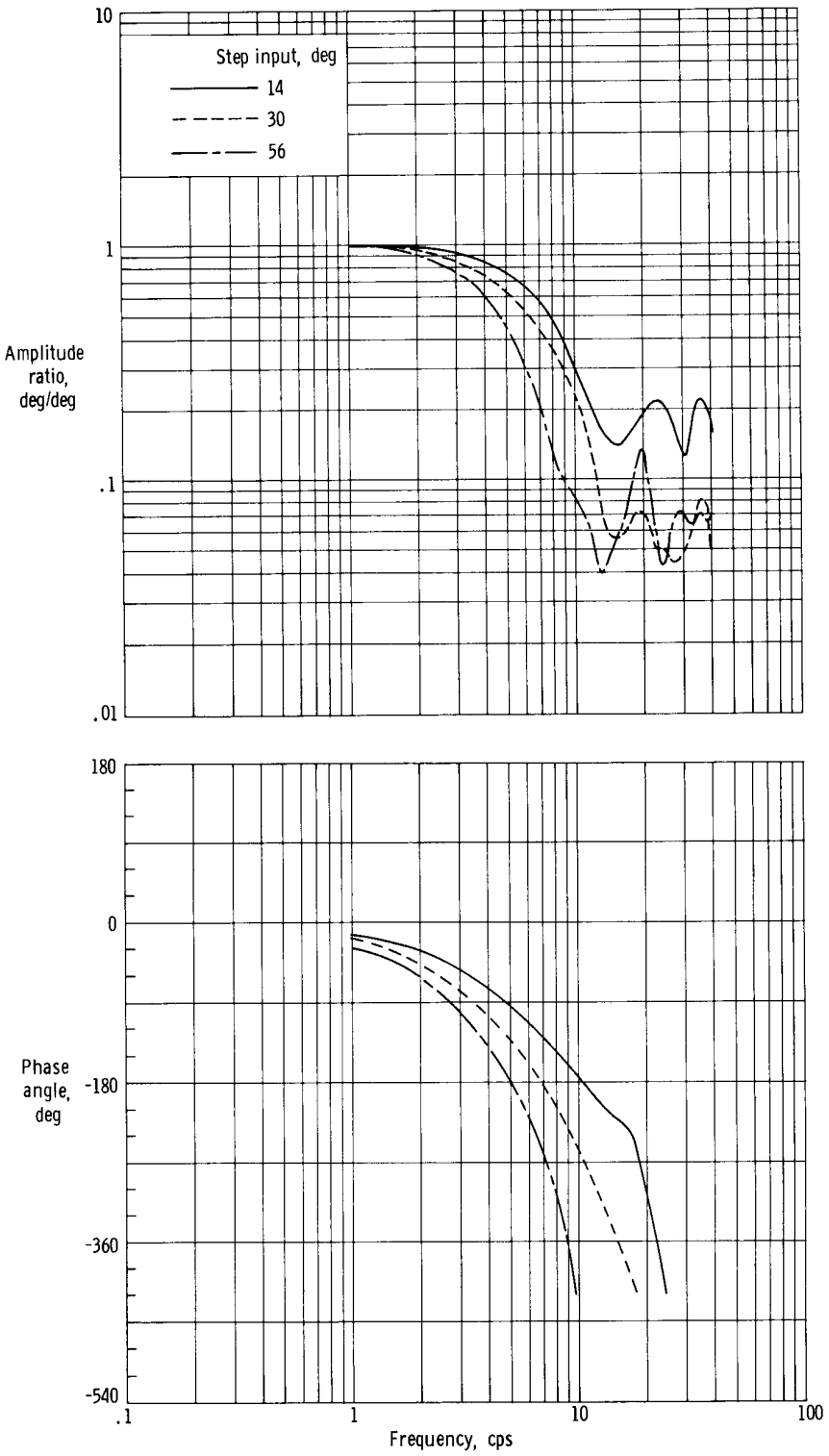

Figure 6. – Frequency response of T-33 bank-angle indicator.

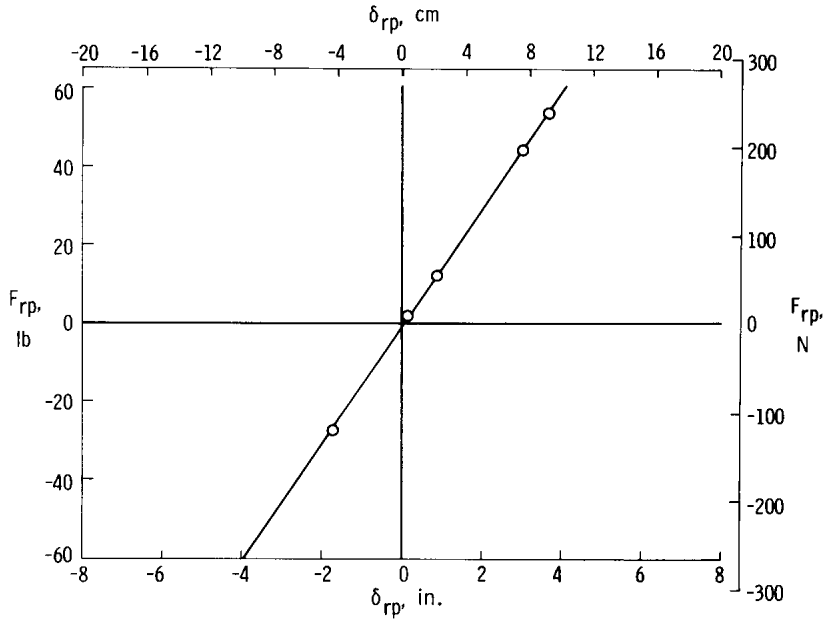

(a) Rudder pedal force.

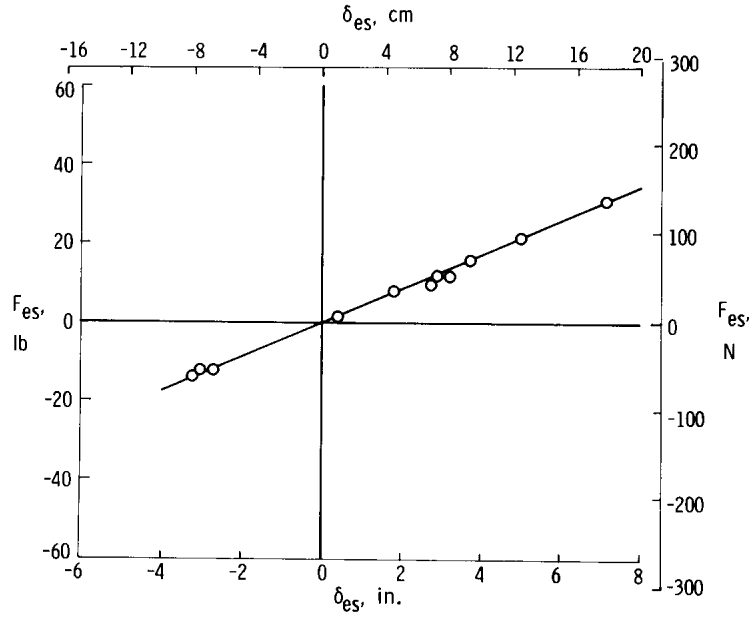

(b) Elevator stick force.

Figure 7. – T-33 rudder pedal force and elevator stick force as a function of displacement.

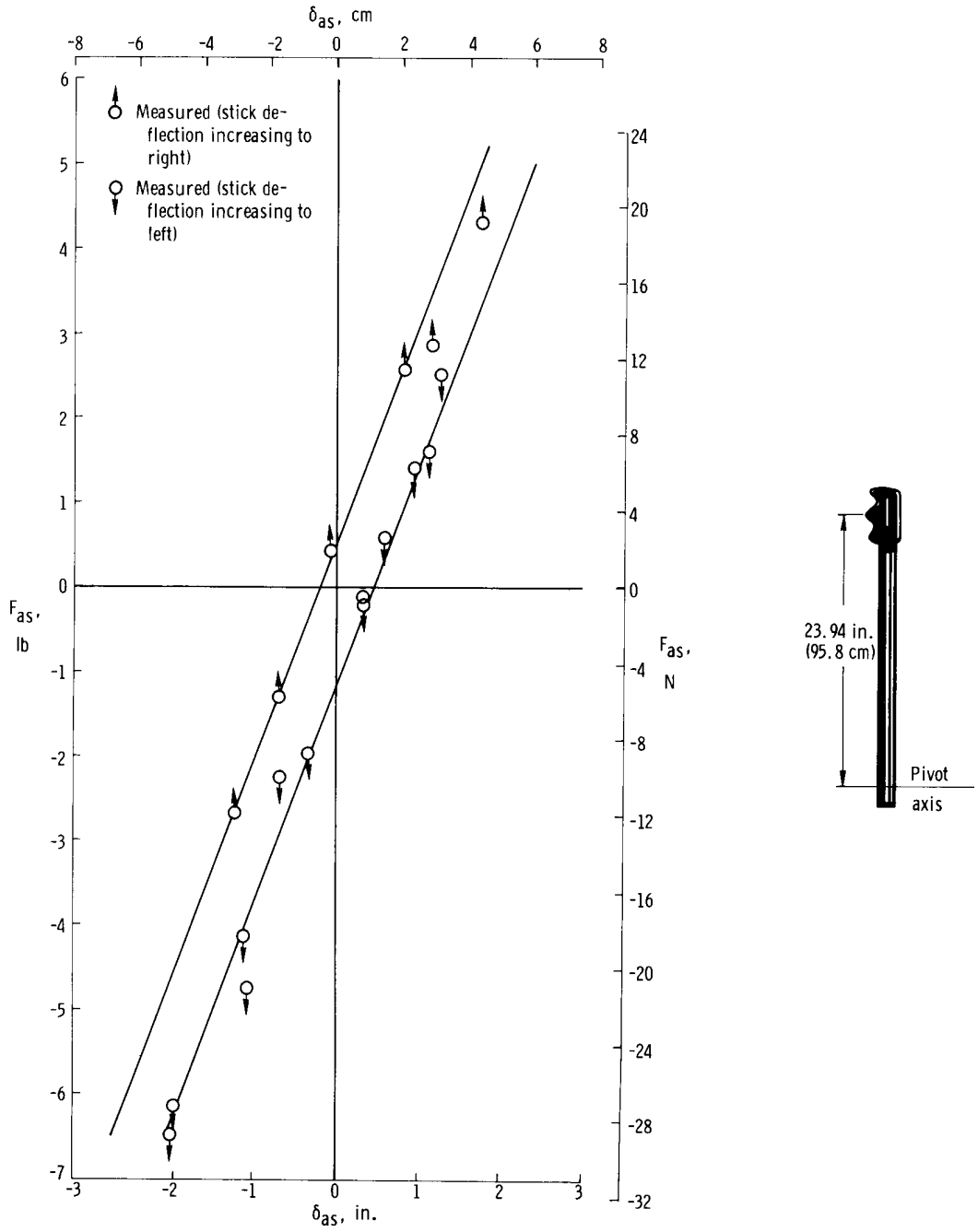

Figure 8. – Hysteresis loop of T-33 aileron stick force as a function of aileron displacement. $\frac{F_{as}}{\delta_{as}}$ = 2.5 lb/in. (4.4 N/cm).

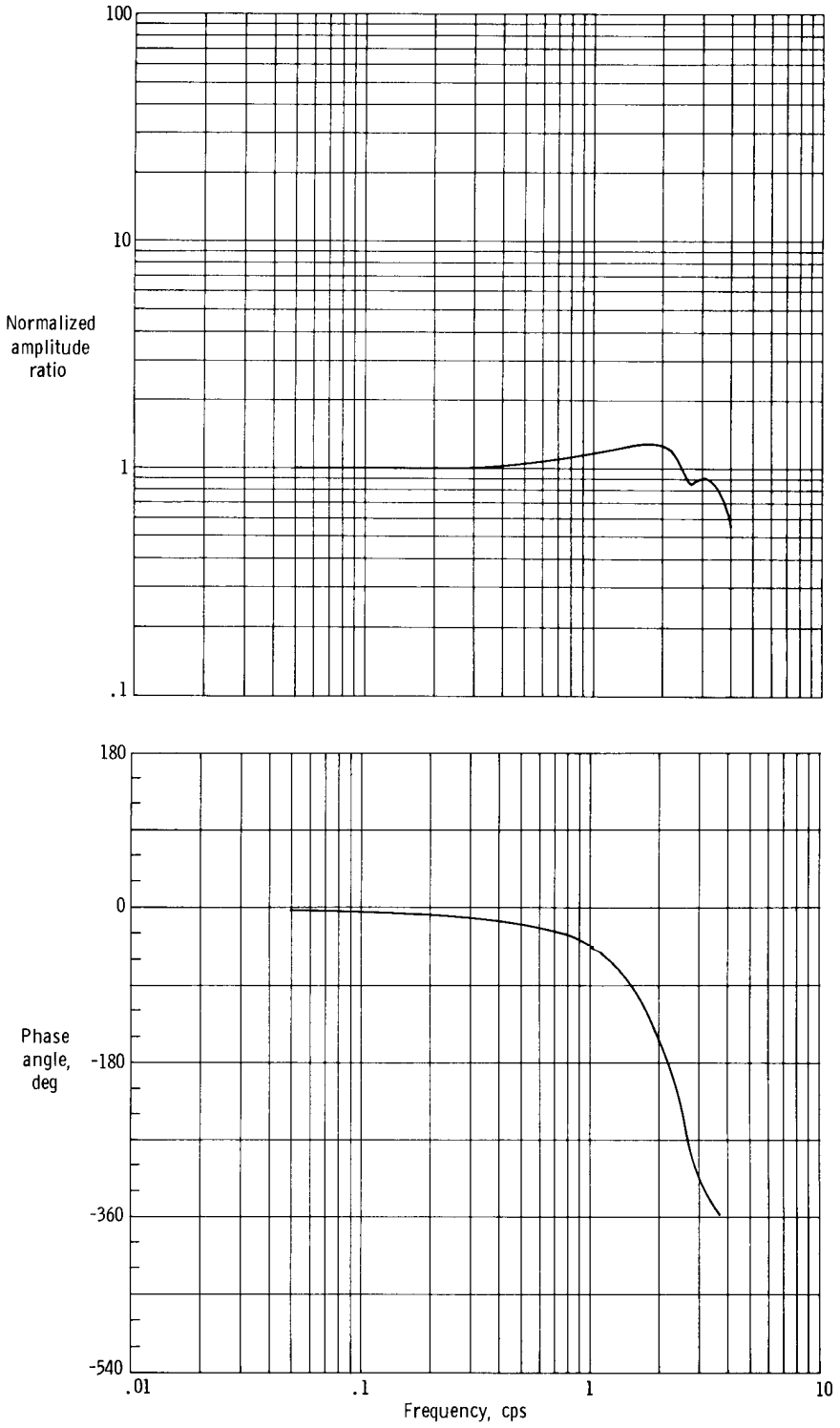

Figure 9. – T-33 aileron stick feel servo dynamics.

E-12544

Figure 10. – Contact-analog cockpit.

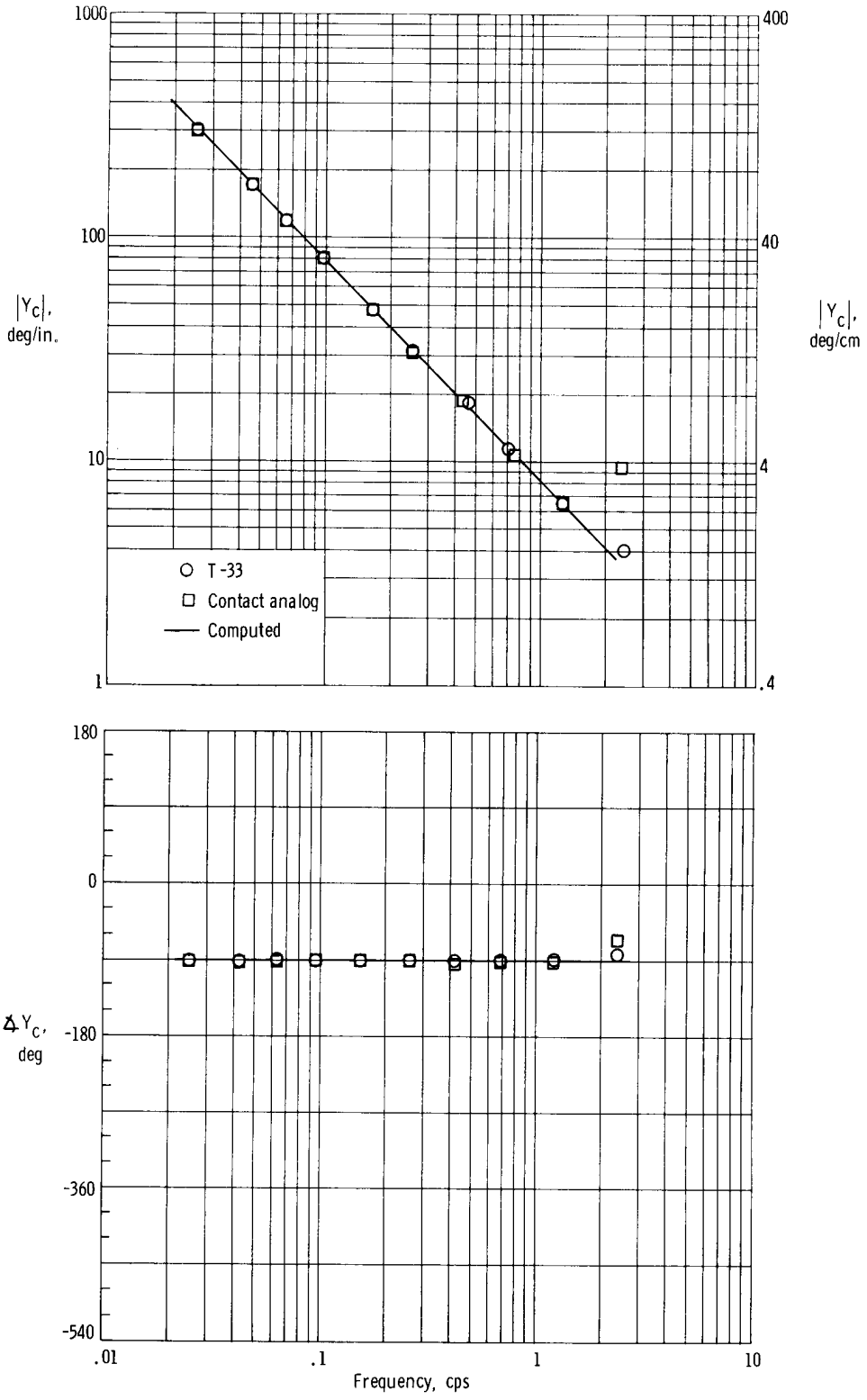

Figure 11. – Comparison of measured and computed Y_c for controlled element $\frac{K}{s}$.

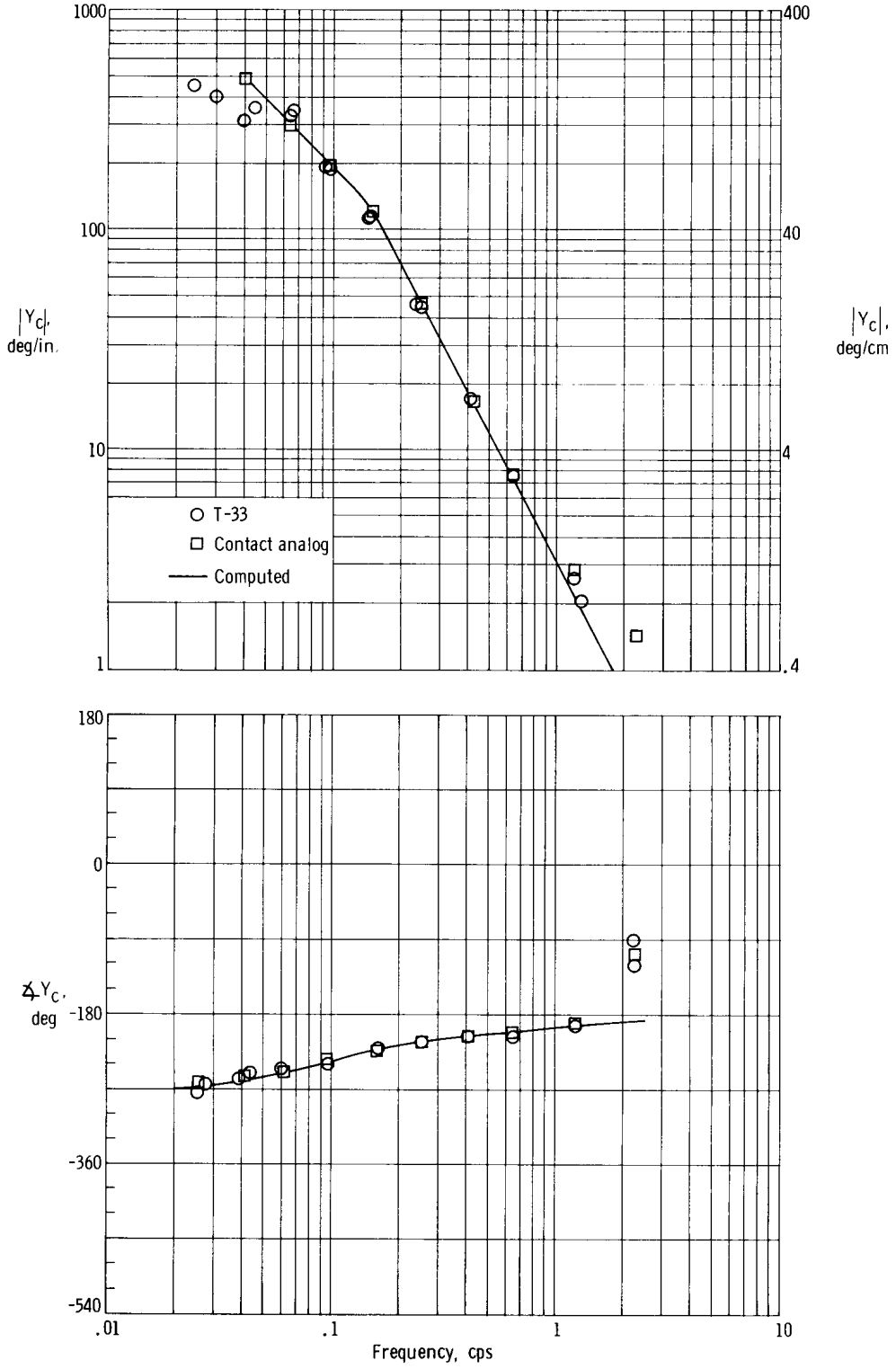

Figure 12. – Comparison of measured and computed Y_c for controlled element $\frac{K}{s(s - \frac{1}{T})}$.

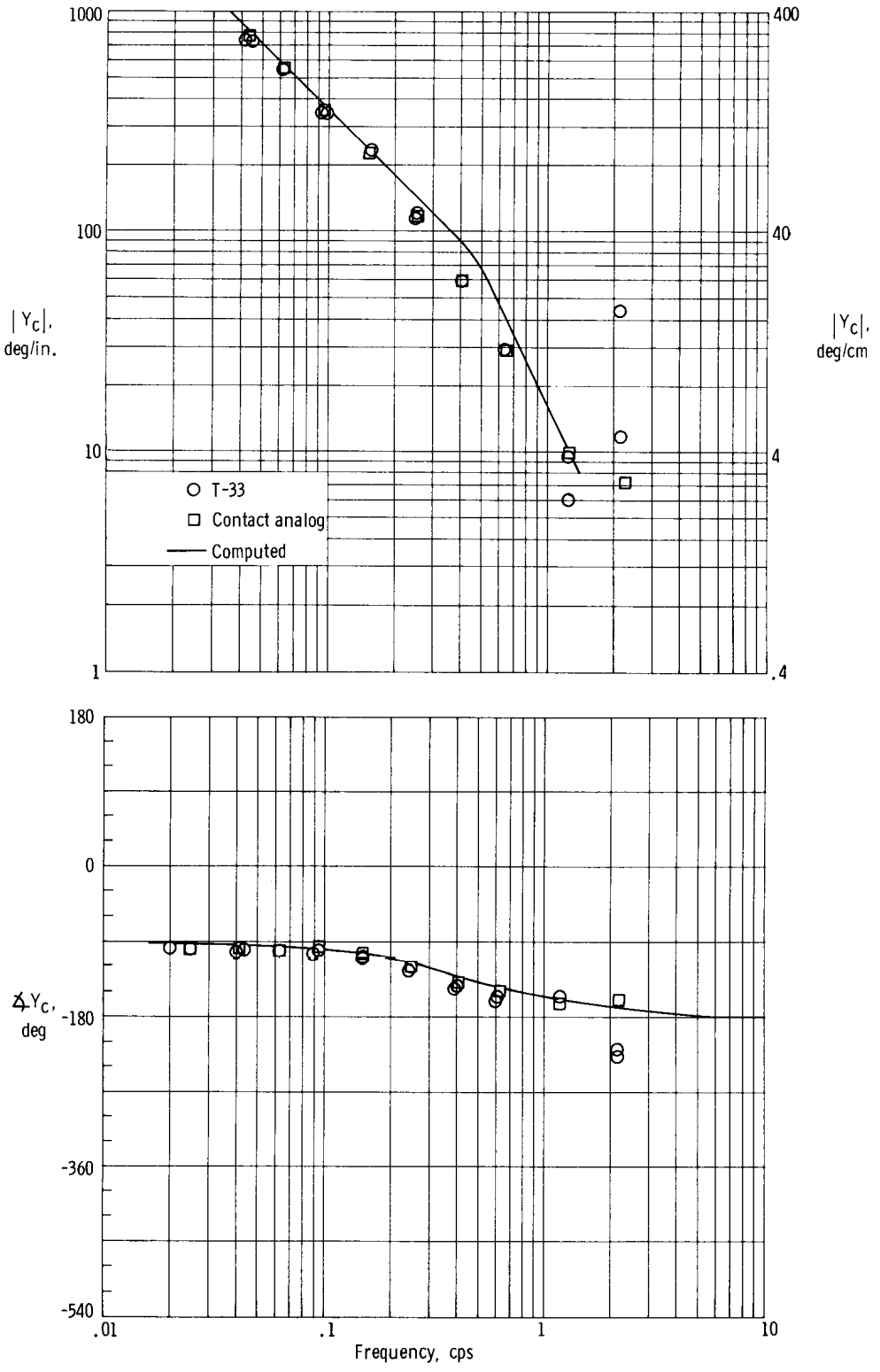

Figure 13. – Comparison of measured and computed Y_c for controlled element A-2*.

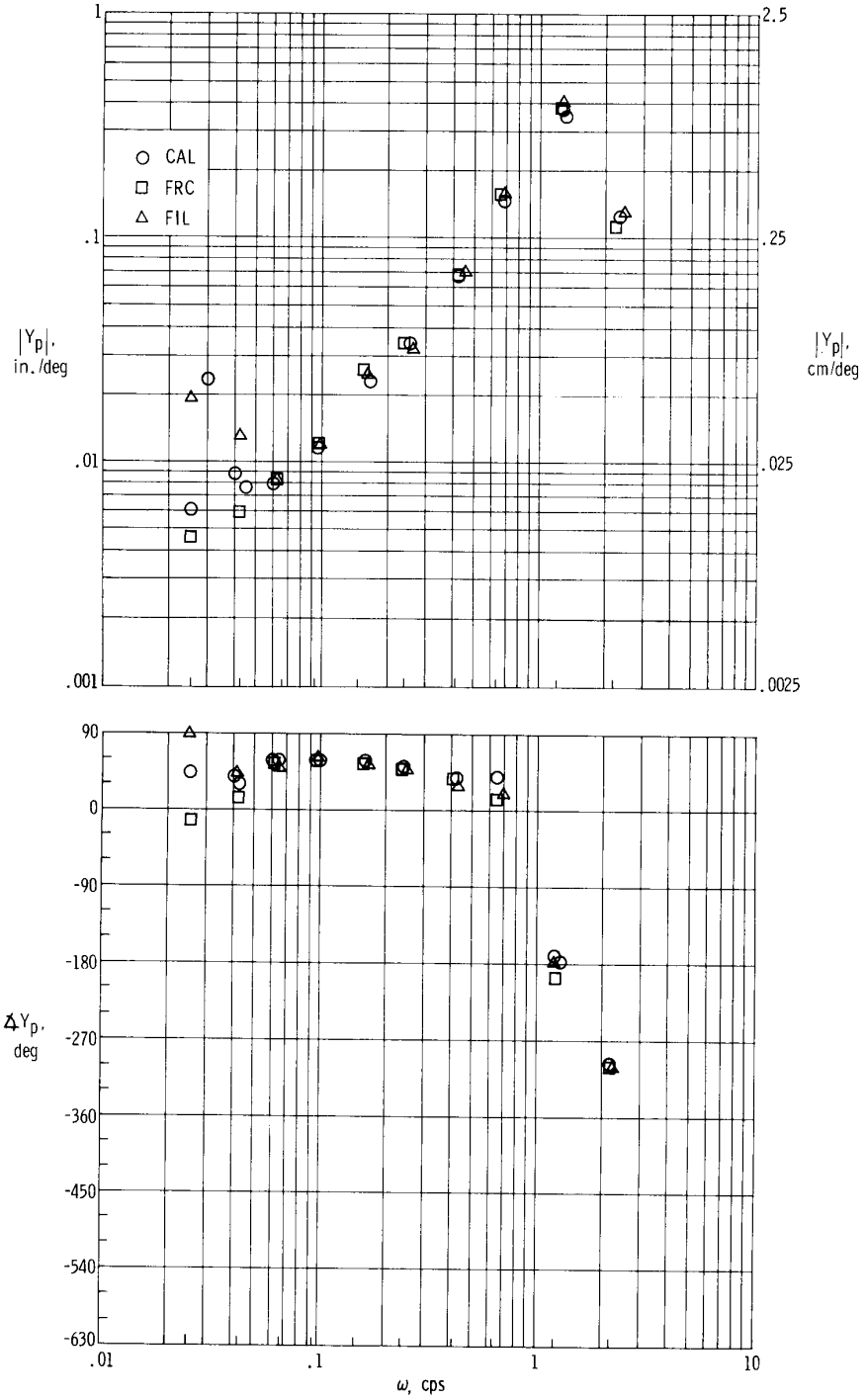

(a) Controlled element $\frac{K}{s(s - \frac{1}{T})}$, run 4.

Figure 14. – Comparison of pilot transfer characteristic Y_p from three different analyses for eight T-33 flight and ground runs.

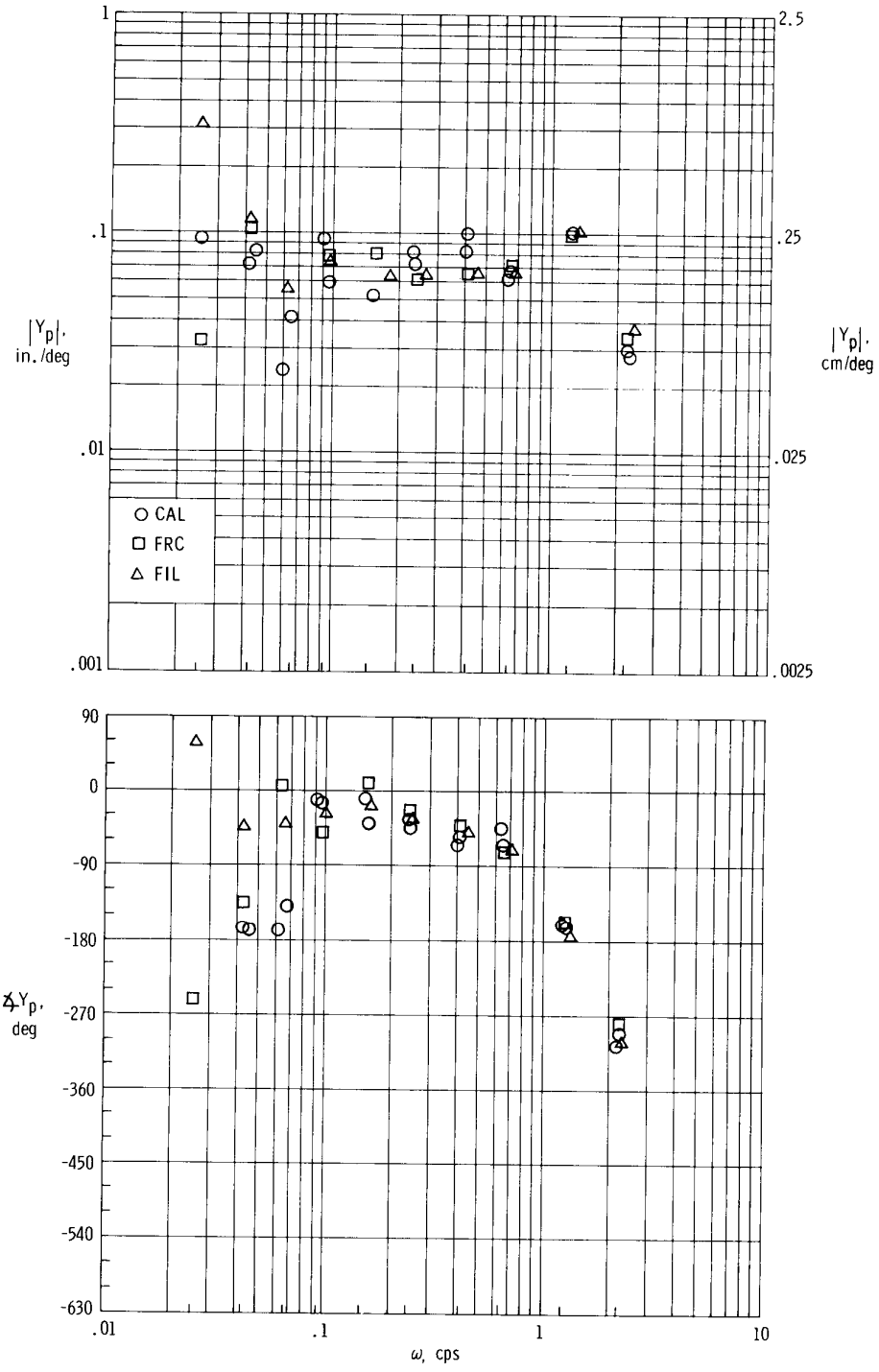

(b) Controlled element $\frac{K}{s}$, run 25.

Figure 14. – Continued.

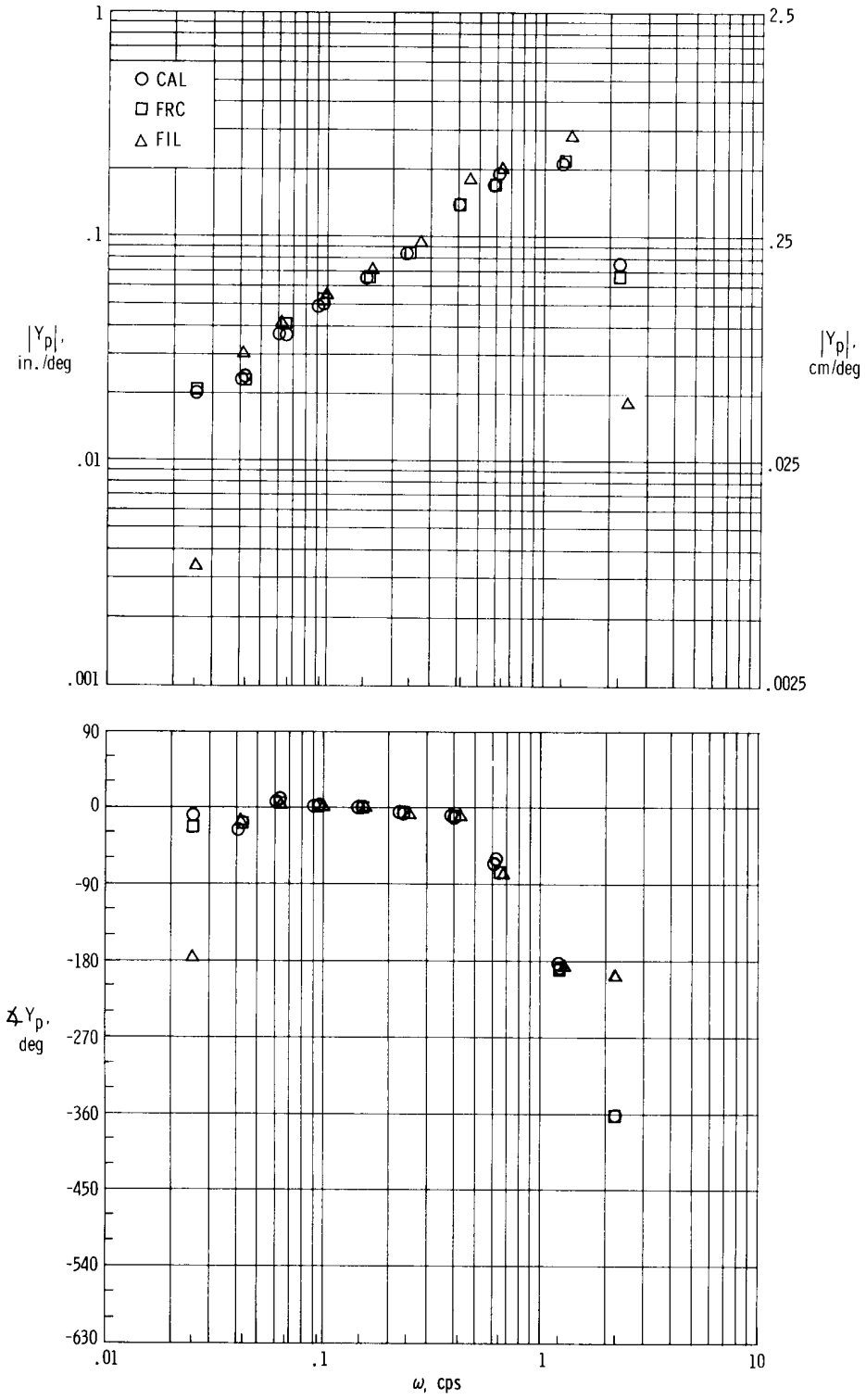

(c) Controlled element A-2 ground, run 39.

Figure 14. – Continued.

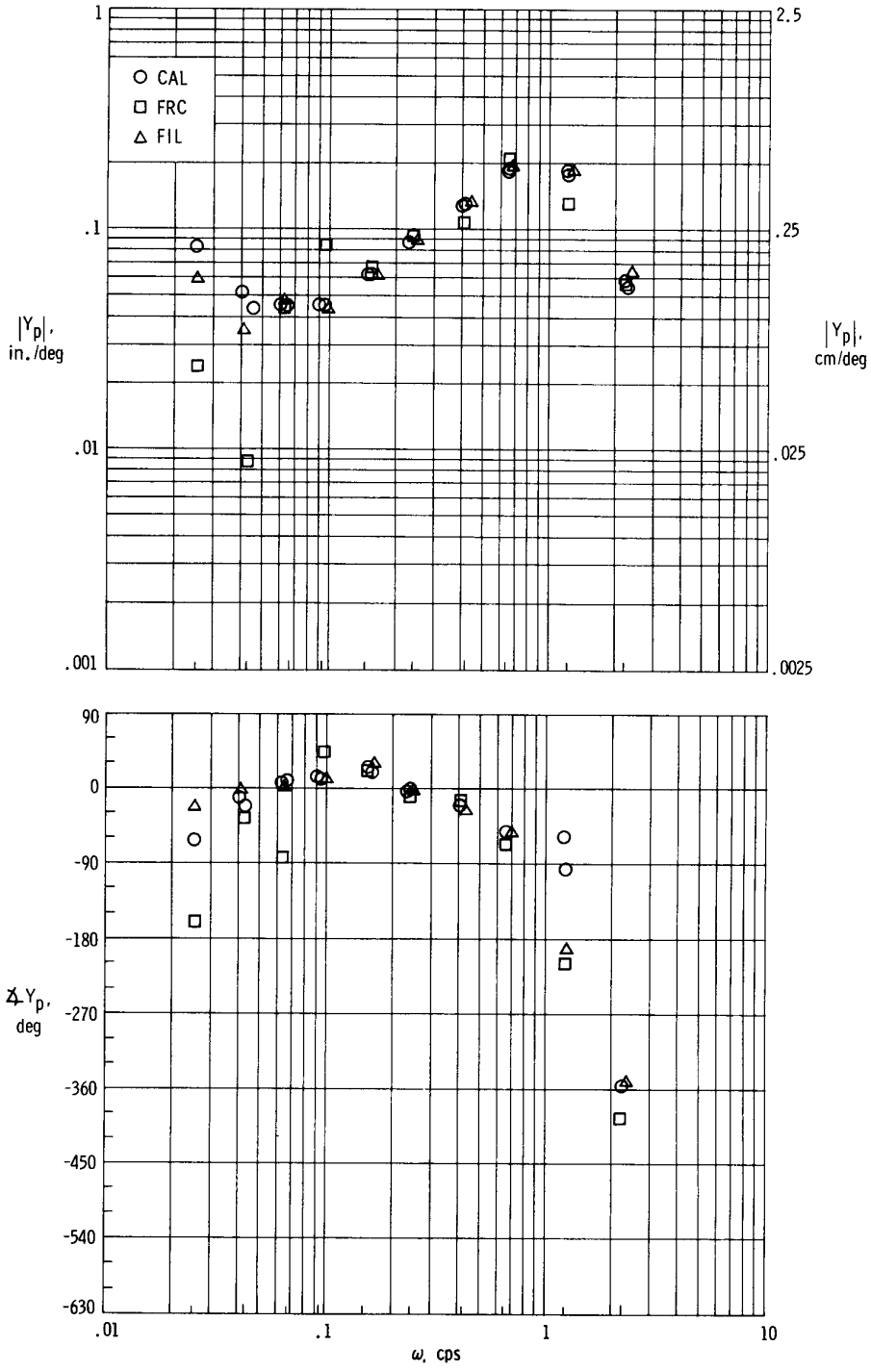

(d) Controlled element A-2* ground, run 60.

Figure 14. – Continued.

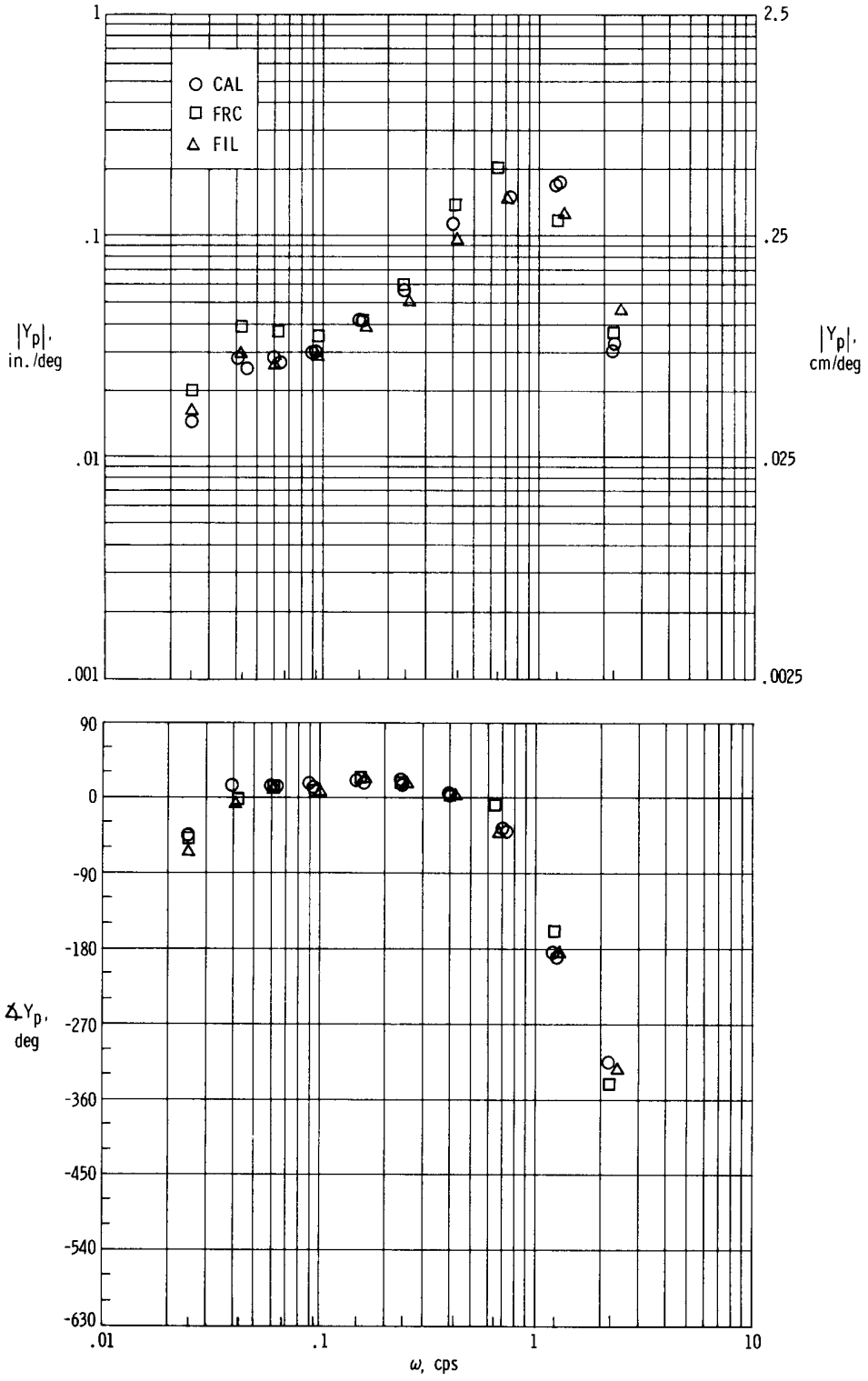

(e) Controlled element A-2* ground, run 69.

Figure 14. – Continued.

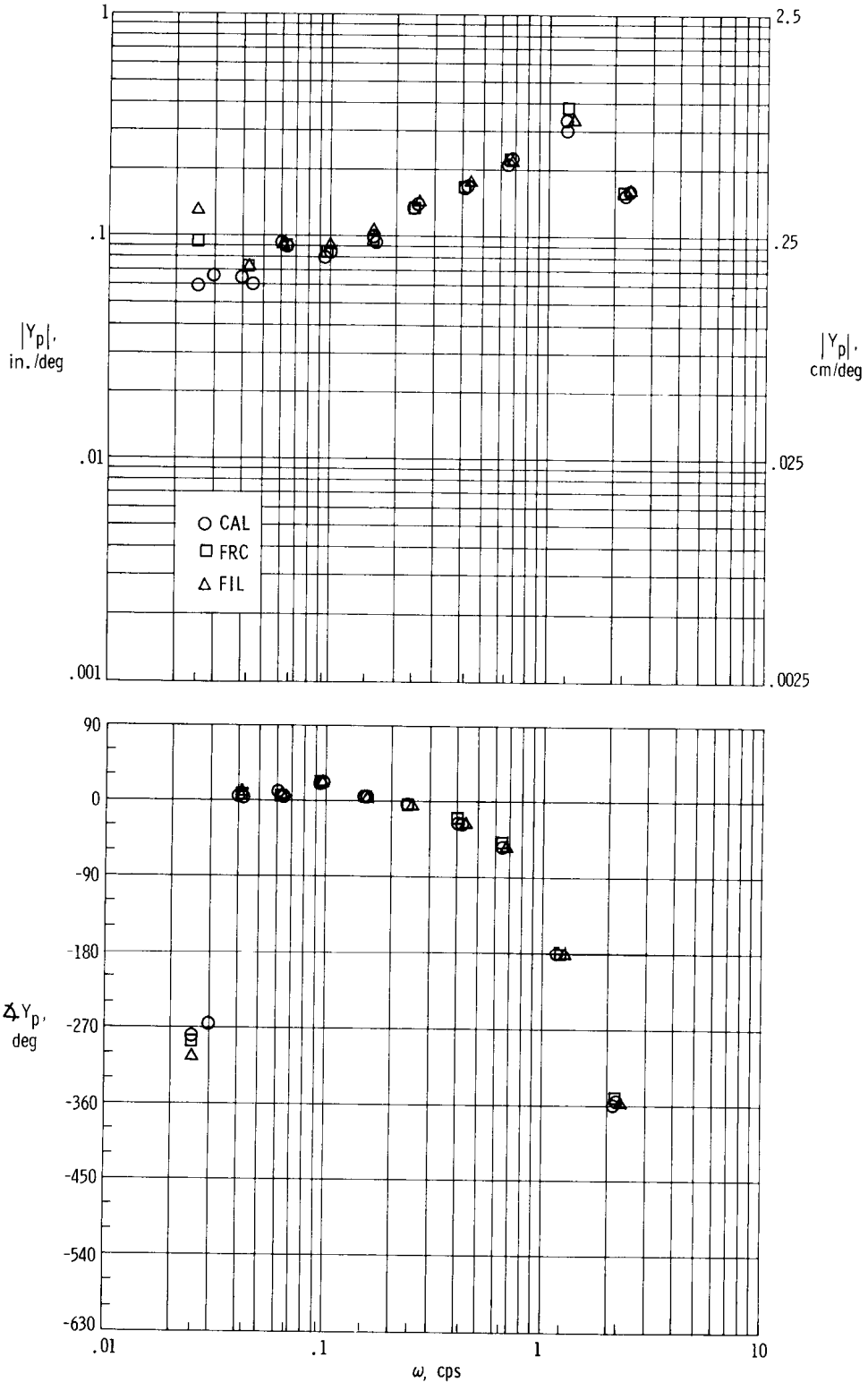

(f) Controlled element A-2* flight, run 90.

Figure 14. – Continued.

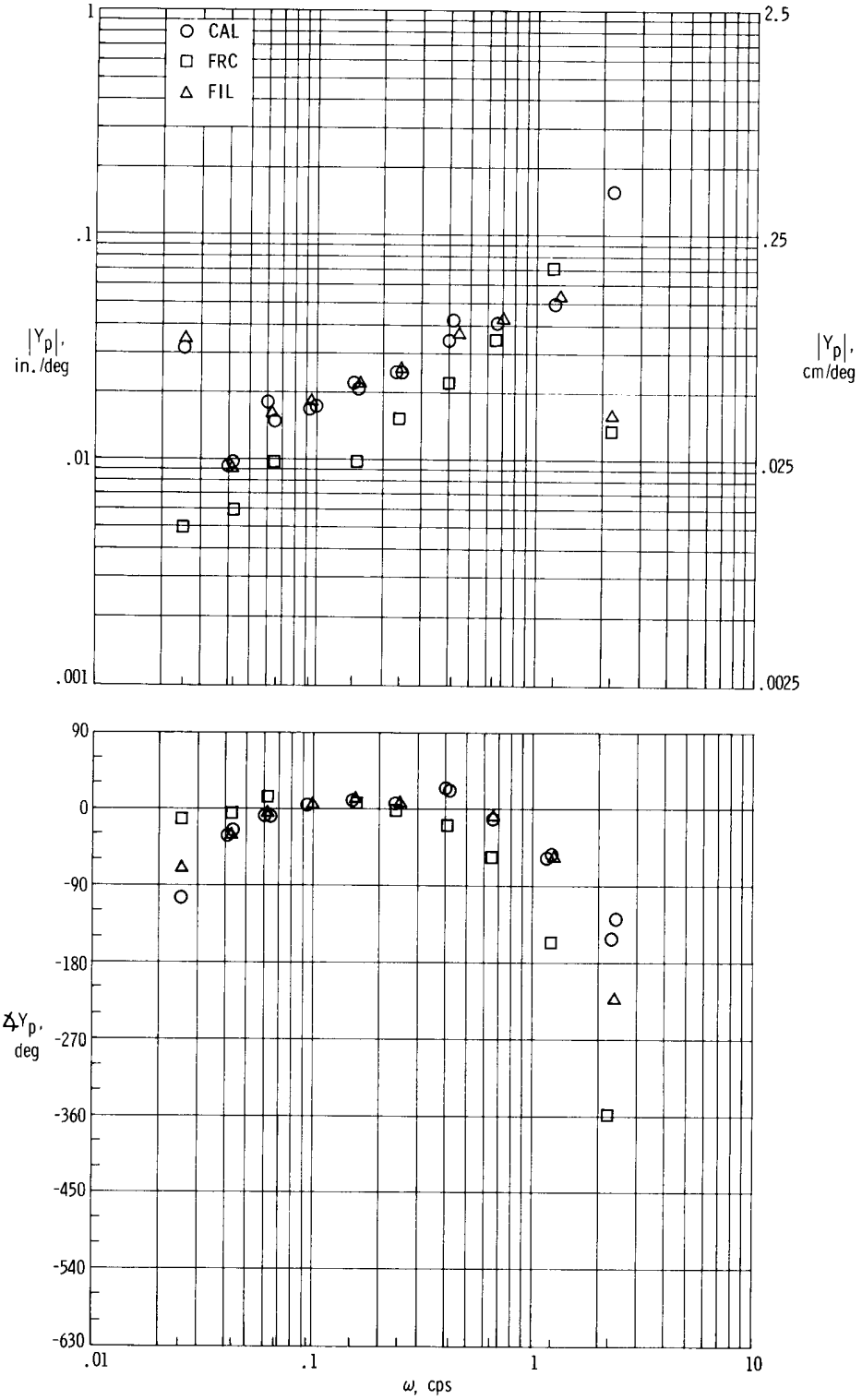

(g) Controlled element A-2 flight, run 97.

Figure 14. – Continued.

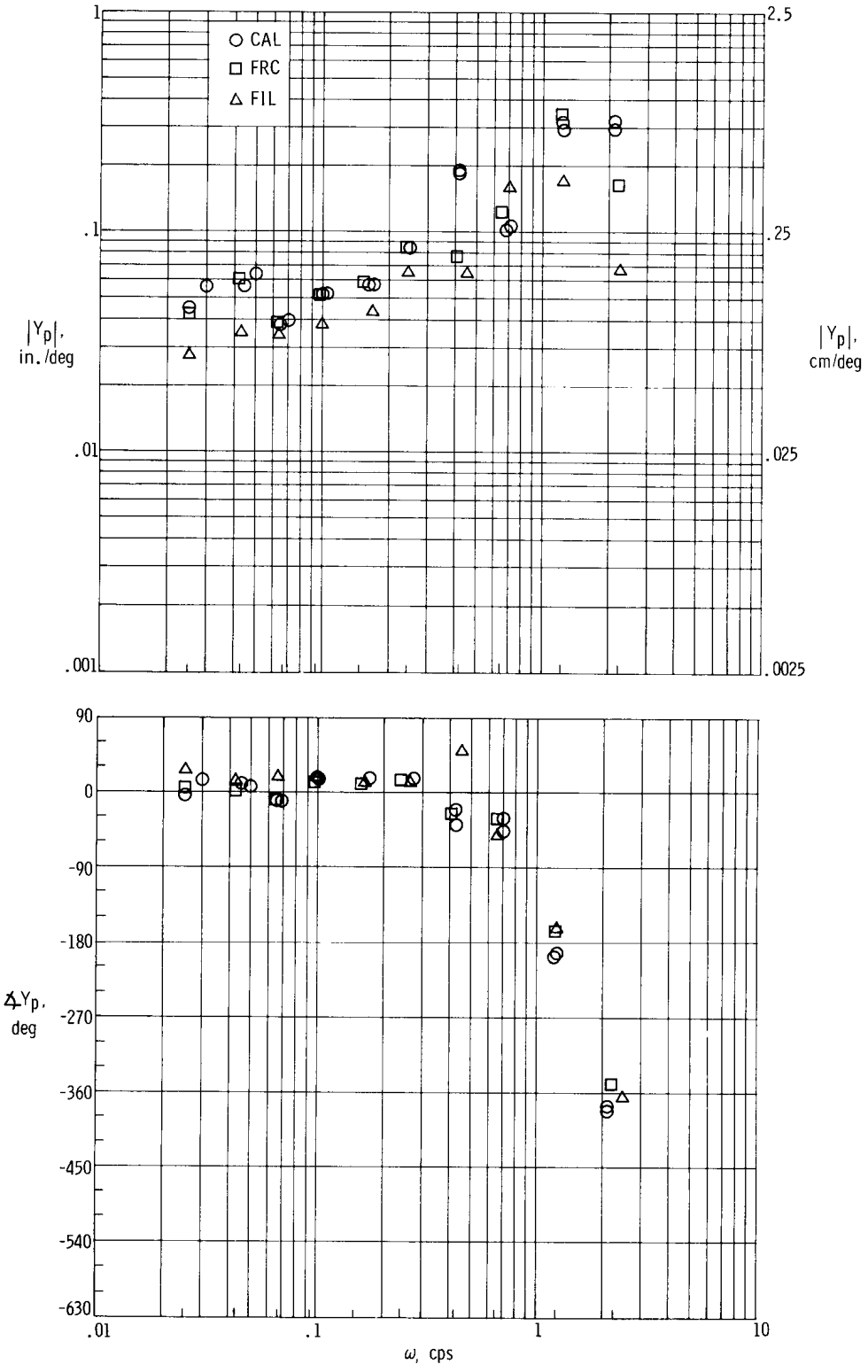

(h) Controlled element A-2 flight, run 118.

Figure 14. – Concluded.

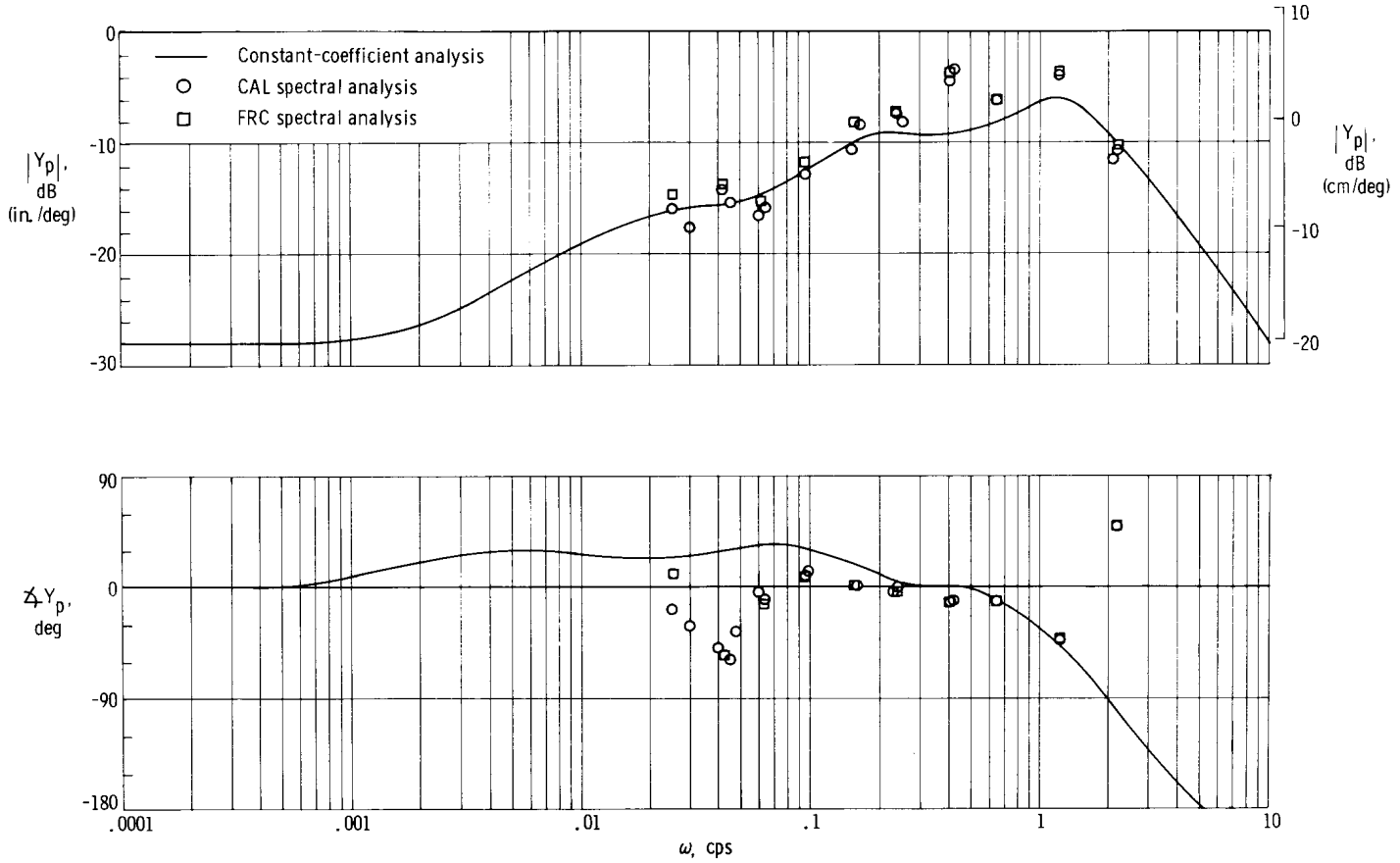

Figure 15. – Comparison of pilot transfer characteristic Y_p obtained from constant-coefficient analyses with those obtained from spectral analyses for controlled element A-2 flight, run 106.

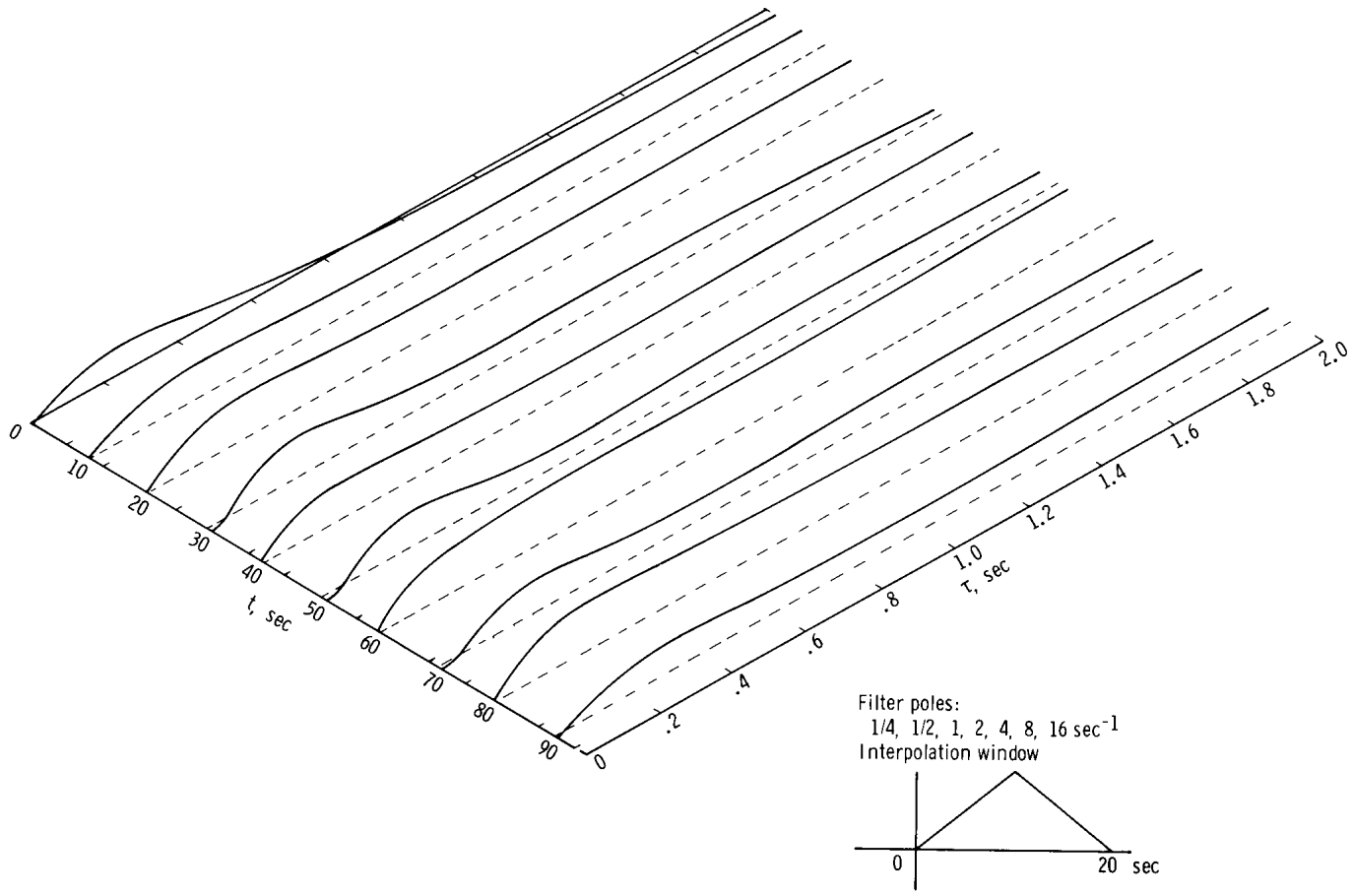

(a) Response of model to step input.

Figure 16. – Output of time varying pilot model.

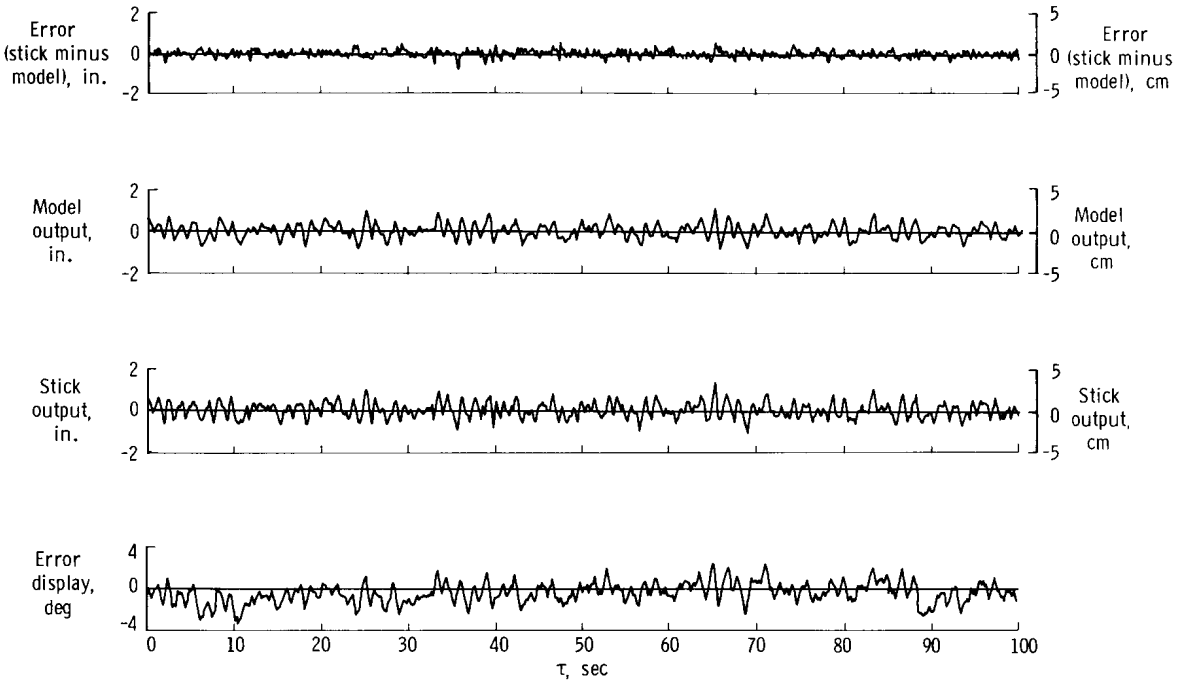

(b) Response of pilot and model to bank-angle disturbance.

Figure 16. – Concluded.

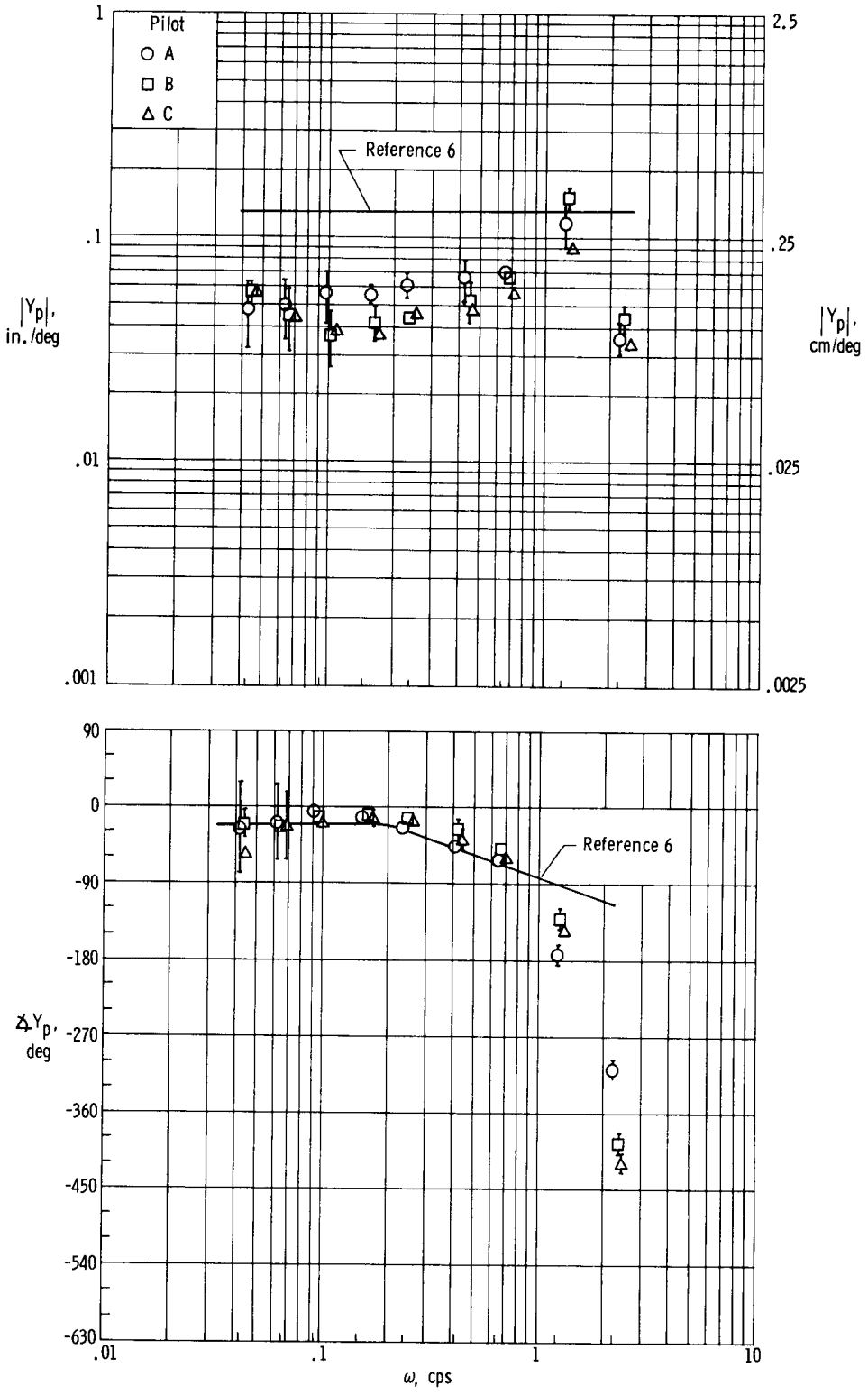

(a) Controlled element $\frac{K}{s}$, T-33 ground.

Figure 17. – Pilot transfer characteristic Y_p for different controlled elements and simulators.

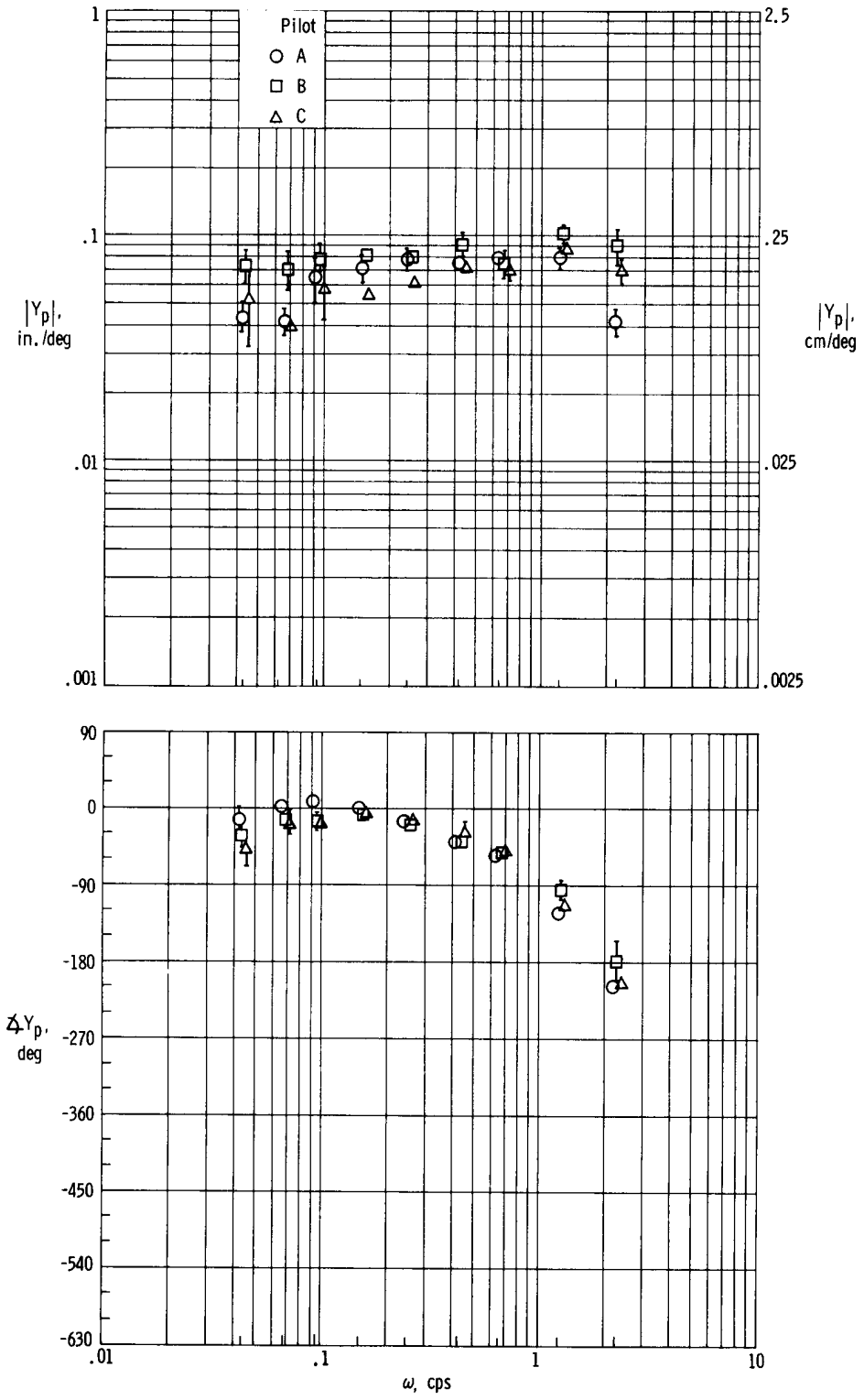

(b) Controlled element $\frac{K}{s}$, contact analog.

Figure 17. – Continued.

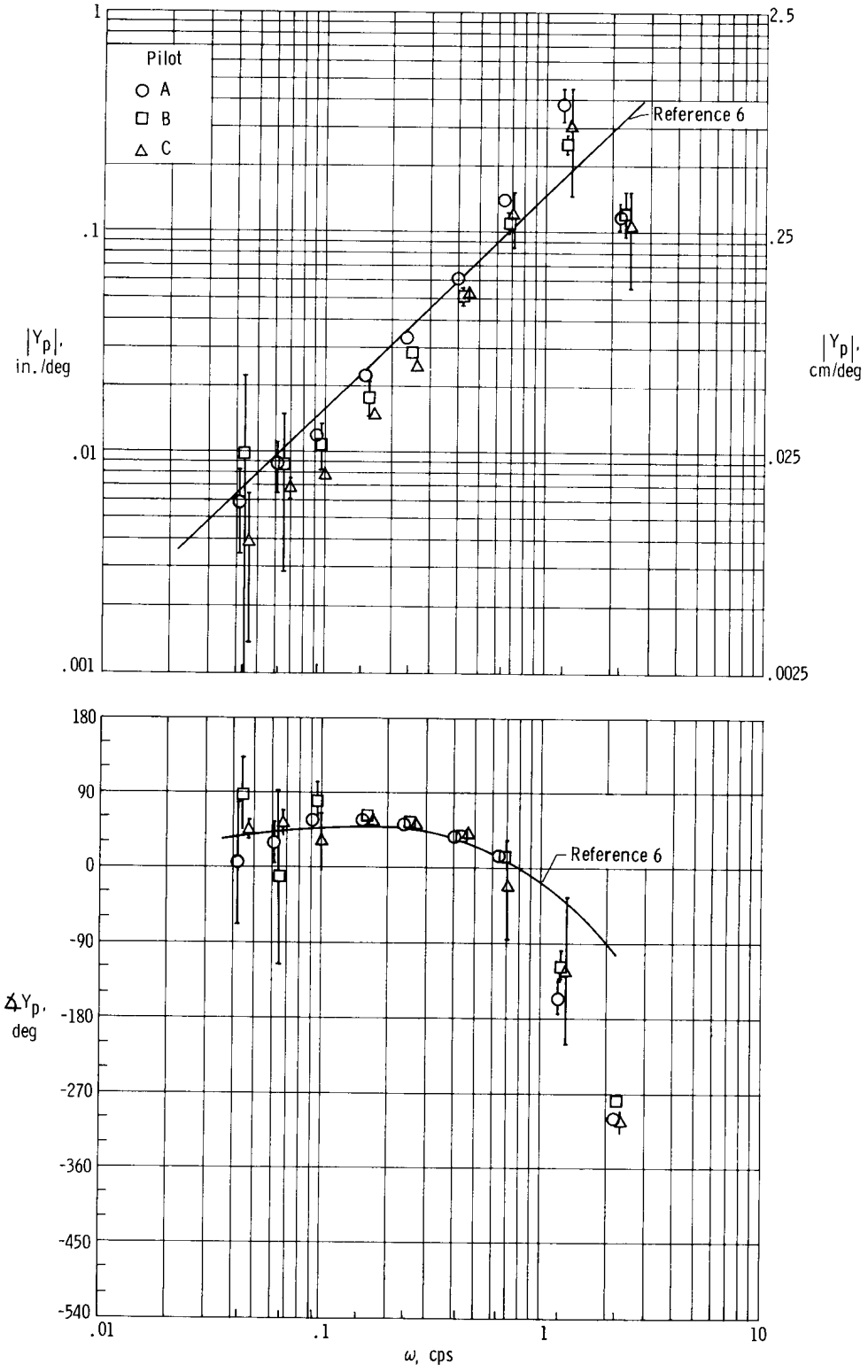

(c) Controlled element $\frac{K}{s(s - \frac{1}{T})}$, T-33 ground.

Figure 17. – Continued.

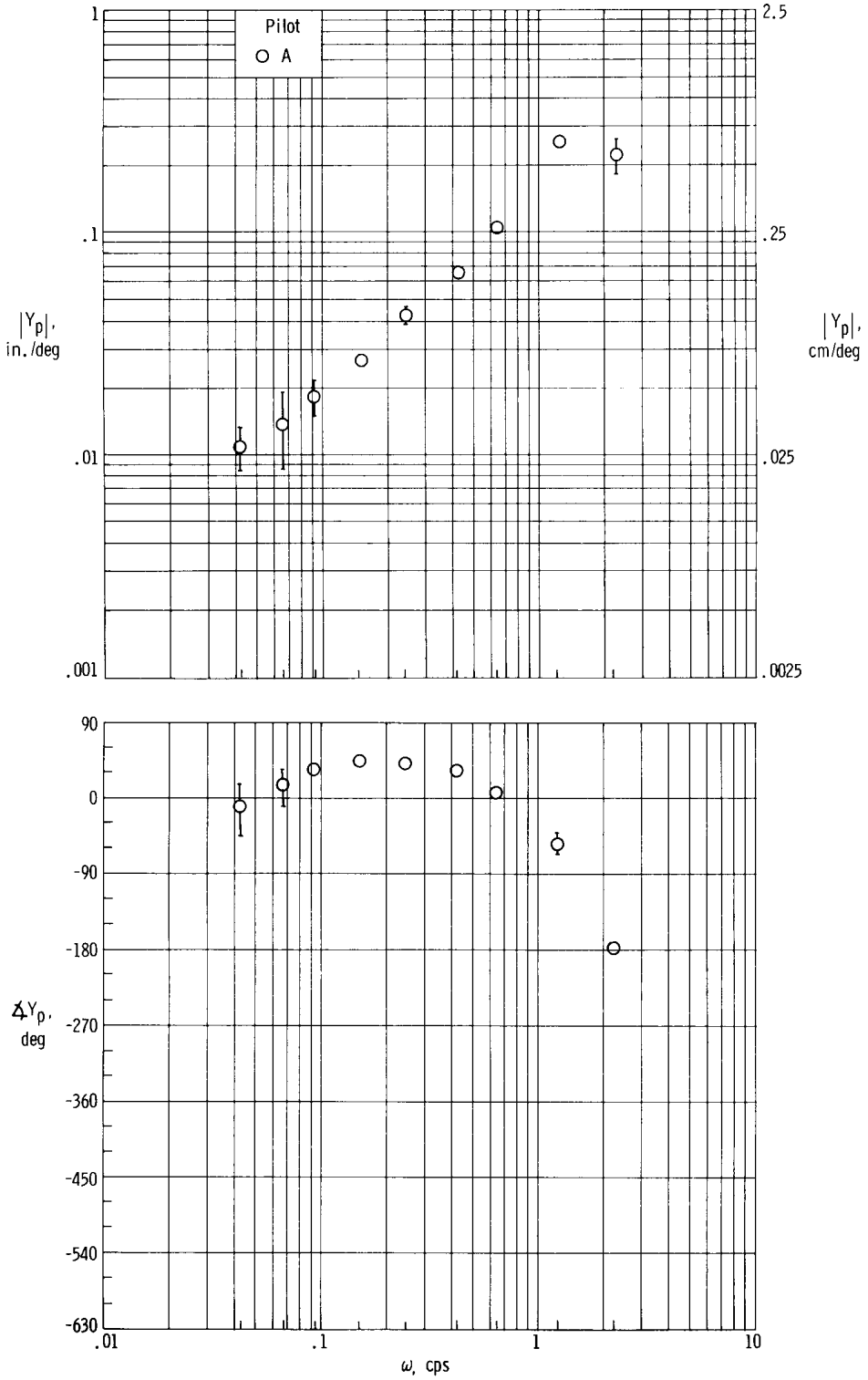

(d) Controlled element $\frac{K}{s(s - \frac{1}{T})}$, contact analog.

Figure 17. – Continued.

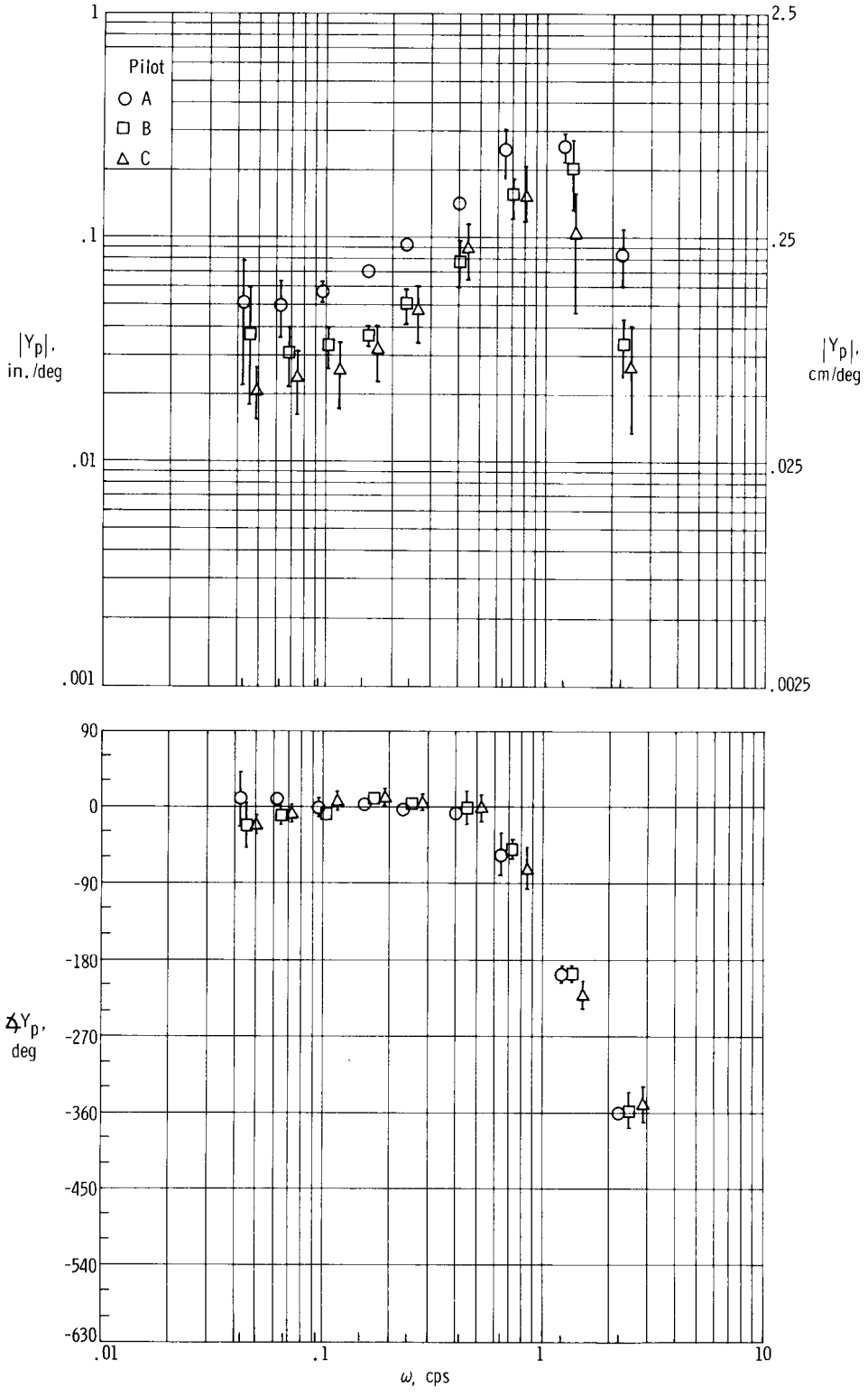

(e) Controlled element A-2, T-33 ground.

Figure 17. – Continued.

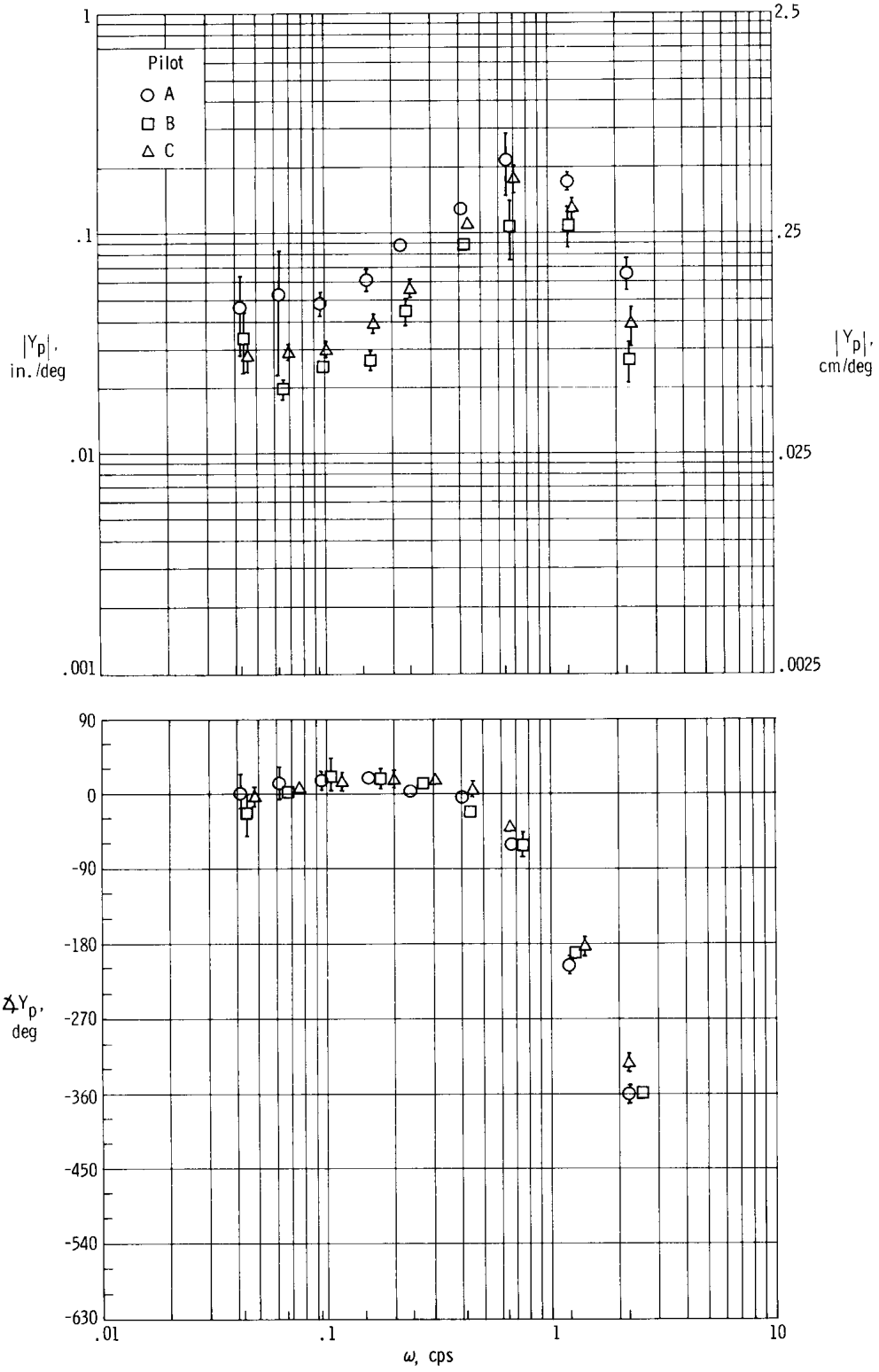

(f) Controlled element A-2*, T-33 ground.

Figure 17. – Continued.

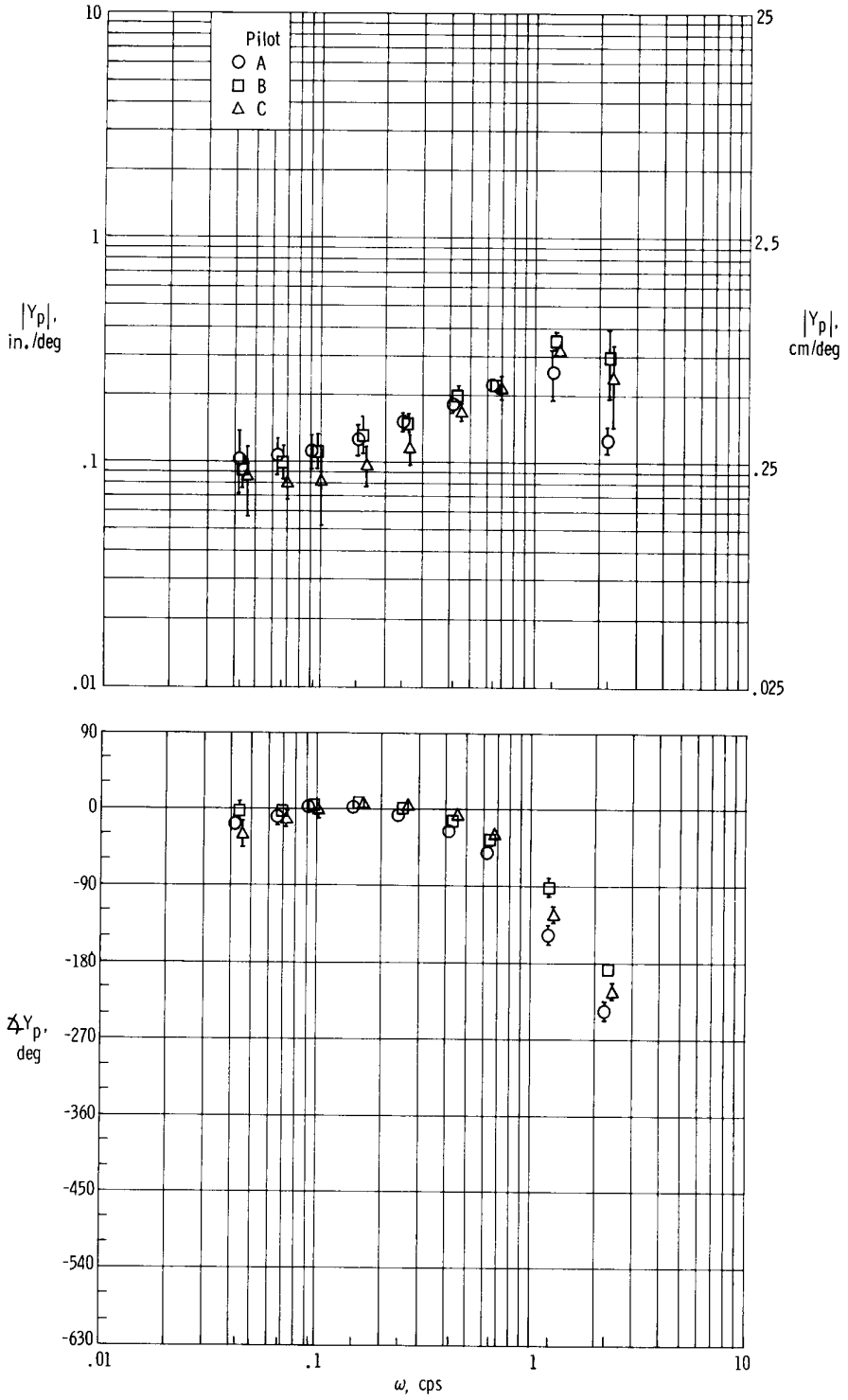

(g) Controlled element A-2*, contact analog.

Figure 17. – Continued.

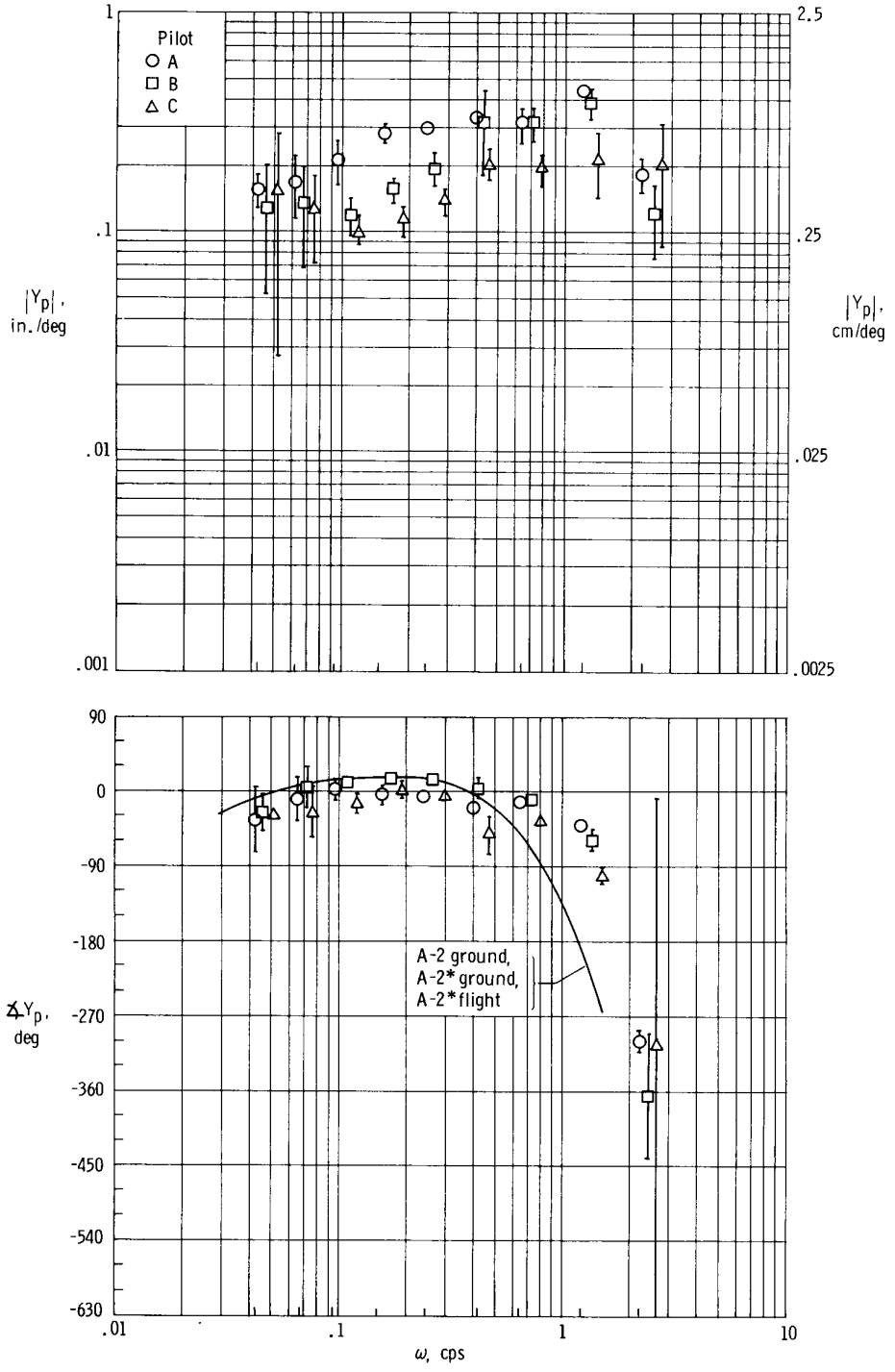

(h) Controlled element A-2, T-33 flight.

Figure 17. – Continued.

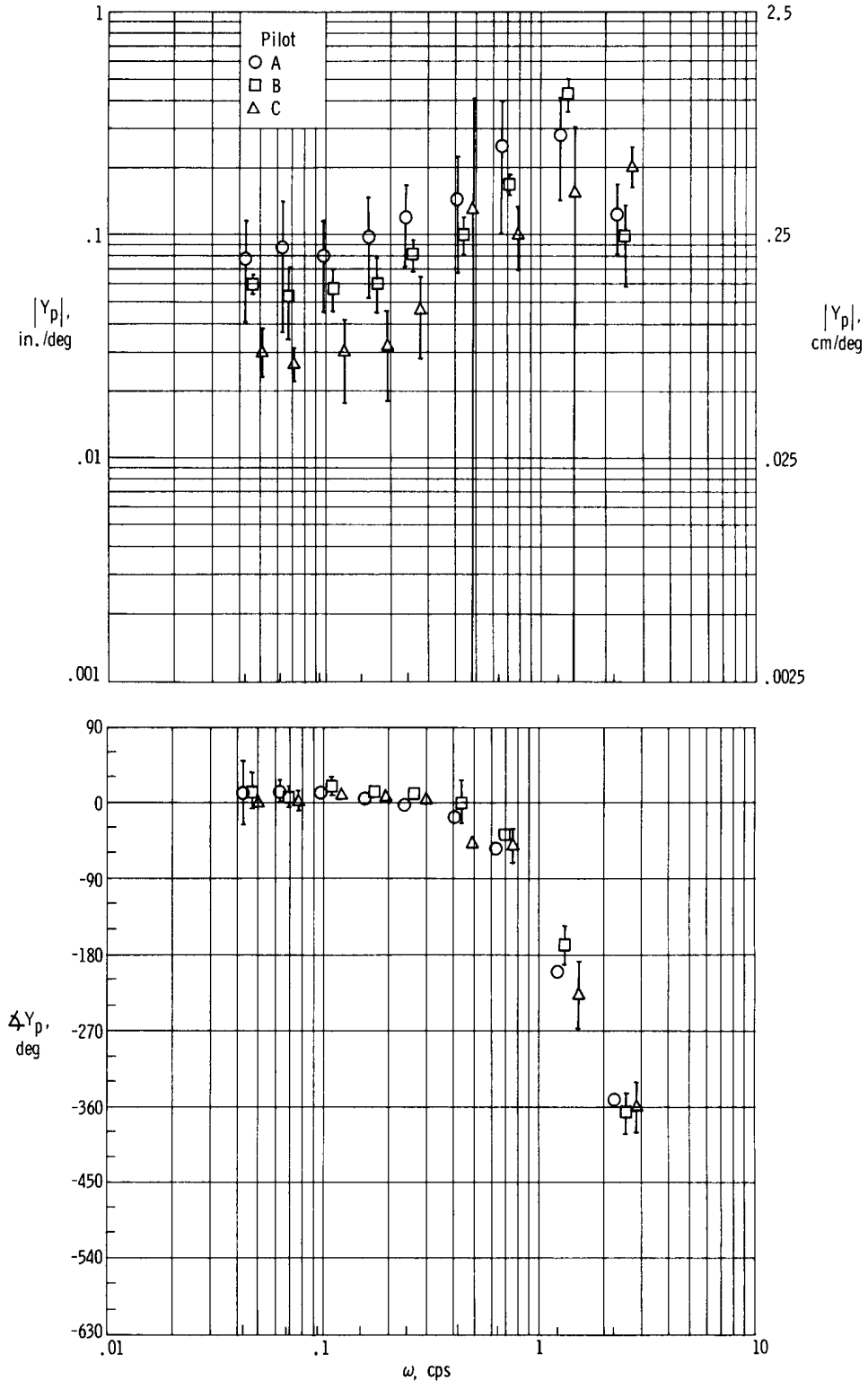

(i) Controlled element A-2*, T-33 flight.

Figure 17. – Concluded.

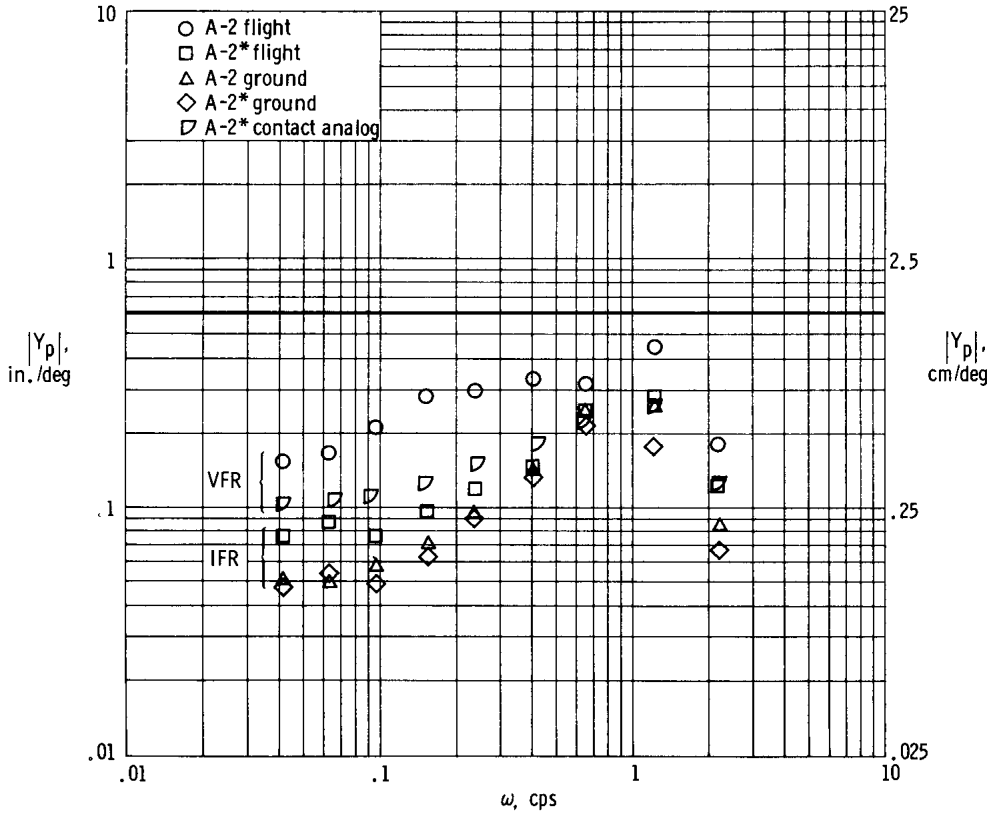

(a) Pilot A.

Figure 18. – Comparison of pilot-transfer characteristic gain $|Y_p|$ for controlled element A-2 and A-2*.

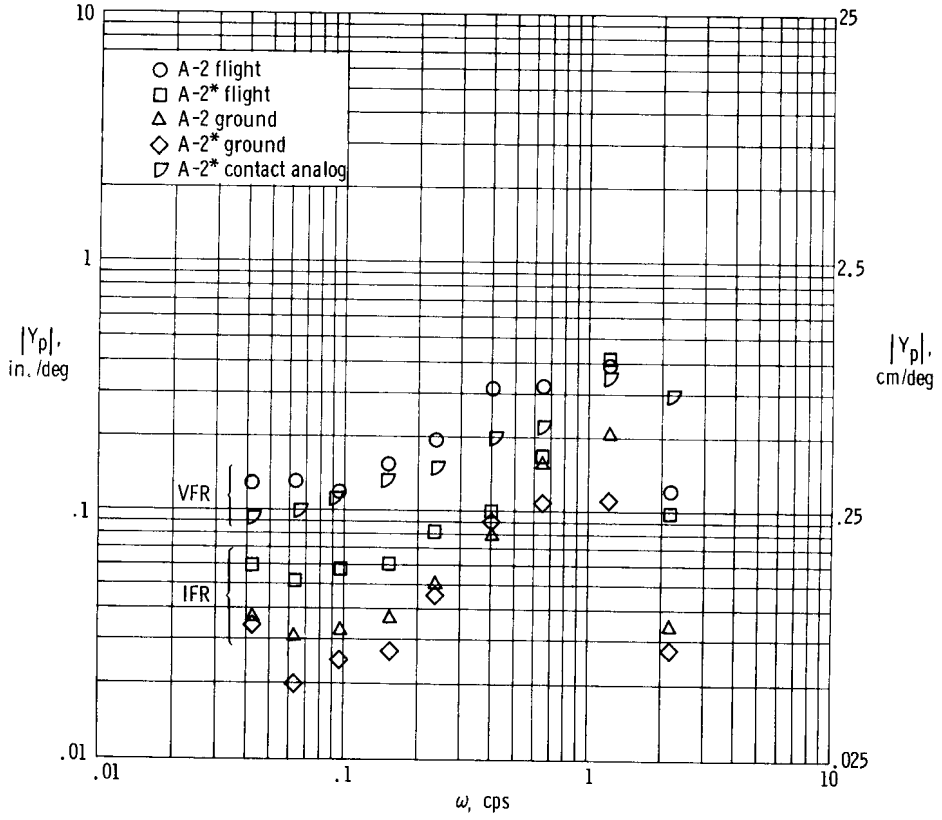

(b) Pilot B.

Figure 18. – Continued.

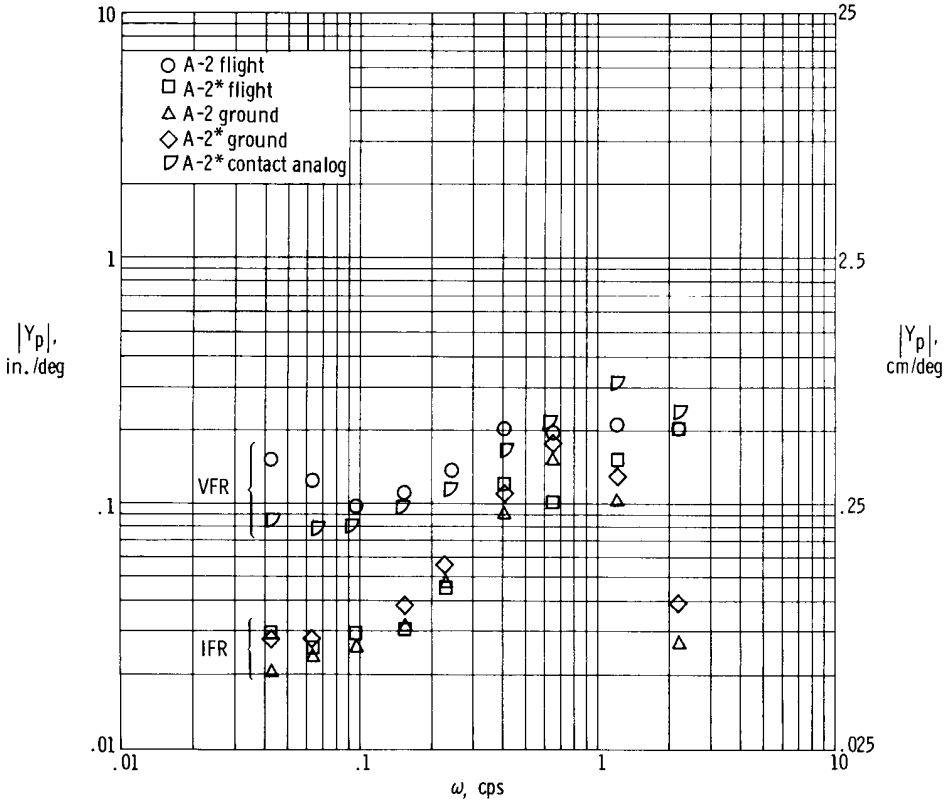

(c) Pilot C.

Figure 18. – Concluded.

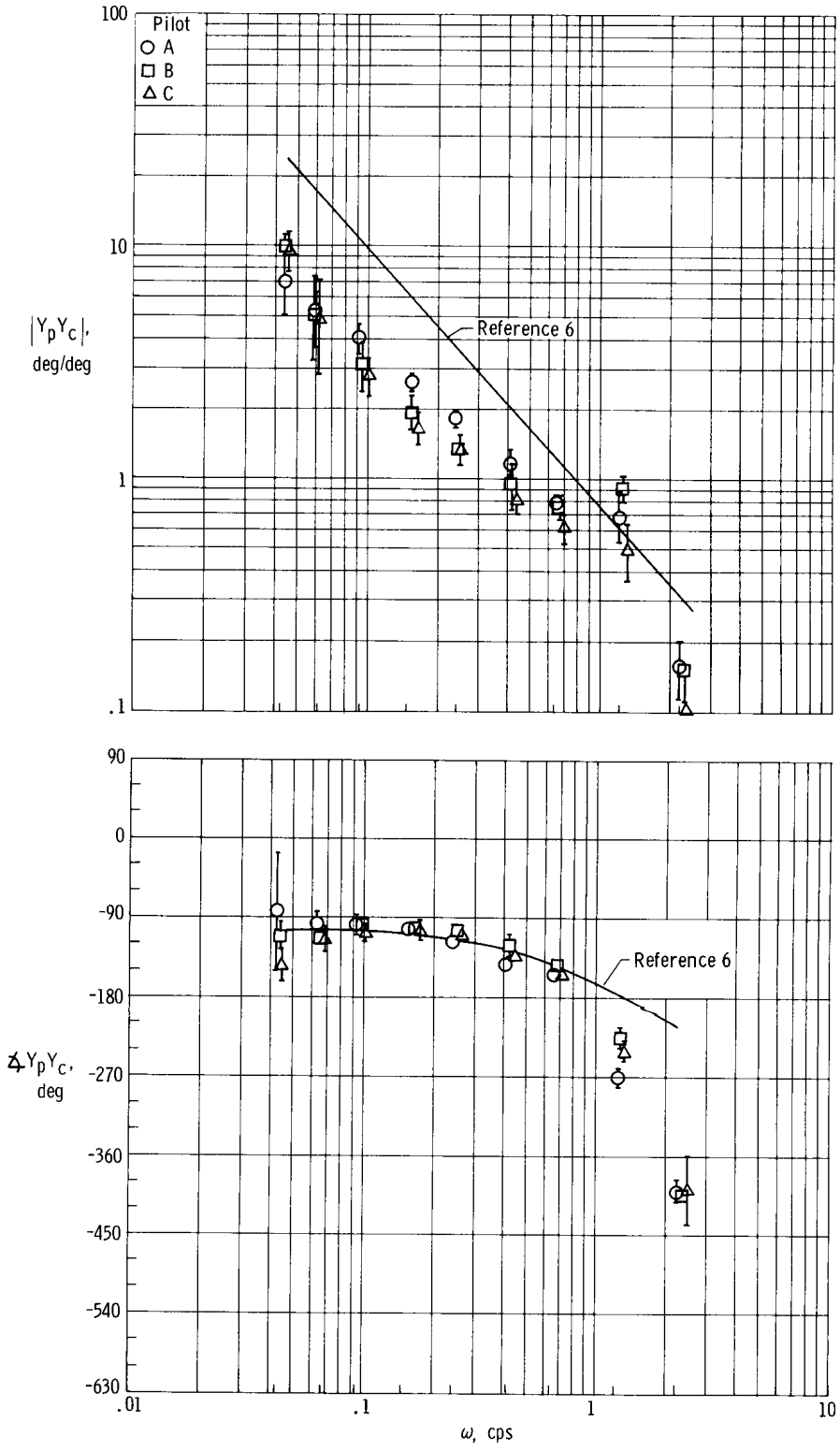

(a) Controlled element $\frac{K}{s}$, T-33 ground.

Figure 19. – Open-loop describing function Y_pY_c for different controlled elements and simulators.

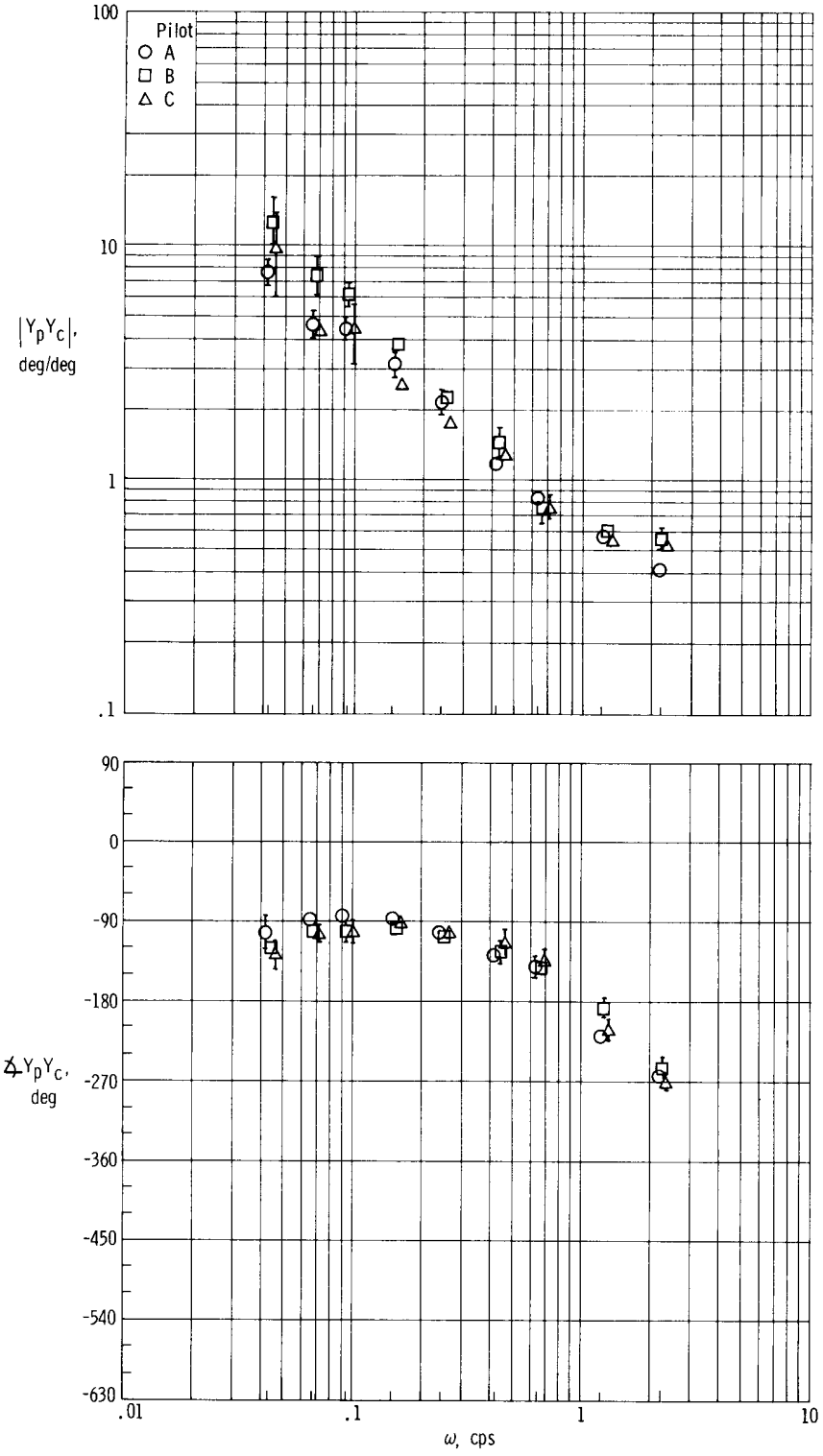

(b) Controlled element $\frac{K}{s}$, contact analog.

Figure 19. – Continued.

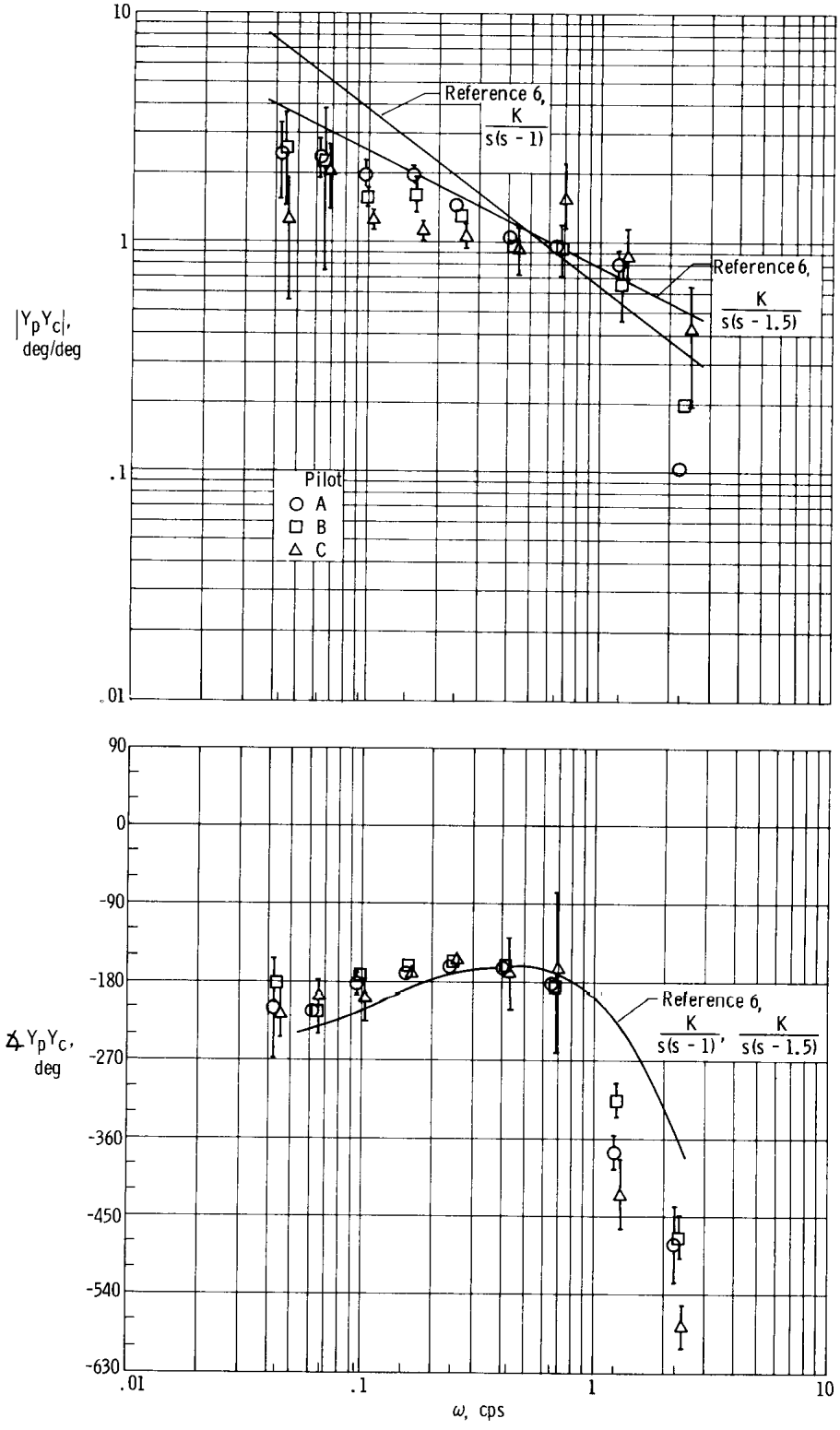

(c) Controlled element $\frac{K}{s(s-\frac{1}{T})}$, T-33 ground.

Figure 19. – Continued.

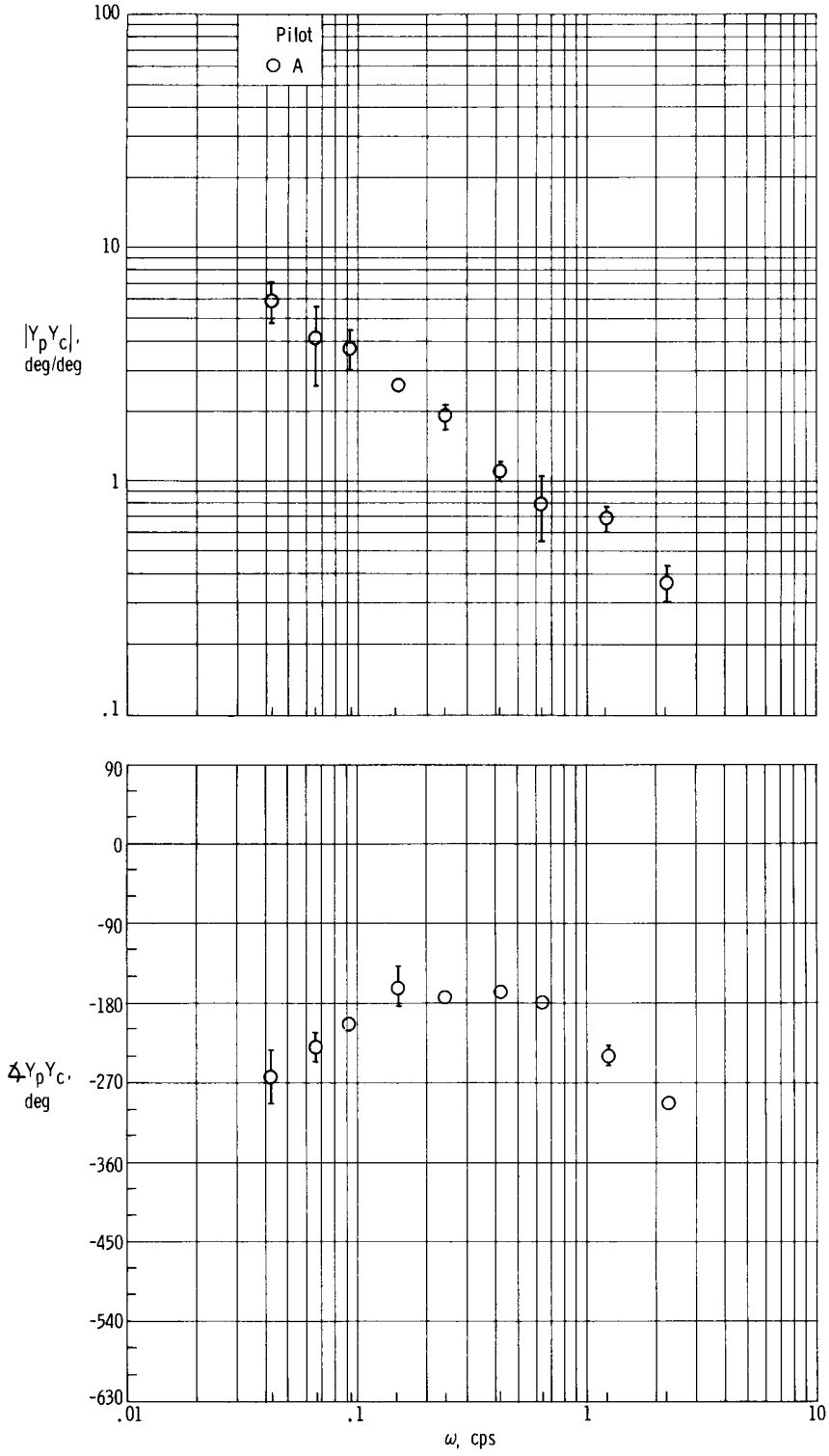

(d) Controlled element $\frac{K}{s(s - \frac{1}{T})}$, contact analog.

Figure 19. – Continued.

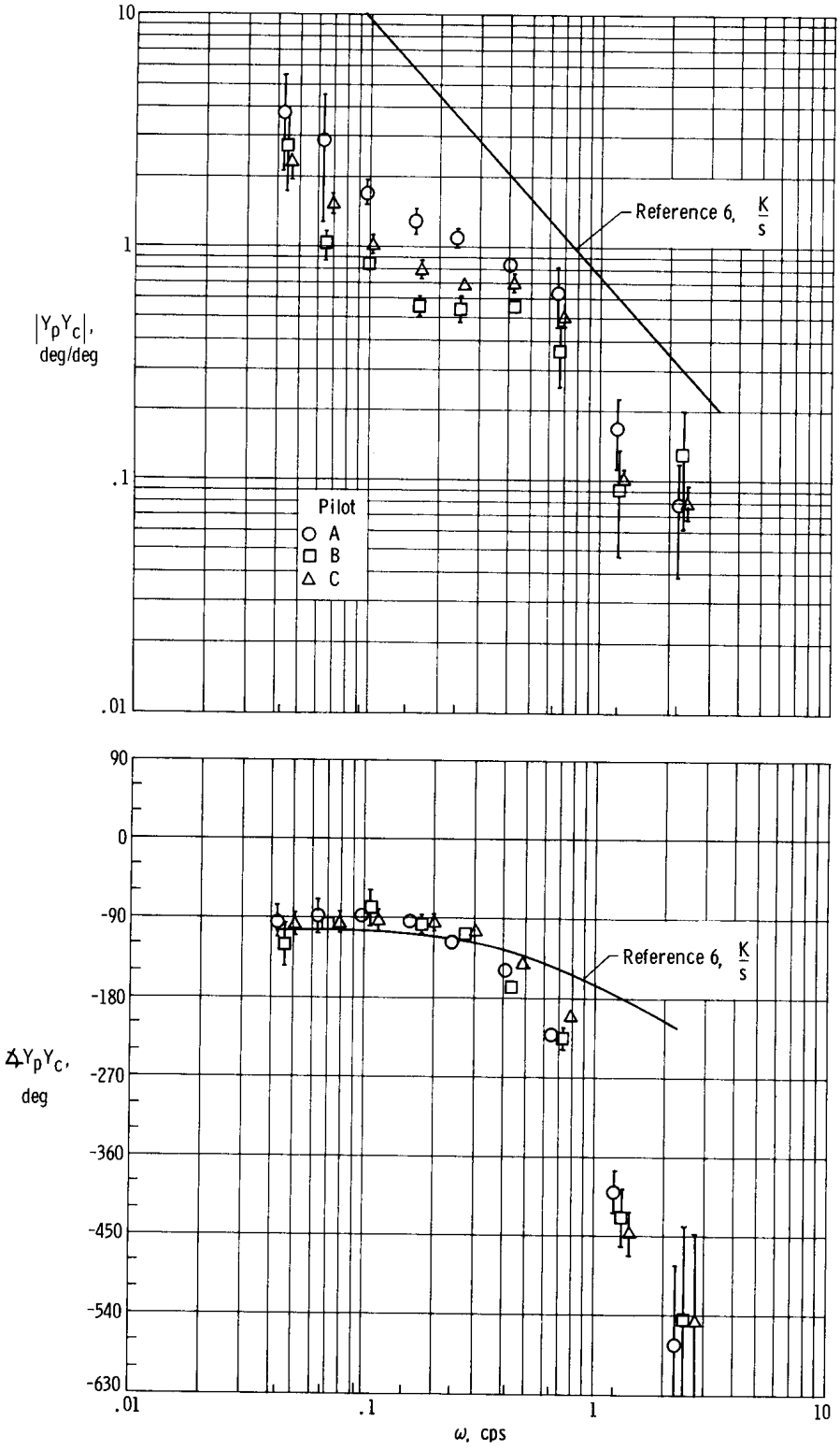

(e) Controlled element A-2*, T-33 ground.

Figure 19. – Continued.

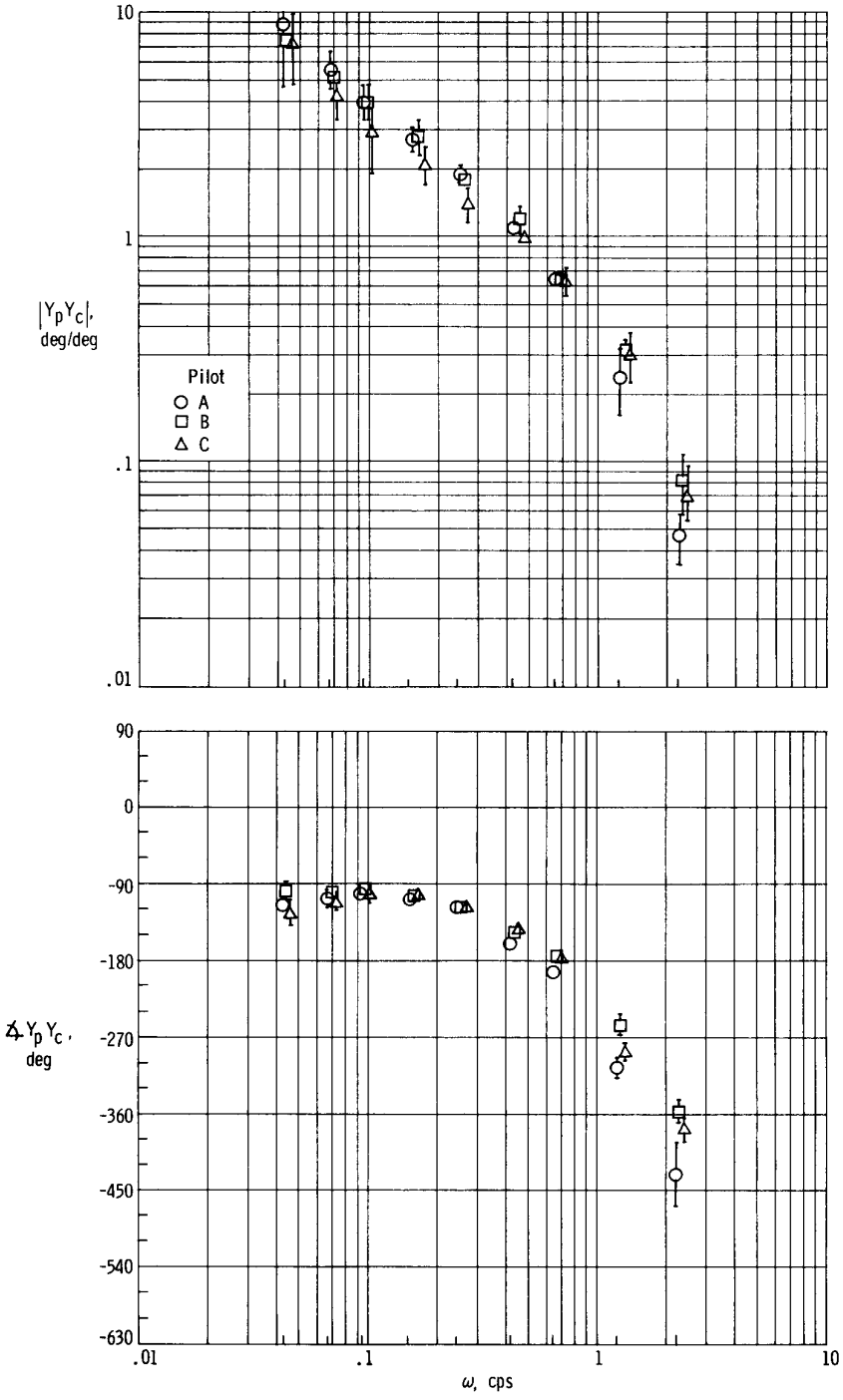

(f) Controlled element A-2*, contact analog.

Figure 19. – Continued.

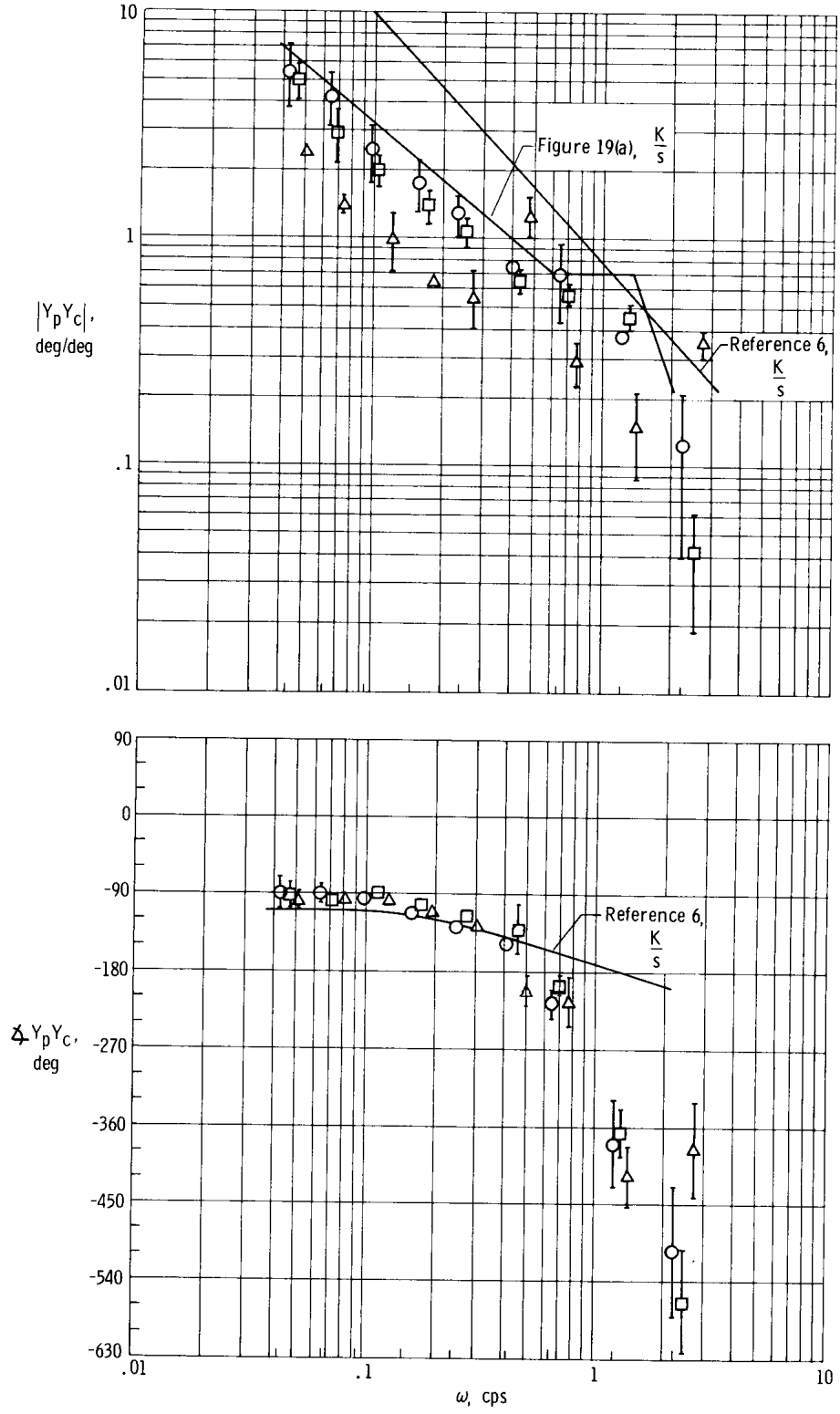

(g) Controlled element A-2*, T-33 flight.

Figure 19. – Concluded.

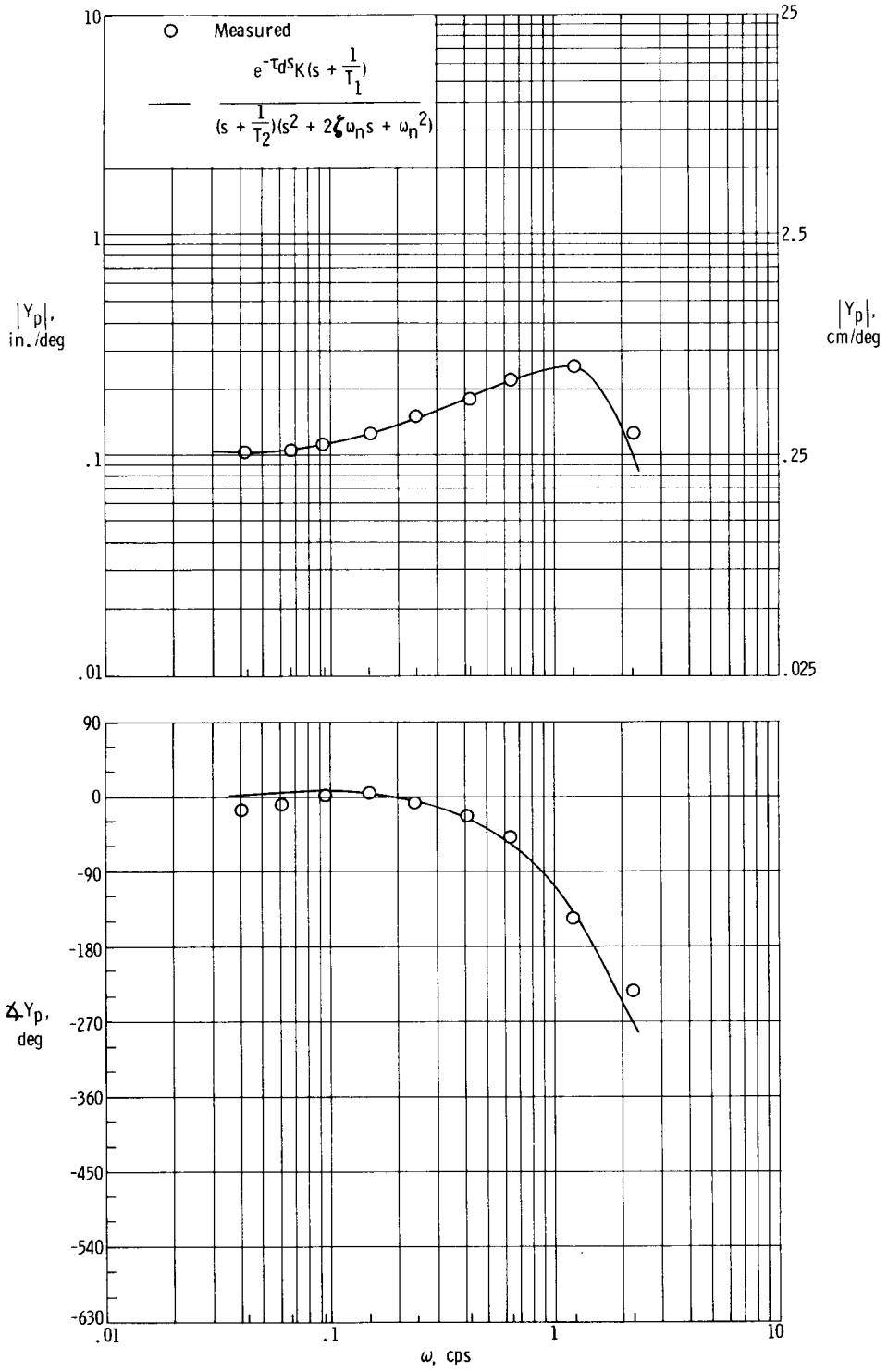

(a) Contact analog.

Figure 20. – Comparison of measured Y_p with $Y_p = \dfrac{e^{-\tau_d s} K(s + \frac{1}{T_1})}{(s + \frac{1}{T_2})(s^2 + 2\zeta\omega_n s + \omega_n^2)}$ for controlled element A-2. Pilot A.

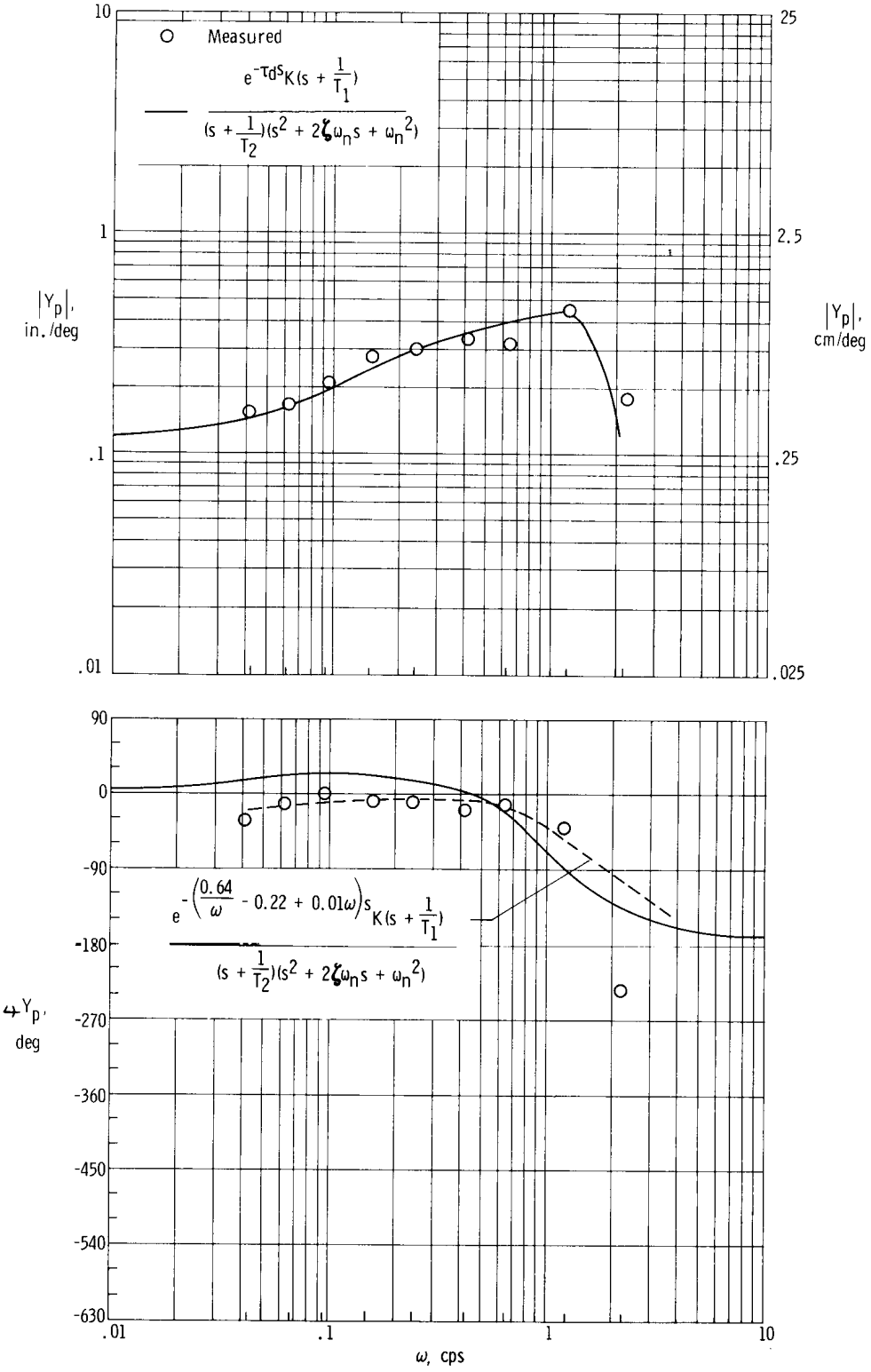

(b) T-33 flight.

Figure 20. – Concluded.

NASA-Langley, 1969 —— 5 H-504